Two-photon multifocus microscopy for real-time cell imaging

(多焦点励起２光子顕微鏡の試作とその実時間細胞動態観察への応用に関する研究)

Katsumasa Fujita

December, 1999

Department of Applied Physics,
Osaka University

Two-photon multifocus microscopy for real-time cell imaging

Katsumasa Fujita

Department of Applied Physics,
Osaka University

Contents

Introduction 1

Chapter 1.
Two-photon multifocus fluorescence microscopy 4

1-1 Principle 4
1-2 Microlens array for multifocus excitation 6
1-3 Spatial resolution 16
1-4 Fluorescence excitation efficiency 18
1-5 Summary 25

Chapter 2.
Development of a two-photon multifocus fluorescence microscope 26

2-1 Optical setup 26
2-2 Experimental results 29
2-3 Summary 37

Chapter 3.
Intracellular Ca^{2+} imaging
with a two-photon multifocus fluorescence microscope 38

3-1 Role of Ca^{2+} in heart muscle cells 38
3-2 Fluorescent Ca^{2+} indicators 45
3-3 Experiments for real-time two-photon Ca^{2+} imaging 48
3-4 Summary 60

Chapter 4.
High resolution microscopy
with a 4pi confocal optical system and phase conjugation 62

4-1 Principle and imaging properties 62
4-2 The use of phase conjugation in a 4pi confocal optical system. 67
4-3 Development of a 4pi confocal microscope with a phase conjugate mirror 72
4-4 Summary 79

Conclusions 83

Acknowledgements 85

References 87

List of publications 91

Introduction

The recent developments in technologies of molecular design and gene manipulation have been providing opportunities to understand the functions and the mechanisms of living bodies with observations by a microscope [Ishikawa, 1995; Endo, 1998]. For example, fluorescent ion indicators made from ion chelators enable us to observe the dynamics of intracellular ions which take on various biological functions, such as muscle constriction, emission of neurotransmitters, communication between intracellular apparatuses, and so on [Minta,1989; Endo 1998]. Expression of fluorescent proteins, known as GFP (Green Fluorescent Protein), in gene-manipulated animals brings fluorescence emission from deep inside of them, where ordinary staining techniques cannot introduce fluorescent dyes [Chalfie, 1994]. This technique can also be applied to the obsevation of the behavior of Ca^{2+} with the combination of two GFPs through the interposition of Ca^{2+}-sensitive calmodulin [Miyawaki, 1998].

In the observation of a living specimen, it is important to reduce physical or physiological damage in the specimen during or even before the observation. For this reason, a confocal fluorescence microscope has been often used to observe those specimens, where the optically sectioned three-dimensional images can be obtained without slicing the specimen mechanically [Gu, 1996; Kawata, 1995]. However, even with the confocal microscope, the observable depth in such specimens is usually mentioned as 50μm, and this observable depth is still not enough to see the functions of whole parts of organs or other apparatuses in bodies [Ishikawa, 1995].

Microscopic techniques have been advanced by the introduction of the two-photon fluorescence microscope realized with the recent development of ultrafast high-power laser systems[Denk, 1990, Denk, 1995]. Since the probability of two-photon excitation is proportional to square of the excitation intensity, the fluorescence emission can be obtained only in the focal volume of an objective lens which illuminates the specimen. This localization of the fluorescence emission brings about three-dimensional resolution, the same as that in a confocal microscope, and reduces photobleaching without exciting out-of-focus planes. Furthermore, the near-infrared light used for two-photon excitation can penetrate more deeply into the specimen than visible light for single-photon excitation [Sheppard, 1990]. Denk et al showed the advantages on a two-photon excitation in their first work for

two-photon fluorescence microscope in 1990 [Denk, 1990]. In 1994, Piston et al. presented the images of the distribution of Ca^{2+} concentration in cultured heart rat cells as the first application of a two-photon microscope in a living biological specimen [Piston, 1994]. Svoboda et al. observed Ca^{2+} dynamics in neocortical pyramidal neurons located at about 300μm depth in a rat brain [Svoboda, 1997]. Squirrell et al. succeeded in imaging mammalian embryos without compromising viability [Squirrell, 1999] Recently, the process of cell division within a cube with 300μm dimensions, in a rat embryo, was recorded by Denk with the help of GFP [Denk, 1999].

Because of the advantages in two-photon excitation shown in the above-mentioned applications, the use of the microscope for real-time imaging of living and moving specimens attracted many researchers. As a first approach for the real-time imaging, Xie et al. developed a realtime imaging system by fast raster scanning of a single focus with a resonating galvanometer mirror, and observed single green algae cells swimming in an aqueous solution [Xie, 1998]. Fan et al used a similar configuration for observing Ca^{2+} concentration in cultured rat heart cells [Fan, 1999]. In another approach, Bewersdorf and his co-workers proposed a multifocus multiphoton excitation microscope, where fluorescence was excited with several tens of focuses produced by a microlens array [Bewersedorf, 1998]. In their microscope, the image acquisition rate was enhanced without increasing the scanning speed of the foci by the use of multipoint excitation. This multifocus excitation technique was also used for measuring fluorescence lifetime of chromophores with a high-speed gating camera [Straub, 1998].

Based on the background presented, the research in this dissertation was carried out to develop a two-photon fluorescence microscope which can be applied to the observation of living and moving specimens with the advantages of the high image-acquisition rate and the high spatial-resolution. For this purpose, the use of both a microlens- and pinhole-array disk was proposed to obtain two-photon excitation at multiple foci, where the image acquisition rate, the spatial resolution, and the observable depth can be enhanced. The developed system was applied to the observation of Ca^{2+} dynamics in cultured rat heart cells and a whole rat heart to verify the usefulness of the proposed microscope. The contents of this dissertation are as follows.

In Chapter 1, the principle and the optical properties of the proposed microscope are described. The design of a microlens- and a pinhole-array disk which realize a uniform scanning and illumination on a specimen with multifocus is shown. The fluorescence

excitation efficiency and its saturation effect are estimated both theoretically and experimentally for the optimization of the optics.

In Chapter 2, the practical system of the proposed microscope and some experimental results are shown. In the experimental results, the enhancement in the spatial resolution and the contrast of obtained images were confirmed in the system with a pinhole-array disk.

In Chapter 3, the techniques for imaging intracellular Ca^{2+} dynamics with the developed microscope are shown. The roles of Ca^{2+} and its behavior in heart muscle cells are also introduced. The experimental results of Ca^{2+} imaging in cultured heart rat cells and a whole rat heart are mentioned to show the versatility of the proposed microscope in the biological field.

The use of a 4pi optical system and phase conjugation for further enhancement of spatial resolution is proposed in Chapter 4. A practical system with 4pi optics was developed and some preliminary experiments were performed. The experimental results show an increased spatial resolution of about 120μm brought about by the 4pi optics and its capability of compensating for aberrations generated in a specimen. A multifocus excitation microscope using these techniques is introduced at the end of this chapter.

The conclusion of this research and its perspective for the future are given at the end of this dissertation.

Chapter 1.

Two-photon multifocus fluorescence microscopy

In this chapter, the use of a microlens- and pinhole-array scanner is proposed to increase the image acquisition rate of the two-photon fluorescence microscope with multifocus excitation. The use of a confocal pinhole-array in a multifocus two-photon microscope brings about the enhancement of spatial resolution and contrast of fluorescence images into the microscope. With the proposed setup, the image acquisition rate can be increased several ten times larger than that with a single-focus scanning microscope. In the following sections, the principle and the optical properties of the proposed microscope are described. The estimation of fluorescence excitation efficiency given in the fourth section of this chapter reveals that the sufficient use of laser light is important for multifocus fluorescence microscopes.

1-1 Principle

Fig. 1-1 shows the optical setup of a two-photon multifocus fluorescence microscope [Fujita, (in press)] with a microlens- and pinhole-array scanner. In this optical system, the beam from the laser is divided to a number of beamlets at a microlens-array disk and produces focusing spots on a pinhole-array disk. Each focusing spot is imaged into the specimen as a two-photon excitation spot by an objective lens. The fluorescence excited at each spot is collected by the same objective lens and detected by a CCD camera after being reflected by a dichroic mirror. Rotation of the microlens-array disk scans the specimen with excitation spots so that the fluorescence image is obtained by the CCD camera at video rate or higher [Bewersdorf, 1998, Brackenhoff, 1998; Fujita, 1999]. The microlenses on the disk are arranged on a helical order in order to scan the specimen uniformly [Xio, 1987]. In this microscope, fluorescence detection is done through a pinhole-array disk. This brings about the benefits of confocal detection to the microscope, which are the enhancement of the three-dimensional spatial resolution and the image contrast [Nakamura, 1993; Sheppard, 1990].

As shown in Fig. 1-2, the excitation of fluorescence is localized at the focal plane of the

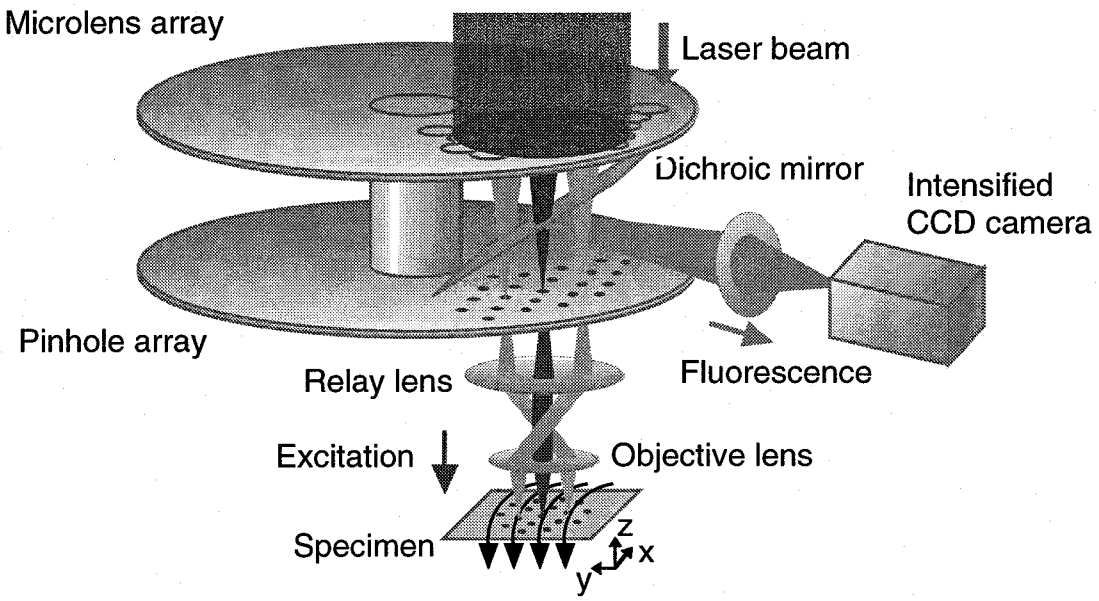

Fig. 1-1 An optical setup of a two-photon multifocus fluorescence microscope with a microlens- and pinhole-array scanner.

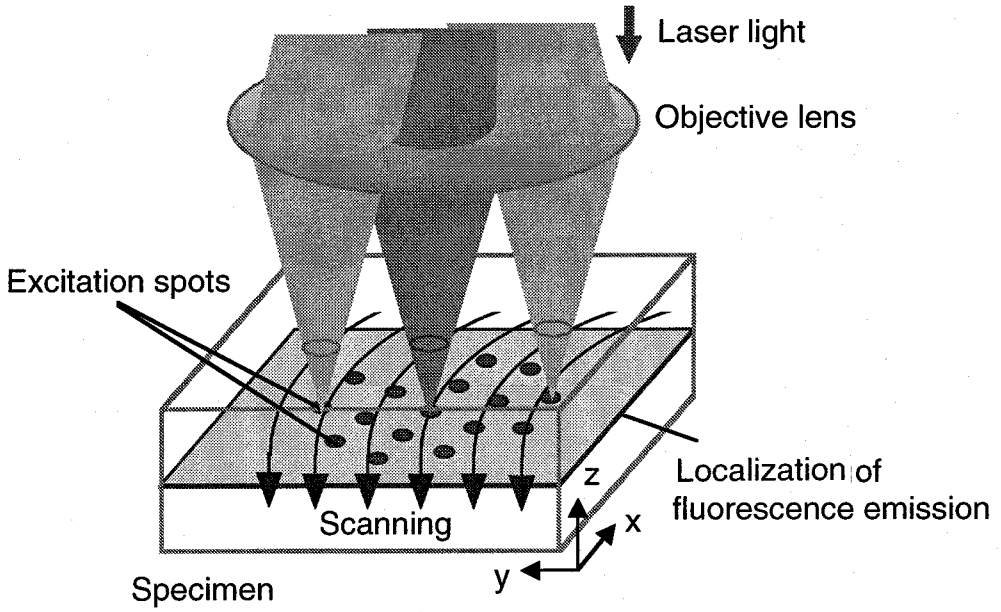

Fig. 1-2 Localized fluorescence emission at a focal plane of an objective lens.

As shown in Fig. 1-2, the excitation of fluorescence is localized at the focal plane of the objective lens, and only the fluorescent plane in the specimen is imaged onto the CCD camera. Optical sectioning can be achieved with this microscope as well as a typical two-photon fluorescence microscope with single-focus excitation. For this reason, an observed specimen does not have to be sliced before observation under this microscope. Other advantages in two-photon excitation, such as long penetration depth with near infrared excitation and less photobleaching at the out-of-focus plane, are also available in this microscope.

The most significant point of this optical setup exists in the multifocus excitation. The enhancement of image-acquisition rate in this microscope relies upon the enhancement of fluorescence-acquisition rate with multifocus excitation. This cannot be achieved in a typical two-photon fluorescence microscope using single-focus scanning. Here, let us think about a typical two-photon fluorescence microscope for the comparison. Even with the excitation by a single focus, it is possible to increase the scanning speed by using a resonant galvanometer mirror or a polygonal mirror [Vukobratovich, 1982; Xie, 1998]. However, the amount of fluorescence detected per unit time decreases proportionally with the increase of scanning speed. The lower amount of the detected fluorescence surely brings about lower signal to noise ratio and lower contrast of obtainable images. Introducing higher intensity of the excitation to solve this problem is not a good idea in two-photon excitation because less of cell viability or nonlinear optical phenomena such as self-focusing, continuum generation, or ablation easily appear with the increase of excitation power. From the above reasons, multifocus excitation has a big advantage to a typical single-focus scanning system.

The confocal detection system introduced in this microscope gives twice higher spatial resolution and higher contrast in images of specimens as mentioned in the third section of this chapter. In addition to this advantage, confocal detection also gives longer penetration depth of observation. This issue will be discussed in the second chapter.

1-2 Microlens array for multipoint excitation

An arrangement of microlenses in a microlens-array scanner is one of the important factors in the multifocus-excitation technique. An inappropriate arrangement of microlenses may cause

inaccurate image reconstruction in the microscope. The following points are required for the arrangement of microlenses to obtain appropriate imaging property of a two-photon fluorescence microscope.

1) Uniform scanning and illumination

Without uniform scanning and illumination, the density of excitation light varies at each position on a specimen. Under this condition, the fluorescence image of the specimen cannot represent the distribution of the fluorescent dye in the specimen properly. For uniform scanning, the density of excitation spots must be the same at any position on the specimen. This can be achieved by setting the separation of the lenses constant at any part of the scanner disk. In the multifocus scanning microscope, the scanning speed of the spots is not constant at a whole view area because the linear velocity of the scanning depends on the radius of the disk. The scanning speed of focuses generated from the microlenses at outer side of the disk run faster than that at the inside. Given the above mentioned conditions, the number of microlenses must be increased along the distance from the center of the disk. A helical arrangement shown in Fig. 1-3 with a constant separation of the lenses can be chosen to satisfy above requirements for the microlens array. The radius of the spiral at the position of i-th microlens can be given as[Ichihara, 1996]

$$r_i = r_0 + \theta_i \frac{m\,d}{2\pi} \tag{1-1}$$

where r_0 is the radius at the microlens nearest to the center of the disk, m is the number of the spirals on the disk, and d is the separation of center of each microlens. The distance along the spiral from r_0 to r_i can be given as

$$\begin{aligned} L_i &= \int_0^{\theta_i} r_i \, d\Omega \\ &= r_0\,\theta_i + \frac{m\,d}{4\pi}\,\theta_i^2 \end{aligned} \tag{1-2}$$

By solving this equation for θ_i, we can obtain the following equation

$$\theta_i = \frac{2\pi}{m\,d}\left(-r_0 + \sqrt{r_0^2 + \frac{L_i\,m\,d}{\pi}}\right) \tag{1-3}$$

Because of $L_i = d\,i$, the angle θ_i can be obtained from the equation (1-2) as

$$\theta_i = \frac{2\pi}{m\,d}\left(-r_0 + \sqrt{r_0^2 + \frac{i\,m\,d^2}{\pi}}\right) \tag{1-4}$$

From Eqs. (1-1) and (1-4), the arrangement of the microlens on the scanner can be calculated when d, r_0, and m are given. Fig. 1-4 shows the arrangement of the microlens with d = 250μm, r_0 = 15mm, and around 20,000 microlenses.

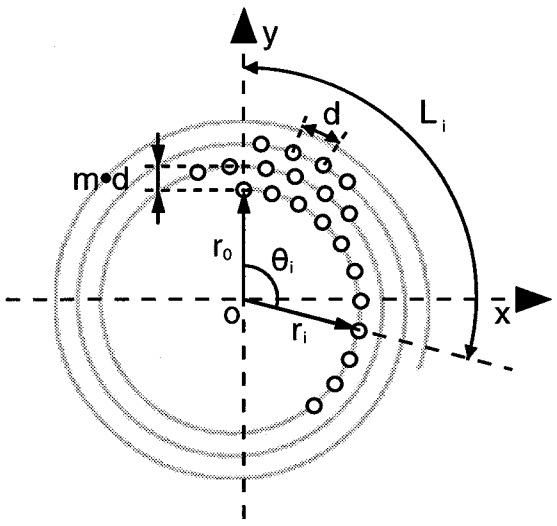

Fig. 1-3 An arrangement of microlenses which gives uniform scanning and illumination density.

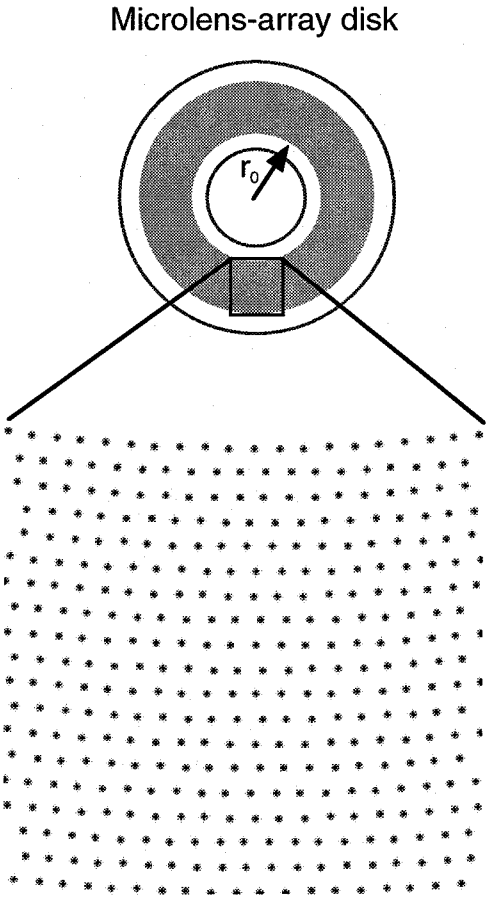

Fig. 1-4 Arrangement of focuses obtained by Eqs. (1-1) and(1-4) with d = 250μm, r_0= 15mm, and around 20,000 microlenses.

2) Separation of focuses

In the multipoint excitation microscope, there is the possibility of interference between the focuses in the specimen which changes the imaging property of the microscope. Too short separation of the focuses brings the overlap of wave front of light between each focus, and this overlap changes the distribution of the intensity of the focus. In laser scanning microscopes, the spatial resolution is proportional to the volume of the excitation spot at the focus [Nakamura, 1993; Gu, 1996]. The overlap of the wave front degrades the spatial resolution in the multifocus fluorescence microscope.

To know the spatial resolution dependence on the separation of focuses, let us calculate the three-dimensional distribution of the intensity of an excitation spot surrounded by other spots. The distribution of the intensity of a single focus is given by the point spread function (PSF) [Born, 1959] as

$$I_s(u,v) \propto \left| \int_0^1 J_0(|v|\rho) \exp(-\frac{1}{2} i u \rho^2) \rho \, d\rho \right|^2 \tag{1-5}$$

where u and v are the normalized value with NA of a lens and wavelength of light λ. The definitions of u and v are

$$u = \frac{2\pi}{\lambda} NA^2 z \tag{1-6}$$

and

$$v = \frac{2\pi}{\lambda} NA\, r \tag{1-7}$$

where z and r are the axial and the lateral positions respectively, when the geometrical focus is located at the origin. Fig. 1-5 shows the PSF of the single excitation spot calculated from Eq. (1-5). When we assume that the arrangement of the focuses forms a pentagon as shown in Fig. 1-6 and the intensity of the center focus can be affected by the wave front of the nearest five focuses, the intensity distribution of the center spot is obtained simply as

$$I_m(u,v) \propto \left| \int_0^1 J_0(v\rho) \exp(-\frac{1}{2} i u \rho^2) \rho \, d\rho + \int_0^1 J_0(|v-v_1|)\rho) \exp(-\frac{1}{2} i u \rho^2) \rho \, d\rho + \cdots\cdots + \int_0^1 J_0(|v-v_5|\rho) \exp(-\frac{1}{2} i u \rho^2) \rho \, d\rho \right|^2 \quad (1\text{-}8)$$

where, v_1, ..., and v_5 represents the lateral position of the surrounding focuses.

Fig. 1-7 shows the PSFs of the excitation spots with the surrounding focuses calculated with several separations $\Delta v = |v_1| = \ldots\ldots = |v_5|$ at the x-z plane shown in Fig. 1-6. From the comparison of Fig. 1-5 and Fig. 1-7, it can be seen that the overlap of the wave front from the surrounding focuses brings about an increase in the intensity at the out-of-focus position on v axis. The increase in intensity moves toward the center with a decrease in the separation. This can be imagined easily by considering a geometrical model of focuses approaching each other. Figs. 1-8 and 1-9 show the intensity along the x and y axis of the calculated results shown in Fig. 1-7. In Fig. 1-8, some sub-peaks appear in the PSF at a separation of $\Delta v \leq 25$, but not at a separation of $\Delta v \geq 30$. From this result, it seems that the focusing spots give the appropriate resolution in the lateral direction when the separation is $\geq$ 30. In the results of Fig. 1-9, several sub-peaks also appear on the axial direction when the separation is small. However, these sub-peaks still clearly appear at a separation of $\Delta v = 50$. In the plot where $\Delta v = 55$, the sub-peaks are still remaining, but their intensity is lower than that of the sub-peaks which appear in the PSF of a single focus. It can be considered that these sub-peaks at a separation of $\Delta v = 55$ do not affect the spatial resolution so much because of their considerably low intensity. From the above-calculated results, it can be concluded that a separation of $\Delta v \sim 50$ is required to obtain the proper spatial resolution in a multifocus excitation microscope. The separation of $\Delta v \sim 50$ corresponds to about 6μm when 800nm wavelength and an objective lens with an NA of 1.0 are used.

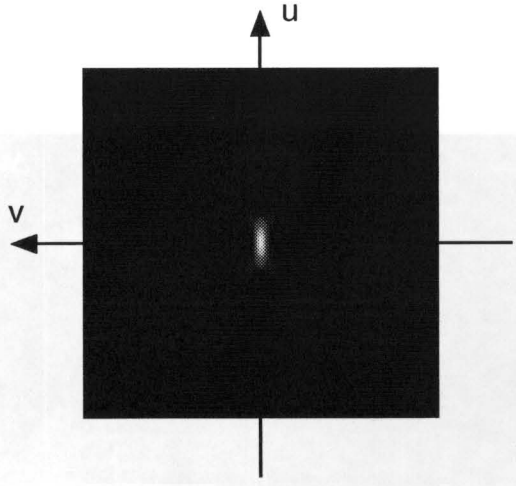

Fig. 1-5 The point spread fuction (PSF) of a single focus.

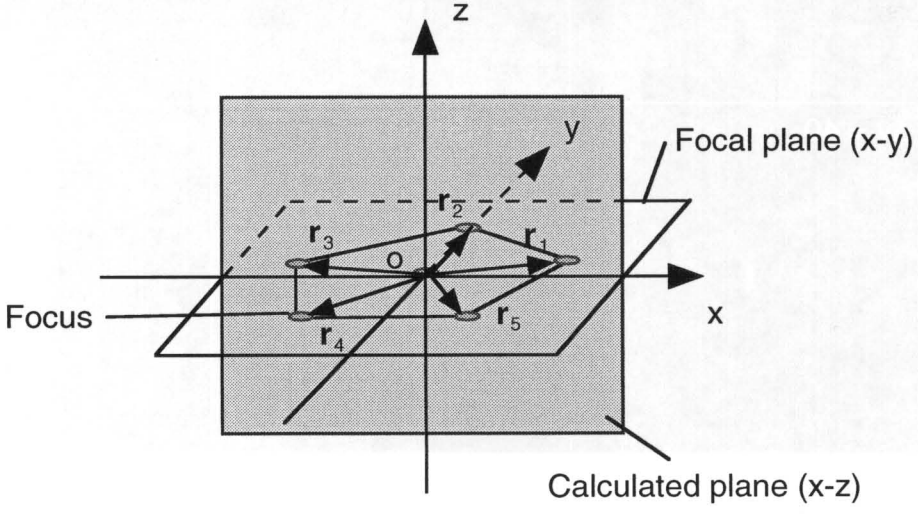

Fig. 1-6 A model for calculation of the interaction between focuses

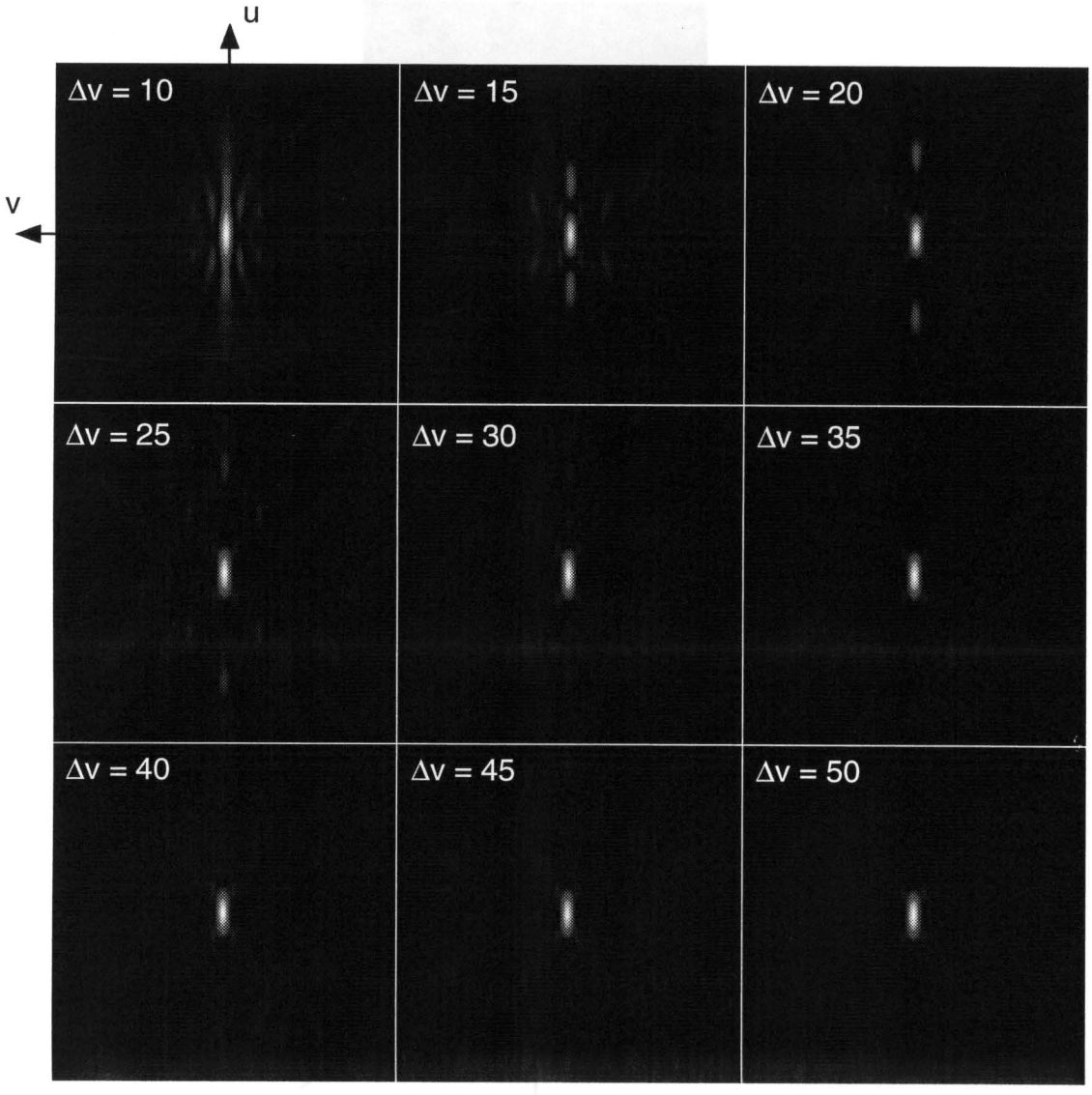

Fig. 1-7 The PSFs of the center focus at several separations to five surrounding focuses.

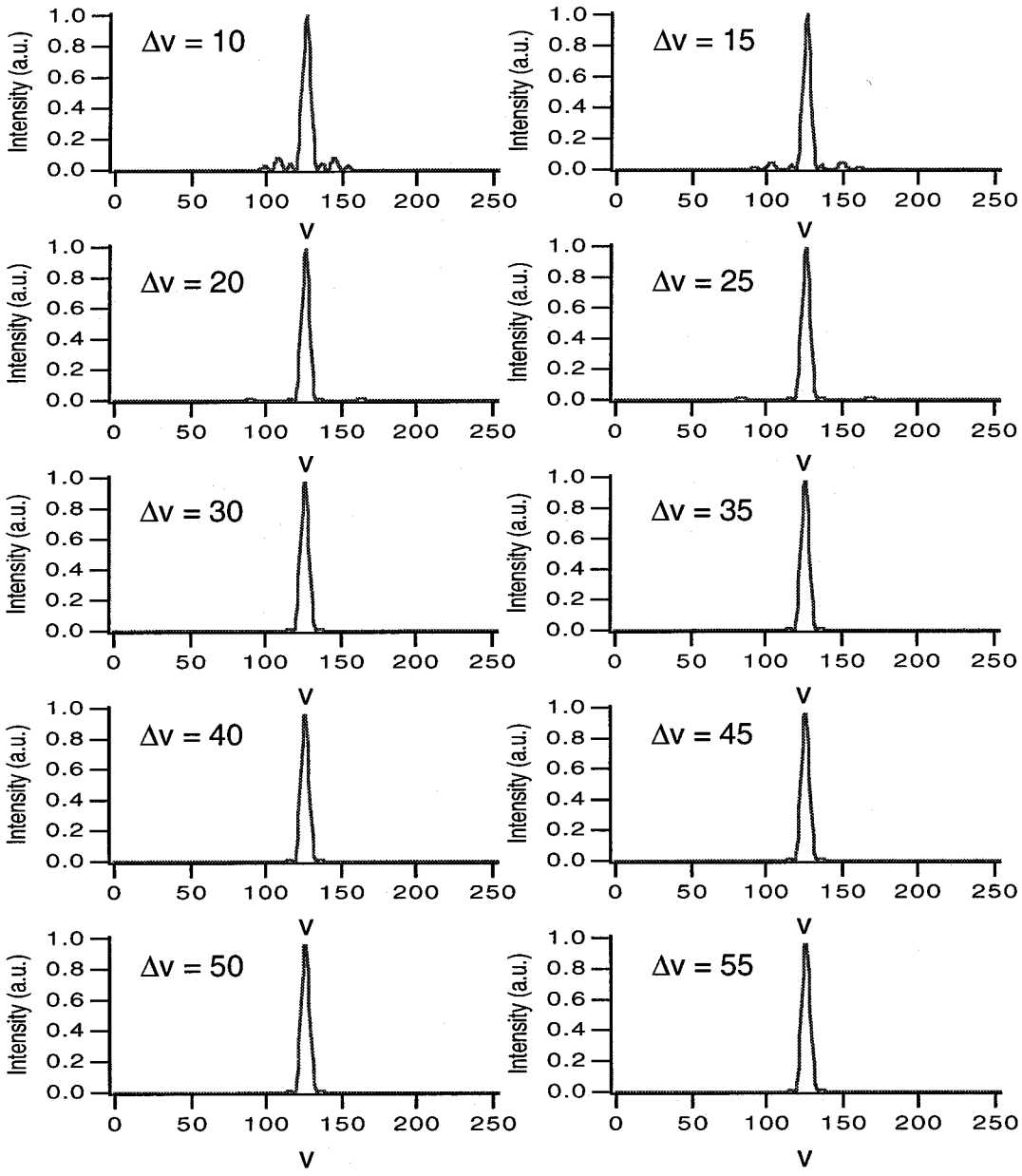

Fig. 1-8 Plots of the intensity of the center focus along the lateral direction

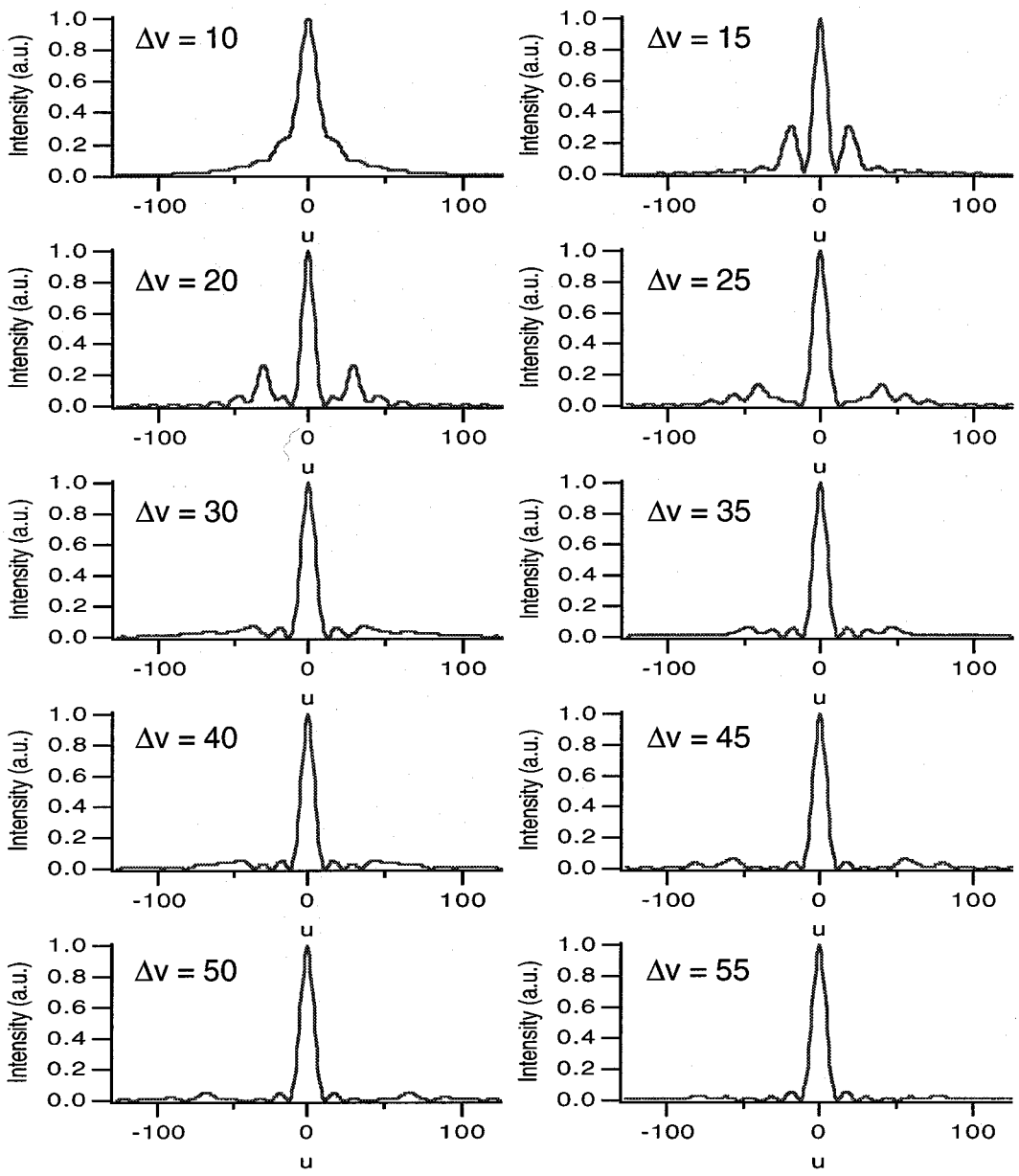

Fig. 1-9 Plots of the intensity of the center focus along the axial direction

1-3 Spatial resolution of two-photon multifocus microscopes

The imaging property of a multipoint two-photon excitation microscope can be considered to be the same as that of a typical two-photon excitation microscope which scans a single focus, when the excitation spots have a separation large enough so as not to interfere with each other in the specimen. As shown in the previous section, with 6μm separation of the excitation spots in the specimen, the volume of the excitation spot is not affected by other focuses. Under this condition, the spatial resolution of a two-photon multifocus microscope can be estimated by using the theory for a typical two-photon excitation microscope with single-focus scanning [Sheppard, 1990; Nakamura, 1993; Gu, 1996]. Fig. 1-10(a) and 1-10(b) show the frequency of a non-zero value in the optical transfer function (OTF) of the two-photon multifocus microscope with and without confocal detection by a pinhole array. For comparison, the OTF of a conventional fluorescence microscope and a single-photon confocal fluorescence microscope are shown in Fig. 1-10(c) and 1-10(d), respectively. In the calculations, it is assumed that the wavelength of light for two-photon excitation is twice longer than that for single-photon excitation (wavelength λ), and the wavelength of fluorescence light is almost half of that of the excitation in two-photon excitation and almost the same in one-photon excitation. From the comparison between Fig. 1-10(a) and (c), it is shown that the lateral resolution is almost the same, but axial resolution is obtained only in two-photon excitation. In a two-photon excitation process, the spatial resolution for the z axis can be obtained without exciting fluorescence dyes positioned out of focus, because the fluorescence emission is localized within a focal volume represented by the square of the PSF [Denk, 1990]. From the comparison between Fig. 1-10(a) and (d), the spatial resolution in the two-photon multifocus microscope is around half of that in a confocal microscope because twice-longer excitation wavelength is used for two-photon excitation. The same as a one-photon excitation microscope, the spatial resolution in a two-photon excitation microscope can be increased by detecting fluorescence through a confocal pinhole. The OTF of the two-photon microscope with confocal detection shows almost the same spatial resolution as that of a single-photon confocal microscope even though twice longer excitation wavelength is used.

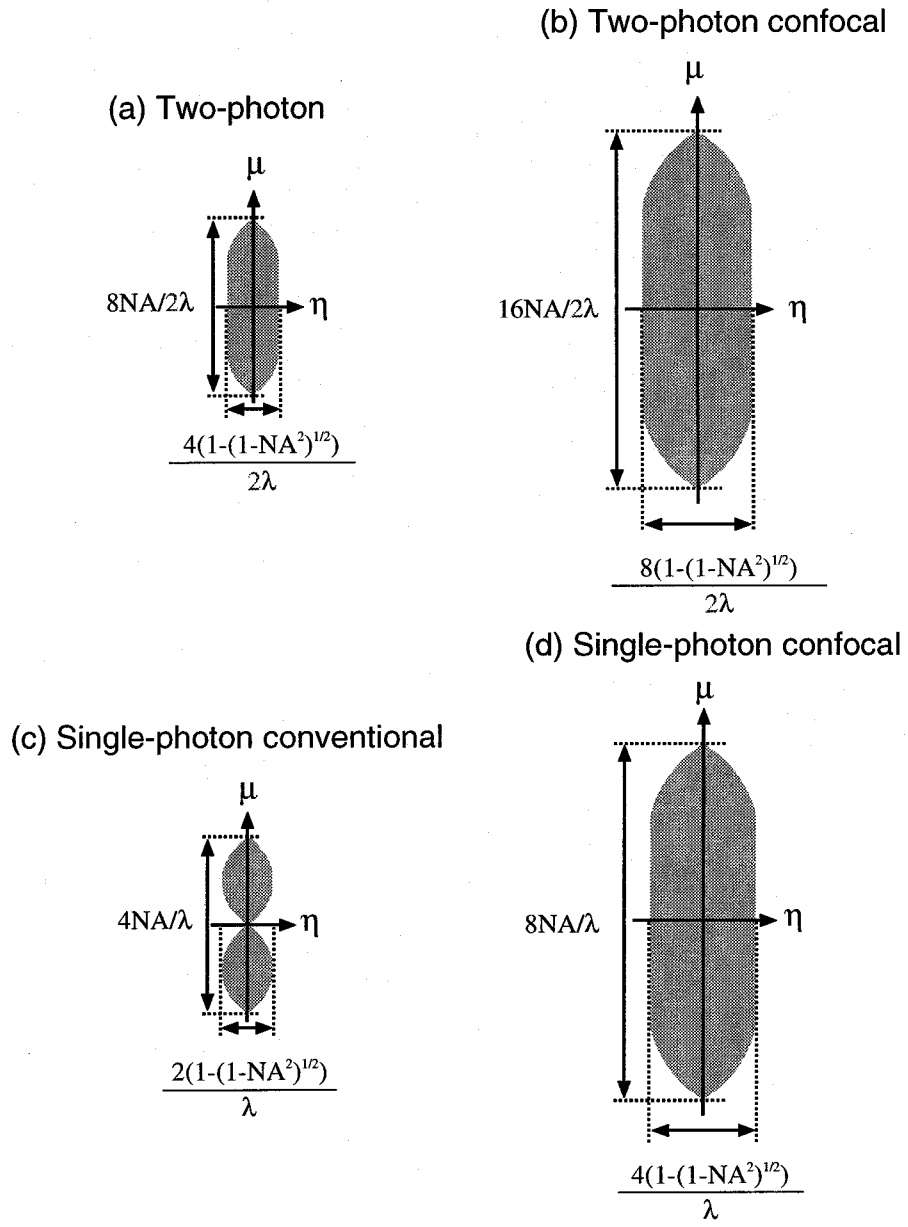

Fig. 1-10 The OTFs of (a) a two-photon fluorescence microscope, (b) a two-photon confocal fluorescence microscope, (c) a conventional fluorescence microscope, and (d) a single-photon confocal fluorescence microscope.

1-4 Fluorescence acquisition efficiency in a multifocus scanning microscope

In the two-photon multifocus microscope, it is important to make sufficient use of a limited light intensity from a laser system because it requires higher excitation intensity for multiple focuses than in a single-focus scanning one, and it is proportional to the number of focuses. For this reason, the fluorescence excitation efficiency must be considered for optimizing the parameters of the system, such as the output power, the repetition rate and pulse width of the laser, and the number of focuses.

1) Fluorescence excitation efficiency in a single focus

It is convenient to consider the amount of fluorescence emitted in a single focus before considering the case with multifocus. The amount of fluorescence emitted from a focus in a specimen can be shown as

$$F(t) \propto C\,\eta\,R(t) \tag{1-9}$$

where C is concentration of fluorescent molecule, η is the quantum yield, and $R(t)$ is the excitation rate of the molecules. The excitation rate of the molecules with a short-pulsed laser can be obtained by considering a simple two-level system of the molecules. Fig. 1-11 shows the model of the two-level system used for estimation. The number of molecules in the excited state and those at ground state can be described with rate equations given as

$$\frac{dn_{ex}}{dt} = n_g(t)\,r_{ex}(t) - \frac{n_{ex}(t)}{\tau_{ex}} \tag{1-10}$$

and

$$\frac{dn_g}{dt} = -n_g(t)\,r_{ex}(t) + \frac{n_{ex}(t)}{\tau_{ex}} \tag{1-11}$$

where n_{ex} is the population of the excited molecules, n_g is the population of molecules in the ground state, r_{ex} is the excitation probability, and τ_{ex} is the lifetime of the excited molecules depending on the relaxation time. The excitation rate of the molecules r_{ex} is given by

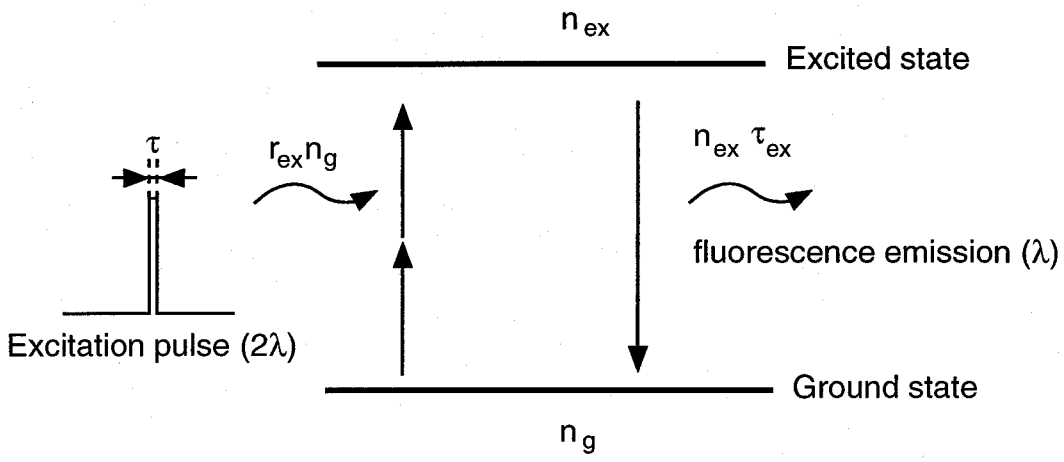

Fig. 1-11 A model of the two-level system used for the calculation of the excitation rate *R(t)*.

considering the photon density at the focus to be given by

$$r_{ex}(t) = \sigma_{2p}\, \Phi^2_{peak}(t) \tag{1-12}$$

where σ_2 is the two-photon absorption cross-section of the molecule and Φ_{peak} is the photon density at the focus given by

$$\Phi_{peak}(t) \simeq \frac{NA^2}{4\hbar c\lambda} \frac{I_{ave}(t)}{f\tau} \tag{1-13}$$

where λ is the wavelength of the excitation light, c is the speed of light in vacuum, NA is the numerical aperture of the objective lens used to focus the light into the sample, I_{ave} is the average power of the incident light, τ and f are the pulse width and the repetition rate of the pulse laser, respectively.

Since the relaxation time from the excited state can be assumed to about 10ns for many fluorescence molecules, τ_{ex} can be omitted from the equations when a pico- or femtosecond laser is used for the excitation. So, Eqs.(1-10) and (1-11) can be simplified as

$$\frac{dn_{ex}}{dt} = n_g(t)\, r_{ex}(t) \tag{1-14}$$

and

$$\frac{dn_g}{dt} = -\, n_g(t)\, r_{ex}(t) \tag{1-15}$$

If we assume a rectangle pulse of the pulse laser and no melecule is at the excited state before the incidence of the pulse, the above equations can be solved by using $n_{ex}(0) = 0$ and $n_{ex} + n_g = 1$, thus giving

$$n_{ex}(t) = 1 - \exp(-r_{ex}\, t) \tag{1-16}$$

and

$$n_g(t) = \exp(-r_{ex}\, t) \tag{1-17}$$

where r_{ex} is a constant coefficient determined by Eq. (1-12) with the peak intensity of the pulse laser. When a laser beam with pulse width τ is focused into the specimen, the excitation rate of the molecules with one pulse can be given from Eq. (1-16) as

$$\langle R \rangle_{pulse} \propto 1 - \exp(-r_{ex}\, \tau) \tag{1-18}$$

From Eq. (1-18), the amount of fluorescence emission within one pulse can be described as

$$\langle F \rangle_{pulse} \propto C\,\eta \left[1 - \exp\left\{ -\sigma_{2p} \left(\frac{NA^2}{4\hbar c\lambda} \frac{I_{ave}}{f\tau} \right)^2 \tau \right\} \right] \tag{1-19}$$

If it can be assumed that the all excited molecules go back to the ground state during the absence of the pulse, we obtain

$$F(t) \propto C\,\eta f t \left[1 - \exp\left\{ -\sigma_{2p} \left(\frac{NA^2}{4\hbar c\lambda} \frac{I_{ave}}{f\tau} \right)^2 \tau \right\} \right] \tag{1-20}$$

Fig. 1-12 shows the excitation rate $\langle R(t) \rangle_{\text{pulse}}$ within one pulse when Rhodamine B is excited by a pulse laser with the wavelength of 800nm, a repetition rate of 80MHz, a pulse width of 100fs, and an NA-1.3 objective lens. The solid line plot in Fig. 1-12 shows the calculated result. From this result, it can be seen that the excitation rate is completely saturated with the excitation intensity at about 20mW. The dotted line is the quadratic curve fitted to the calculation result. From the comparison of the dotted line and the solid line, the excitation rate starts to deviate from the quadratic curve at an excitation intensity of about 5mW. The plot with circles shows the experimentally measured intensity of the fluorescence of Rhodamine B under the same condition as that used for calculation. The experimental result is in good agreement with the calculated result such that the saturation effect of the

fluorescence emission starts at an excitation intensity of around 5mW. From this result and Eq. (1-20) , it can be seen that the repetition rate is one of the important factors to determine the amount of fluorescence emission when the saturation effect of fluorescence emission occurs.

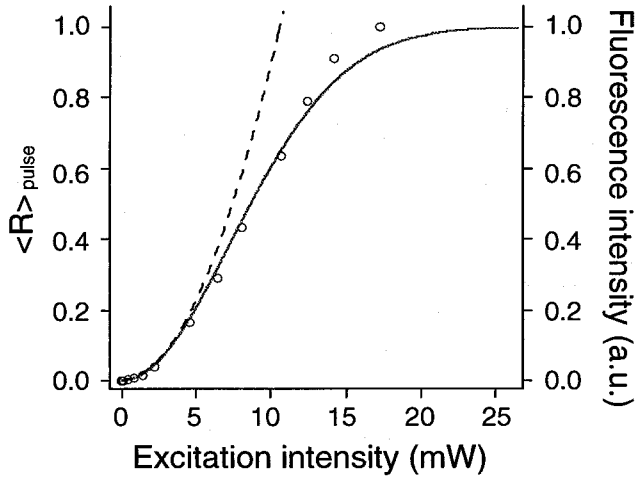

Fig. 1-12 The excitation rate within one pulse calculated for Rhodamine B excitation (solid line). The fluorescence intensity measured in the same condition of the calculation is plotted by circles. The dotted line is the quadratic curve fitted to the calculated result.

2) Fluorescence excitation efficiency in multifocus

In a multifocus fluorescence microscope, a laser beam is divided to a number of focuses. Under this condition, the fluorescence excitation is somewhat different from that with a single focus where the intensity of the excitation laser used can be high enough so as to reach the saturation of the fluorescence emission. When the average power of $I_{total}(t)$ reaches the focal plane of an objective lens, the average intensity of the excitation for each focus $I_{focus}(t)$ is given by,

$$I_{focus}(t) = I_{total}(t) / N \tag{1-21}$$

where N is the number of focuses in use. Substituting Eq. (1-21) into Eq. (1-20), we obtain,

$$F(t) \propto C\,\eta f t N \left[1 - \exp\left\{ -\sigma_{2p} \left(\frac{NA^2}{4\hbar c\lambda} \frac{I_{total}(t)}{f\tau N} \right)^2 \tau \right\} \right] \tag{1-22}$$

From Eq. (1-22), the optimized number of focuses for a laser to be used can be calculated. If we assume that a mode-locked Ti:Sapphire laser with a wavelength of 800nm, a repetition rate of 80MHz, and a pulse width of 100fs is used to induce two-photon excitation in Rhodamine B by a NA-1.3 objective lens, the amount of fluorescence emission at a different number of foci can be calculated as shown in Fig. 1-13. The calculation result shows that the total amount of the fluorescence can be obtained when 12 foci are used for the excitation. When the number of foci is smaller than 12, the amount of the fluorescence is almost proportional to the number of foci. This is because the fluorescence excitation rate is saturated, and the increase in the excitation intensity for each focus does not help to obtain more fluorescence. On the other hand, when the number of foci is lager than 12, the amount of the fluorescence is almost inversely proportional to the square of the number of foci. In this situation, the increase in the number of focuses brings about the lack of excitation intensity at each focus. From this estimation, it can be found that the optimization of the number of the excitation focuses according to the available laser power, specimen, and the objective lens used is important in a multifocus fluorescence microscope.

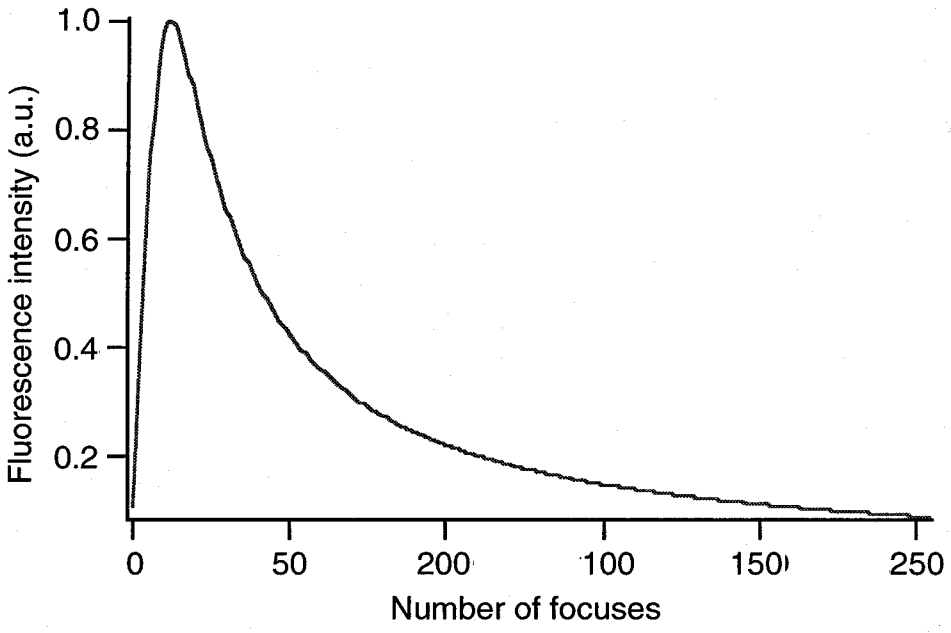

Fig. 1-13 Total intensity of fluorescence induced with a different number of focuses

1-5 Summary

In this chapter, A two-photon multifocus fluorescence microscope using a microlens- and pinhole-array was proposed. The proposed microscope can obtain optical sectioning images by the localization of fluorescence induced by two-photon excitation. With the multifocus excitation used in the microscope, the image acquisition rate can be increased proportionally to the number of focuses. The use of the pinhole array in the multifocus microscope can bring about twice higher spatial resolution as compared to that in a non-confocal system. An arrangement of microlens-array scanner disk which gives uniform scanning and illumination density was presented for the development of the proposed microscope. The calculation of the overlap of the wave front between the focuses revealed that at least 6μm separation between focuses is required in order to achieve the ideal spatial resolution of the microscope when 800nm-wavelength excitation light is focused with an NA-1.0 objective lens. It was also shown that the amount of the fluorescence obtained in multifocus excitation is strongly affected by the saturation of the fluorescence excitation rate. From this effect, in a multifocus fluorescence microscope, the number of the excitation focuses should be optimized according to the experimental conditions, such as the available laser power, the specimen, and the objective lens used.

Chapter 2.

Development of a two-photon multifocus fluorescence microscope.

In this chapter, the techniques for the development of a two-photon multifocus fluorescence microscope are described. Fluorescence images obtained by the developed microscopes show the imaging properties of the proposed microscope. In the obtained images, the enhancement of spatial resolution and image contrast was confirmed. A longer penetration depth was obtained in a confocal setup than that in a non-confocal setup, which is different from the results in a typical two-photon single-focus microscope.

2-1 Optical setup

Fig. 2-1(a) shows an optical setup of the developed two-photon multifocus fluorescence microscope. A laser beam is incident onto a microlens-array disk and produces several tens of focuses at the focal plane where a pinhole-array disk is placed. The two disks were precisely aligned so that each microlens focuses the light into a corresponding pinhole on the disk. The transmission light through the pinhole-array disk was introduced into a conventional fluorescence microscope(Olympus, BX50WI). Since the pinhole-array disk is placed on the imaging plane of the microscope, the pinholes were imaged into a specimen by an objective lens as multiple excitation spots. Fluorescence excited at each excitation spot using the two-photon process was collected by the same objective lens and directed into a intensified CCD camera (Hamamatsu, C24000-35) by a dichroic mirror placed between the two disks. With 1800rpm rotation speed of the disks, 3ms image scanning time was achieved. The developed microscope can also be used as a non-confocal two-photon multifocus microscope by replacing the mirror between the objective lens and the relay lens with a dichroic mirror which reflects NIR light (excitation) and transmits visible light(fluorescence) as shown in Fig. 2-1(b). A photograph of the developed microscope is shown in Fig. 2-2

The microlens- and pinhole-array scanner disk was developed with microlenses and

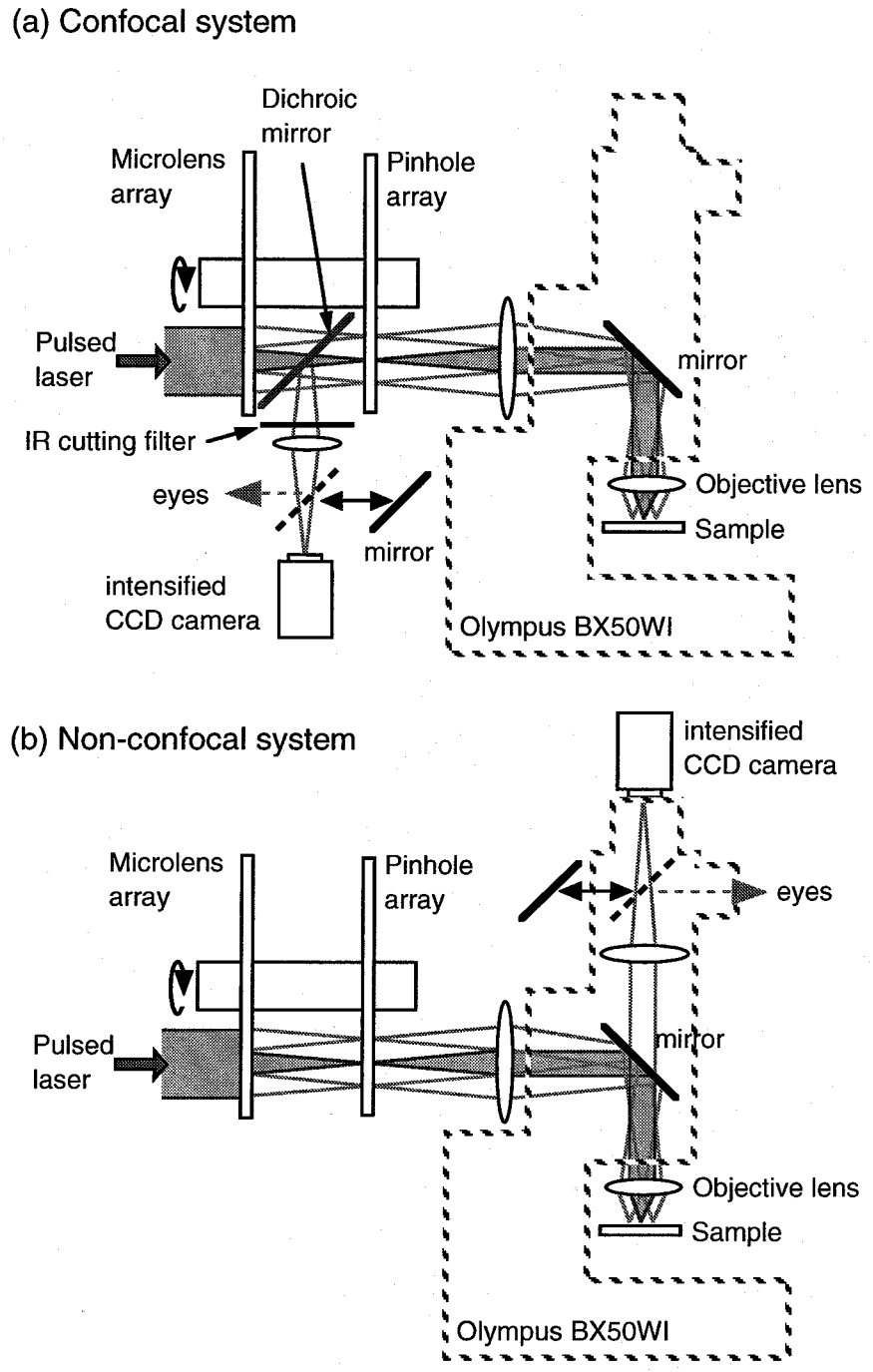

Fig. 2-1 Optical setups of two-photon multifocus fluorescence microscope with (a) confocal detection and (b) without it.

pinholes whose diameters were 250μm and 50μm, respectively. The diameter of the pinhole was determined according to the size of diffraction limited focal spot of fluorescence from the objective. A NA of the microlenses used was 0.0125. Around 20,000 microlenses and pinholes were set on the disks. These disks were made of synthetic silica glass using an etching process. Chromic metal was coated on the glass for the pinhole-array disk.

With the optical setup shown in Fig. 2-1, several specimens were observed to examine the imaging properties of the developed microscope. In the following experiments, a mode-locked Ti:Sapphire laser (Tsunami, SpectraPhysics, pulse width = 80fs, repetition rate = 82MHz) was used as a light source. Fig. 2-3 shows excitation spots generated in a solution of Rhodamine 6G without the rotation of the scanning disks. An oil immersion objective lens whose NA is 1.3 was used for exciting the sample. The separation of each focuses was set at 6μm, which gives adequate spatial resolution according to the calculation performed in Section 1-3 of the previous chapter.

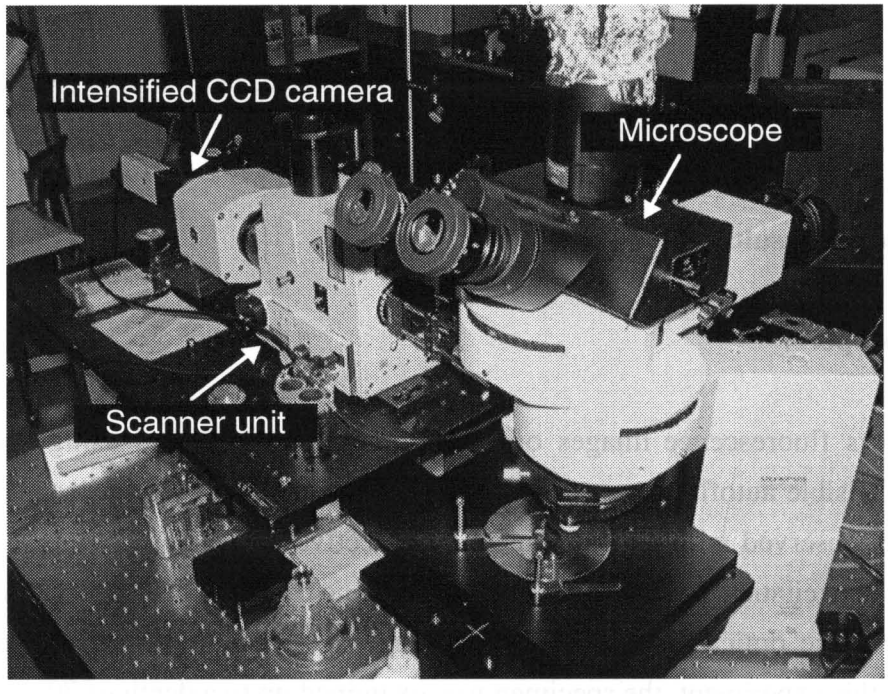

Fig. 2-2 The developed two-photon multifocus fluorescence microscope

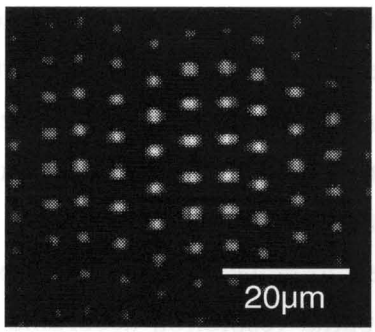

Fig. 2-3 Two-photon excited spots in a solution of Rhodamine 6G. The separation of the spot is 6μm.

2-2 Experimental results

1) Imaging property

Fig. 2-4 shows fluorescence images of convallaria radix obtained using the developed microscope. Visible autofluorescence induced by multiphoton excitation was imaged. The specimen was observed with an oil immersion objective lens whose NA is 1.3. The total intensity for the excitation was 150mW at the focal plane of the objective lens. Each image in Fig. 2-4 shows the optical x-y cross-section image at a depth z from the surface of the specimen. In this experiment, the specimen was examined up to a depth of 70μm. The three-dimensional distribution of particle-like structures in the cell wall is clearly observed. Fig. 2-5 shows the three-dimensional structure of the specimen rendered from the image series in

Fig. 2-4. The boundary of the structure was given at 70% of the normalized fluorescence intensity in the images.

The same specimen was also observed with the non-confocal system as shown in Fig. 2-6. The condition for the observation, such as the excitation intensity and the objective lens used, was the same as that in Fig. 2-4. For the comparison between the imaging properties in the confocal and the non-confocal system, the images obtained at the same depth of the specimen by both systems are shown in Fig. 2-7. Fig. 2-7(a) shows confocal images, and Fig. 2-7(b) shows non-confocal images. From the comparison between Fig. 2-7(a) and 2-7(b), the images obtained with the non-confocal system are more blurred than those with the confocal system, and this blurring phenomenon increases with observation depth. This is caused by fluorescence scattered in the specimen or fluorescence emission by reabsorption of fluorescence. Because the microscope uses the two-dimensional detector array of the CCD camera for image acquisition, scattered or reemitted fluorescence at the out-of-focus region can be imaged as background noise with the non-confocal system. As seen in Fig. 2-7, this effect is more prominent at deeper parts in the specimen. On the other hand, in the confocal images, the scattered or reemitted fluorescence are prevented from being imaged by the pinhole array. This difference of imaging property between the two systems is more obvious in x-z cross-section images shown in Fig. 2-8. From above comparisons, it can be concluded that a longer penetration depth can be obtained in the confocal system than in the non-confocal system.

This result is quite different from results using a single-focus scanning two-photon microscope. In a typical two-photon microscope, a confocal pinhole is not used to observe a deep part of a specimen because the scattered fluorescence does not affect the reconstruction of fluorescence images in a single-scanning case. Scattering of fluorescence might decrease the detectable fluorescence, but it does not give background noise. For this reason, in the single-scanning system, it is reasonable for observing a deep part of a specimen to detect as much fluorescence as possible without the pinhole. However, as shown in the experiments above, it was found that this cannot be applied for the multifocus system where a two-dimensional detector array is used to image a specimen.

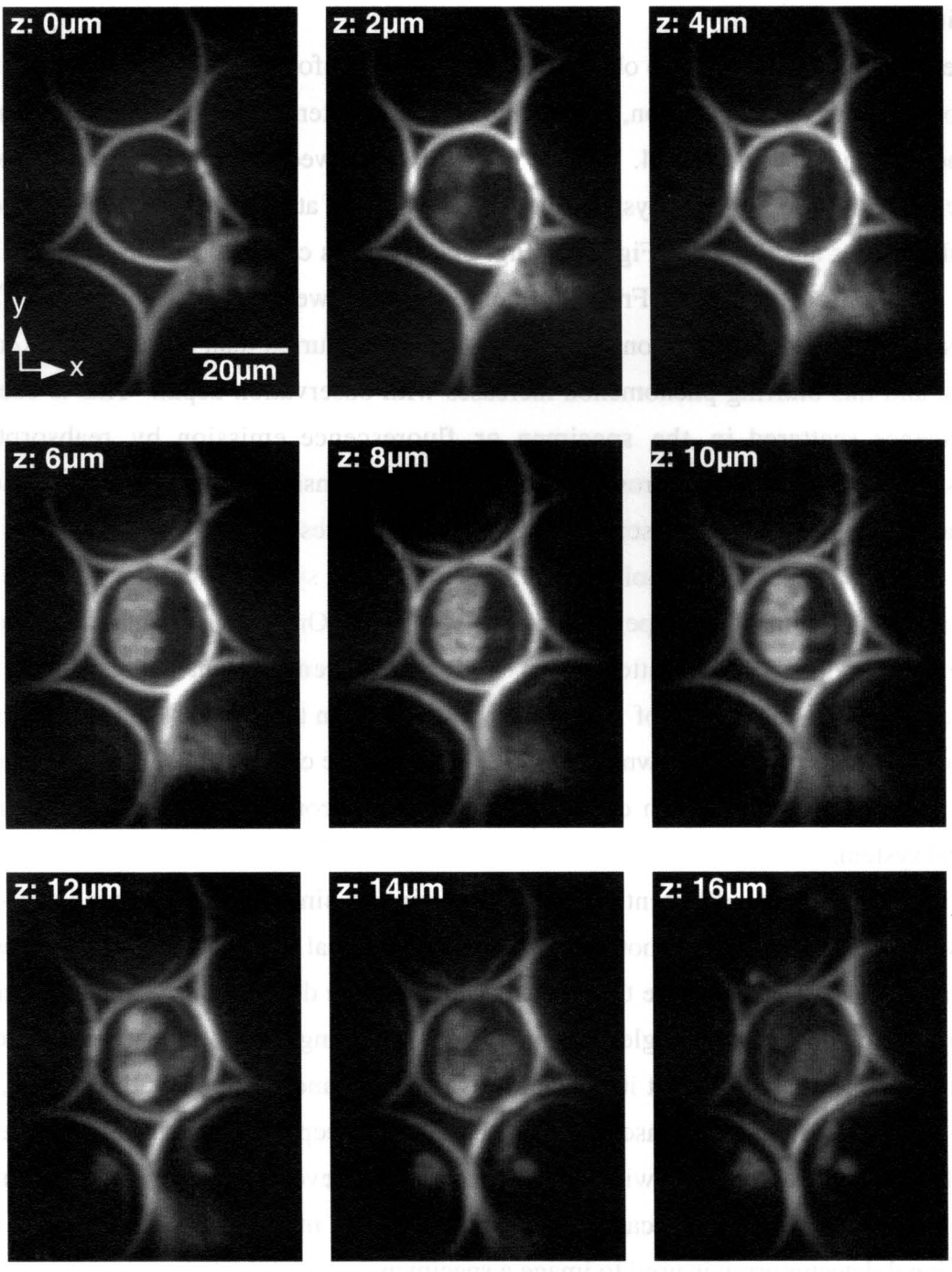

Fig. 2-4 Confocal fluorescence images of convallaria radix obtained by the developed microscope. Each image was taken at depth of every 1μm.

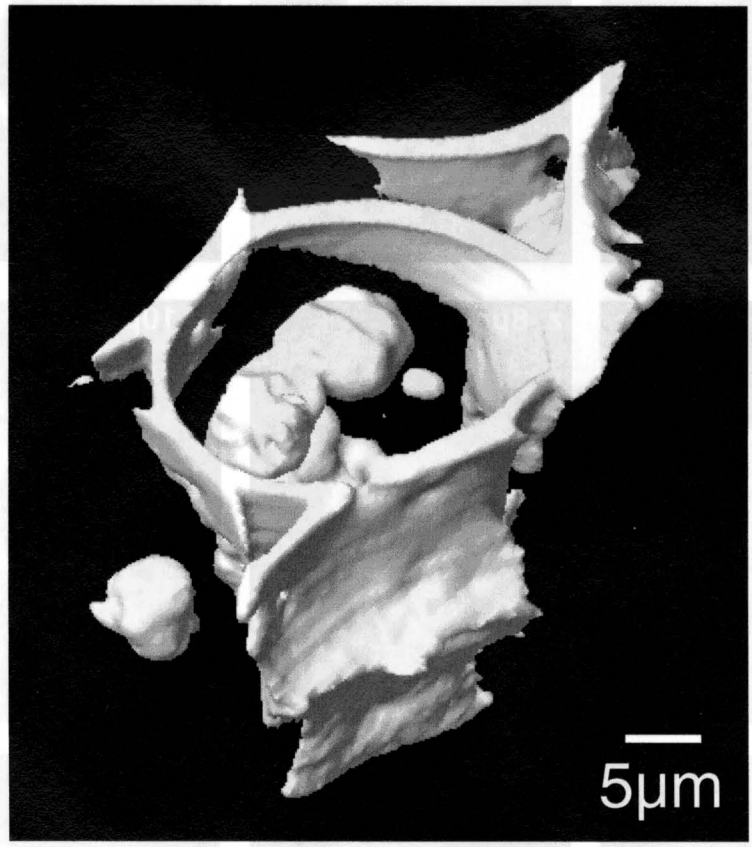

Fig. 2-5 The three-dimensional structure of convallaria radix rendered from the image series in Fig. 2-4.

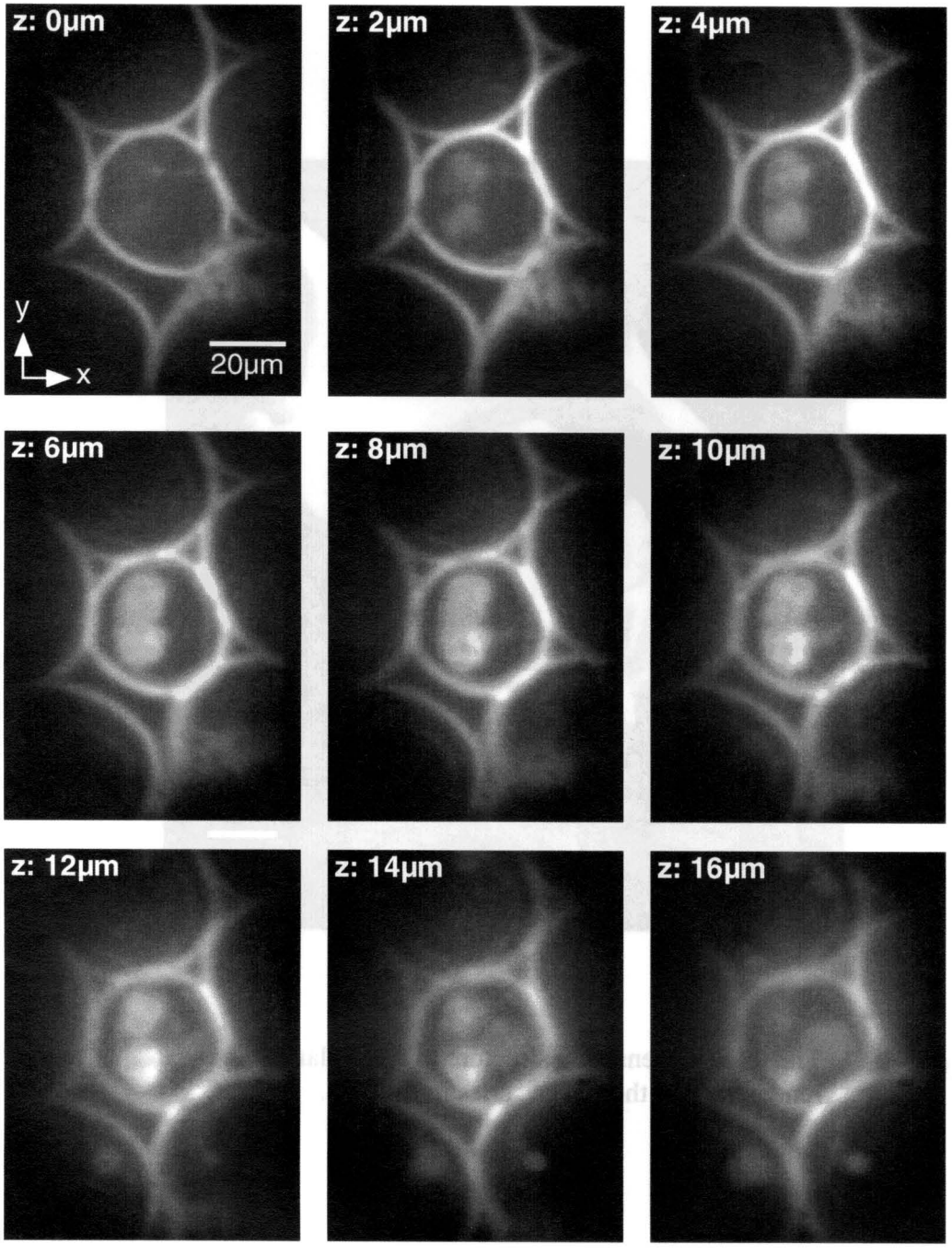

Fig. 2-6 Non-confocal fluorescence images of convallaria radix obtained by the developed microscope. The same position of the specimen as Fig. 2-4 was observed.

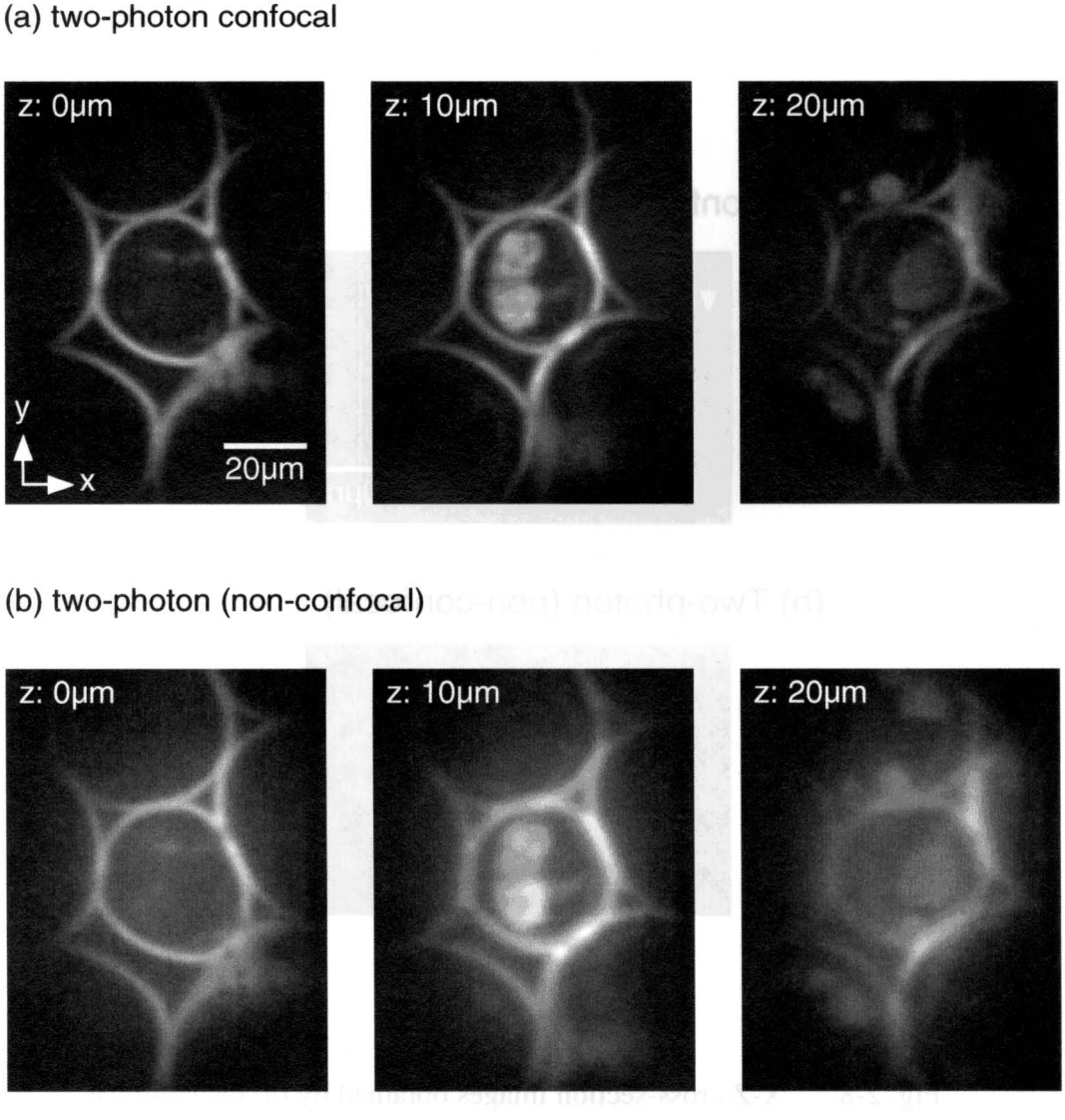

Fig. 2-7 Comparisons of the images obtained by the confocal system and the non-confocal system.

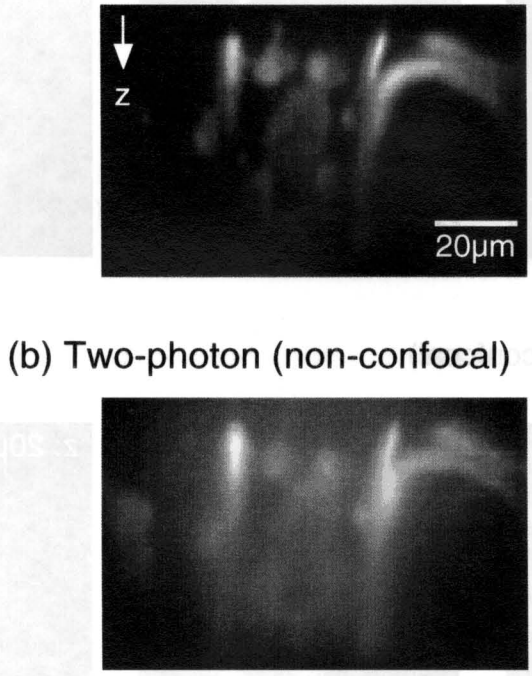

Fig. 2-8 X-Z cross-section images obtained by (a) the confocal system and (b) the non-confocal system

2) Axial resolution

For the comparison of the axial resolution in the two systems, their axial responses were obtained. Fluorescence particles with a diameter of 1μm were used as a sample. The particles were spread and fixed on a slide glass so that the particles did not create multiple layers. The fixed particles were covered by a cover slip with immersion oil. The sample was scanned along the axial direction through the foci while measuring the intensity of the fluorescence from the sample. A piezo-electric scanning stage (MellesGriot, Nanoblock) was used for scanning the sample, and a photomultipler tube (Hamamatsu, H5784) was used for measuring the intensity of the fluorescence. An oil immersion objective with an NA of 1.3 was used for this experiment.

Fig. 2-9 shows the axial responses obtained in the experiment. The solid line and the dotted line in the figure show the confocal response and the non-confocal response, respectively. A comparison of these responses show an increase in the axial resolution in the confocal detection system. Since the size of the particle was not small enough as compared to the size of the focuses with the used objective lens, the responses do not show the actual resolution limit of those system. However, the increase in the axial resolution in the confocal system can be clearly seen from the slope of the responses.

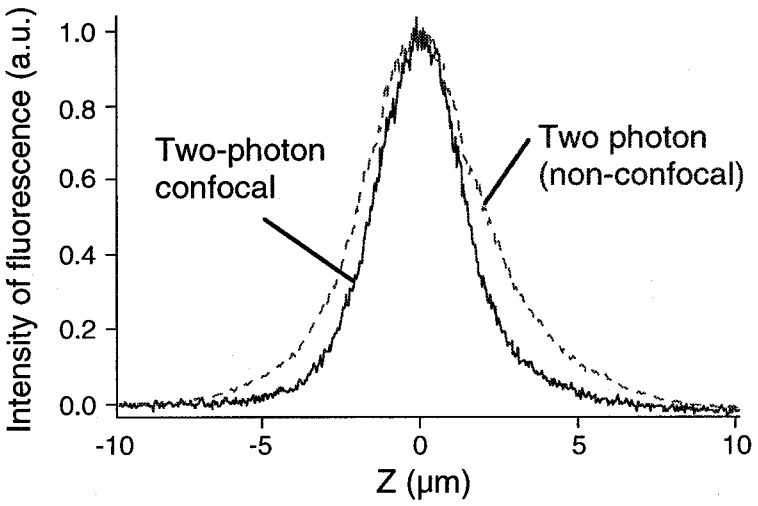

Fig. 2-9 Axial responses of the confocal system and the non-confocal system obtained with fluorescent beads of which diameter was 1μm.

2-3 Summary

In this chapter, the techniques for the development of a two-photon multifocus fluorescence microscope were presented. In the experimental results from the observation of convallaria radix, the observation depth of 70μm was achieved. The comparisons between the optical system with and without the pinhole array revealed that both the spatial resolution and the contrast of the images were highly enhanced with the confocal system. It was also shown that those advantages appear more prominently in the observation of deeper parts of the specimen. In the experiments, it was also found that the penetration depth with the confocal system was longer than that with the non-confocal system, which is completely different from what people have obtained in experiments with a single-scanning two-photon microscope.

Chapter 3.

Intracellular Ca^{2+} imaging with a two-photon multifocus fluorescence microscope

In this chapter, techniques for Ca^{2+} imaging in rat heart cells with a two-photon multifocus microscope developed in the previous chapter are shown. Ca^{2+} imaging in biological specimens is one of the important applications of real-time imaging microscopes, where the dynamics of ion concentration is vital in the investigation of the mechanisms occuring in living bodies.

In the first section of this chapter, the role of Ca^{2+} in heart muscle cells is discussed, which is necessary to understand the experimental results in the following section. The second section shows fluorescent Ca^{2+} indicators used in the experiments. The practical techniques for imaging the Ca^{2+} concentration in both cultured rat-heart cells and those in a rat whole-heart are mentioned in the third section.

3-1 Role of Ca^{2+} in heart muscle cells

The most important function of the heart in a living body is in providing blood for the body. This function is regulated by controlling the concentrations of several ions inside and outside the heart muscle cells. Ca^{2+} plays important roles in heart muscle cells, such as inducing muscle constriction, and is a second messenger between ion channels in the cell membranes and ion storage in the cells [Alberts, 1990].

1) Muscle constriction with Ca^{2+}

Fig. 3-1 shows the main contents of muscle cells in a human heart. The heart muscle cells consist of actin filament, myosin filament, sarcoplasmic reticulum (SR), cell membrane including channels for several ions, and a nucleus [Alberts, 1998]. Muscle constriction is

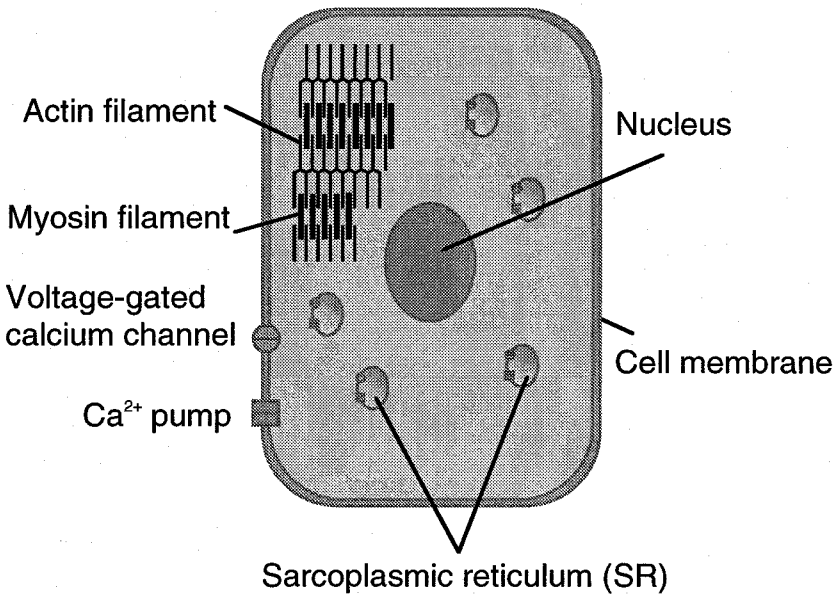

Fig. 3-1 Contents of muscle cells of a human heart.

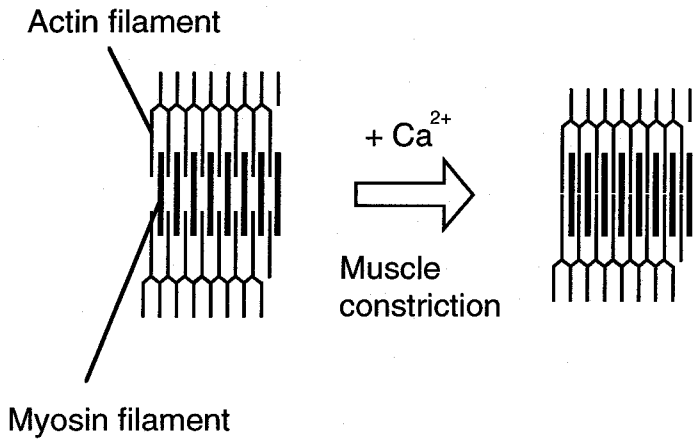

Fig. 3-2 The arrangement of actin and myosin filaments with and without Ca^{2+}

induced directly by the movement of the actin and myosin filaments with the existence of Ca^{2+}, and the mechanism is the same in all muscle cells in other parts of the body, such as skeletal and smooth muscles [Alberts, 1990]. Fig. 3-2 shows the movement of actin and myosin filaments to induce the muscle constriction. Basically, actin and myosin filaments are convinative with each other. However, without Ca^{2+}, the connective part in actin filament is covered by tropomyosin. Tropomyosin is stably conjugated to actin filament with a complex of three kinds of polypeptides which are toroponin-T (Tropomyosin-binding activity), -I (Inhibitory activity), and -C (Calcium-binding activity). With the existence of Ca^{2+}, troponin-T receives Ca^{2+} and removes troponin-I. This induces conformation change of tropomyosin and surfaces the portion on the actin filament supposed to be connected to the myosin filament. When the myosin filament conjugates to the actin filament, the conformation of the actin filament changes, thus, the movement of the filaments is induced.

2) Increase of Ca^{2+} concentration

The constriction of all heart muscles is controlled to provide blood for the body [Brown, 1997]. In other words, the concentration of Ca^{2+} must be controlled to give the rhythm of "heartbeat". A signal which gives the rhythm is produced by the sinoatrial (SA) node. The SA node is positioned at near the joint of the vena cava and the right atrium as shown in Fig. 3-4. The signal from the SA node propagates from cell to cell through the membranes. The signal itself on the membrane is formed as the difference of ion concentration between the inside and outside of the cells, and this is known as membrane potential. As shown in Fig. 3-4, the membrane potential propagates through the right and the left atrium following many different paths while inducing the constriction of the muscles, and gatheres at the atrioventricular (AV) node. At the AV node, the signal starts propagating to the right and the left ventricle after a certain delay. This delay works to create the rhythm of the heartbeat which enables the heart to permeate blood through the body properly. It is already known what kind of signal is generated in the SA node. However, the mechanism of the delay in the signal at the AV node is not yet understood.

The concentration of Ca^{2+} in the cells increases with the propagation of the membrane potential. Basically, without the signal, the concentration of Ca^{2+} out of the cells is about 10,000 times higher than that in the cells. At the arrival of the signal of the membrane

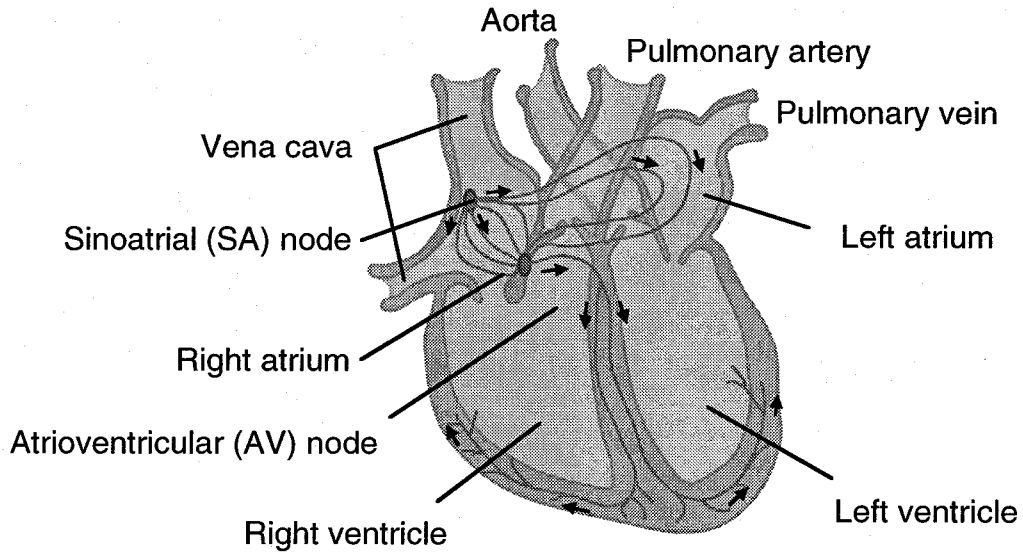

Fig. 3-3 Propagation of membrane potential in a human heart

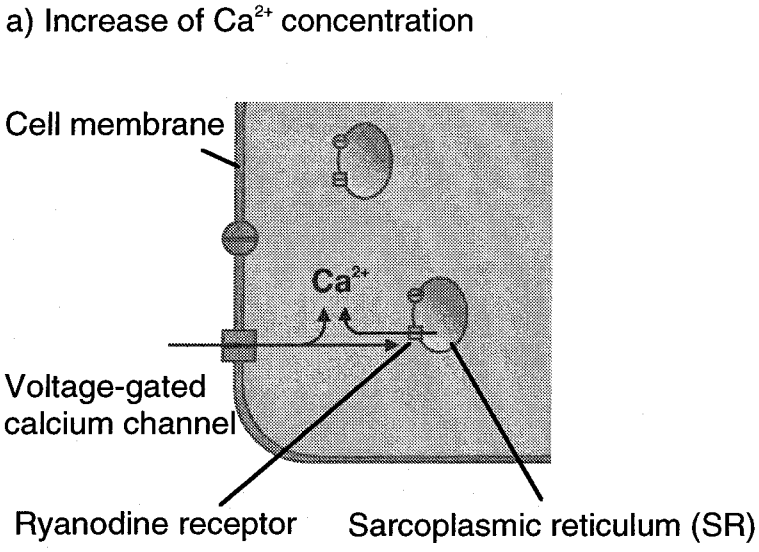

Fig. 3-4 Increase and decrease of Ca^{2+} concentration in a heart muscle cell

potential, ion channels in the membrane are opened and ion exchange is started between the inside and outside of the cells as shown in Fig. 3-4(a). At this moment, highly concentrated Ca^{2+} is allowed to flow into the cells to induce muscle constriction.

When Ca^{2+} enters the cells, it also works to bring further increase in its concentration. In the muscle cells, Ca^{2+} is a second messenger for ryanodine receptors of SR. When the receptors are conscious of Ca^{2+}, SR releases Ca^{2+} stored in it [Iino, 1998]. This amplification of Ca^{2+} concentration in muscle cells is called "Ca^{2+}-induced Ca^{2+} release (CICR)" and is known as a mechanism which brings about the propagation of Ca^{2+} concentration in the cells. A schematic diagram of CICR is shown in Fig. 3-5. After a certain period, the concentration of Ca^{2+} is decreased by the Ca^{2+} pump in the SR and the cell membrane as shown in Fig. 3-4(b).

3) Ca^{2+} transient and Ca^{2+} wave

The concentration of Ca^{2+} in muscle cells increases rapidly with the signal from the SA node. This sudden increase of Ca^{2+} concentration is called "Ca^{2+} transient". As mentioned above, this phenomenon is brought about by both Ca^{2+} inflow through ion channels in the cell membrane and CICR. In the case of cultured heart muscle cells, there is no SA node with them. However, a Ca^{2+} transient can be generated because of automaticity which creates the change of the membrane potential even when the cell is isolated [Brown, 1997].

In addition to this phenomenon, it can also be seen that Ca^{2+} concentration increases at a small point in a cell without the signal from the SA node as it propagates within the cell. This is called "Ca^{2+} wave". It is usually said that this might be due to the unexpected release of Ca^{2+} from SR in abnormal cells which are damaged or in unnatural condition. As shown in Fig. 3-4, CICR can propagate Ca^{2+} if Ca^{2+} is generated somewhere in the cell. However, the mechanism of this phenomenon is not known yet and is still under investigation. The Ca^{2+} wave can also induce muscle constriction as same as Ca^{2+} transient. The muscle constriction by Ca^{2+} wave possibly gives abnormal heartbeat which is aberrated from the signal generated in the SA node. Therefore, the Ca^{2+} wave is sometimes assigned as the cause of arrhythmia [Hama, 1998].

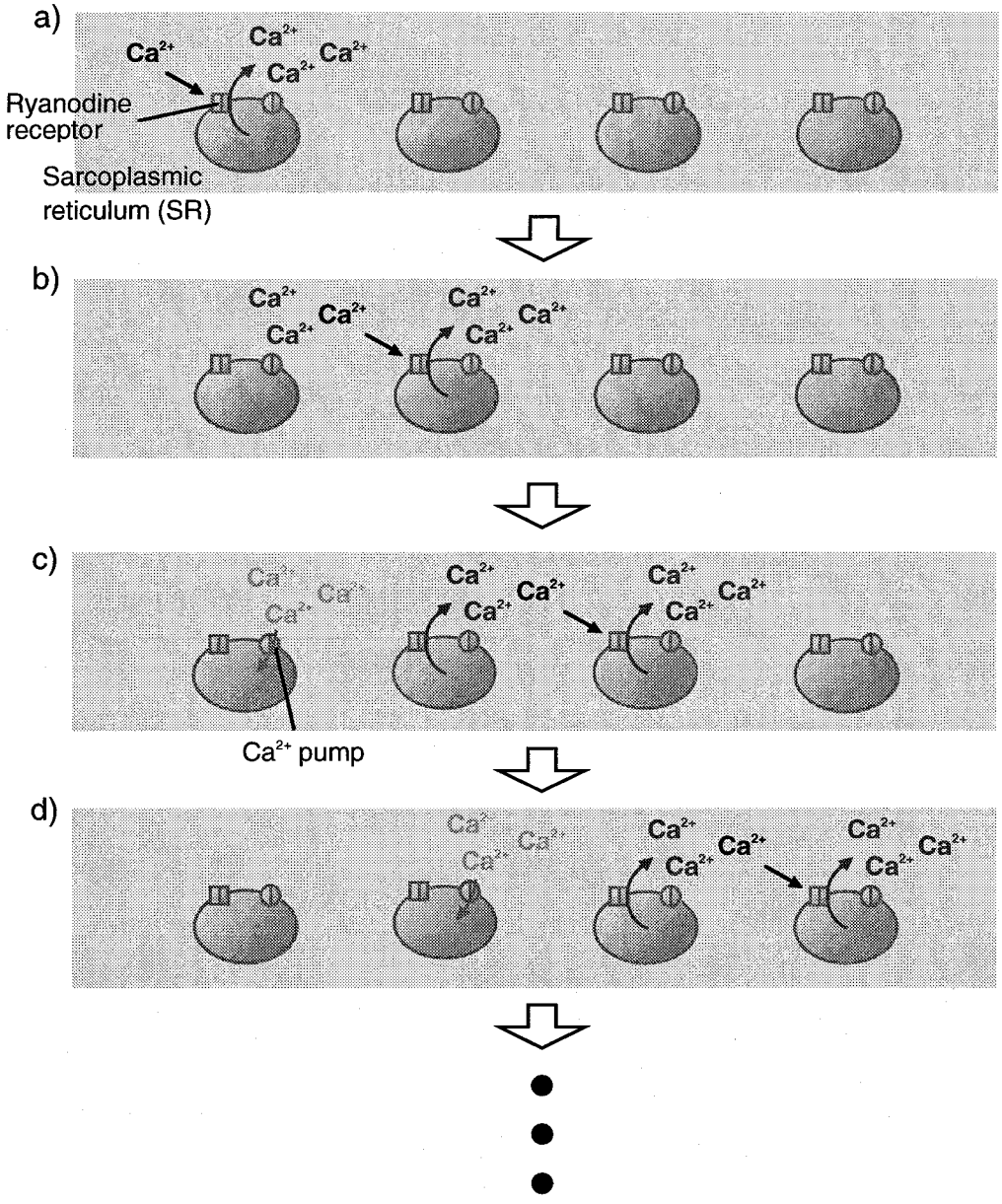

Fig. 3-5 Propagation of Ca^{2+} concentration by Ca^{2+}-induced Ca^{2+} release (CICR)

3-2 Fluorescent Ca^{2+} indicator

1) Fluorescent ion indicators

The development of fluorescent molecules which have a sensitivity to ions enable one to use fluorescence microscopes to measure ion concentration in various biological specimens. These fluorescent molecules are originated in chelating agents which coordinate particular metal ions to make the complex with an increase in fluorescence intensity.

2) Introducing fluorescent indicators into biological cells

Fluorescent indicators do not penetrate readily into cells because of their low fat-solubility [Takesako, 1998]. In a usual case, these fluorescent indicators are loaded into biological cells in the form of acetoxymethyl (AM) ester. Fig. 3-6(a) and 3-6(b) show the molecular structure of Fluo-3 and a AM ester of Fluo-3 (Fluo-3AM) [Haugland, 1996]. The carboxyl group of Fluo-3 is esterified in the Fluo-3AM structure. This esterification increases the fat-solubility of the molecule and its permeability through cell membranes. However, the AM ester cannot form the complex with Ca^{2+} which is required in order to indicate Ca^{2+} concentration, because the coordination of Ca^{2+} is inhibited by the esterification of the carboxyl group.

After Fluo-3AM is loaded into the cells, it is easily hydrolyzed by intracellular esterase. Here, the AM group is released from the molecule so that the molecule forms the complex with Ca^{2+}. The molecular structure becomes the same as that of Fluo-3 after hydrolyzation. In the form of Fluo-3, the molecular permeability through cell membranes becomes low. For this reason, Fluo-3 molecules remain in the cells after hydrolyzation, and the concentration of the molecule in the cells can be kept constant during observation by a fluorescence microscope.

3) Two-photon excitation of Ca^{2+} indicator

Fig. 3-7 shows measured fluorescence intensity from CalciumGreen-1, Fluo-3, and Fluo-4 (all from Molecular Probes), which are suitable Ca^{2+} indicators for observing Ca^{2+} concentration in rat muscle cells. The fluorescence was induced by two-photon excitation

(a) Fluo-3

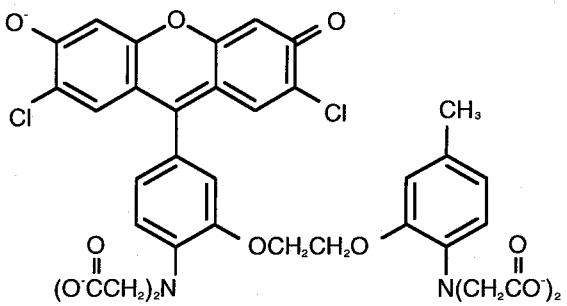

(b) Fluo-3AM

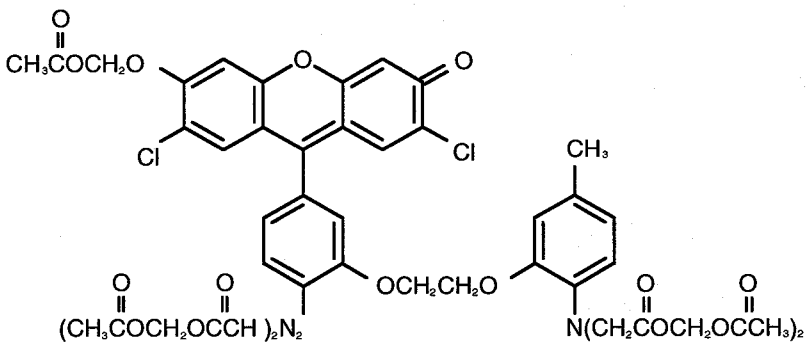

Fig. 3-6 The molecular structure of (a) Fluo-3 and (b) Fluo-3AM.

with an NA-1.3 objective lens (Olympus) and excitation light from a mode-locked Ti:Sapphire laser (Spectra Physics, wavelength = 800nm, pulse width = 80fs, repetition rate = 82MHz). Quadratic dependence of the fluorescence intensity to the excitation intensity in Fig. 3-7 shows that the fluorescence was induced by two-photon excitation. Comparisons between each plot in Fig. 3-7 shows that Fluo-4 gives the highest fluorescence-acquisition efficiency in these indicators.

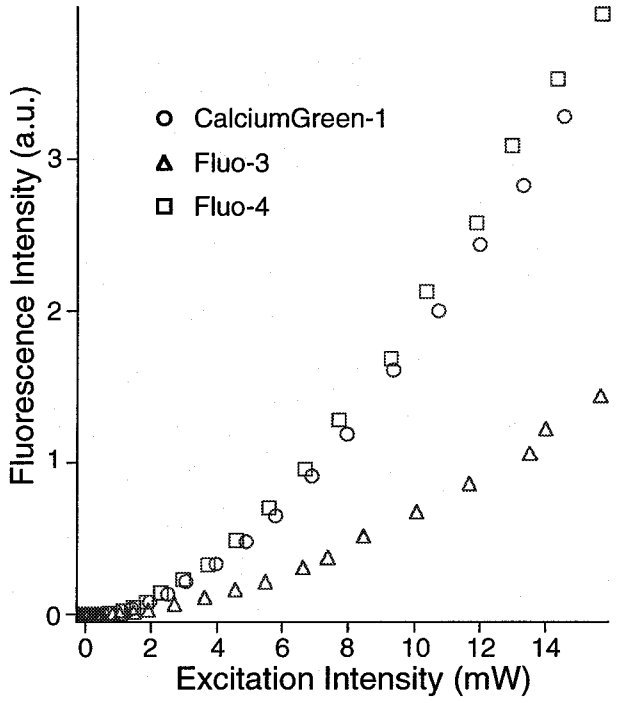

Fig. 3-7 Comparision of fluorescence intensity from CalciumGreen-1, Fluo-3, and Fluo-4. The fluorescence was induced by two-photon excitation in a solution containing a Ca^{2+} indicator (1 mM), $CaCl_2$ (10mM), and HEPES (buffer pH 7.4, 10mM).

3-3 Experiments of two-photon Ca^{2+} imaging

1) Two-photon Ca^{2+} imaging in cultured rat heart cells

In this experiment, the distribution of Ca^{2+} concentration in cultured rat heart cells was observed with the developed two-photon multifocus fluorescence microscope. A mode-locked Ti:Sapphire laser (Tsunami, SpectraPhysics, wavelength = 800nm, repetition rate = 82MHz, average output = 900mW) was used as an excitation light source. A water-immersion objective lens (Olympus, NA = 0.8) was used for excitation and observation of a specimen. Fluo-3AM (Molecular Probes) was used as a fluorescent Ca^{2+} indicator. A frame grabber (AG-6, Scion Corporation, image acquisition time = 33ms) was used to store the image series of the specimen into a computer (Power Macintosh 4400, Apple Computer).

Before the observation, the cultured cells were immersed in a Tyrode solution which contained $CaCl_2$ (1mM), HEPES (buffer, pH = 7.4, 10mM), KCl (4mM), $MgCl_2$ (1mM) and Fluo-3AM (0.018mM) for loading Fluo-3AM into the cells. The Tyrode solution contains ions which are included in the blood of rats, and helps a specimen to survive during fluorescence loading and observation. After 30minutes of loading, the Tyrode solution was removed, and the specimen was rinsed with the Tyrode solution which did not contain Fluo-3AM. During the observation, the cells were immersed in the Tyrode solution without Fluo-3AM.

Fig. 3-8 shows obtained fluorescence image of the distribution of Ca^{2+} concentration in the cultured rat-heart cell. The total excitation power at the focal plane of the objective lens was 152mW. Each image was obtained sequentially with a time resolution of about 33ms. Brighter parts in the images show higher Ca^{2+} concentration in the cell. In Fig. 3-8, a Ca^{2+} wave can be seen as the movement of higher Ca^{2+} concentration from the lower-right edge of the specimen to the upper-left. Fig. 3-9 shows two-photon fluorescence images from the same part of the specimen at different times. In this figure, one can see Ca^{2+} transient with the sudden increase of the Ca^{2+} concentration within the entire cell except the nucleus.

Two different cells which showed different Ca^{2+} dynamics were compared by measuring the decay time of Ca^{2+} concentration after the Ca^{2+} transient. The cell in Fig. 3-9 (Cell-A) was

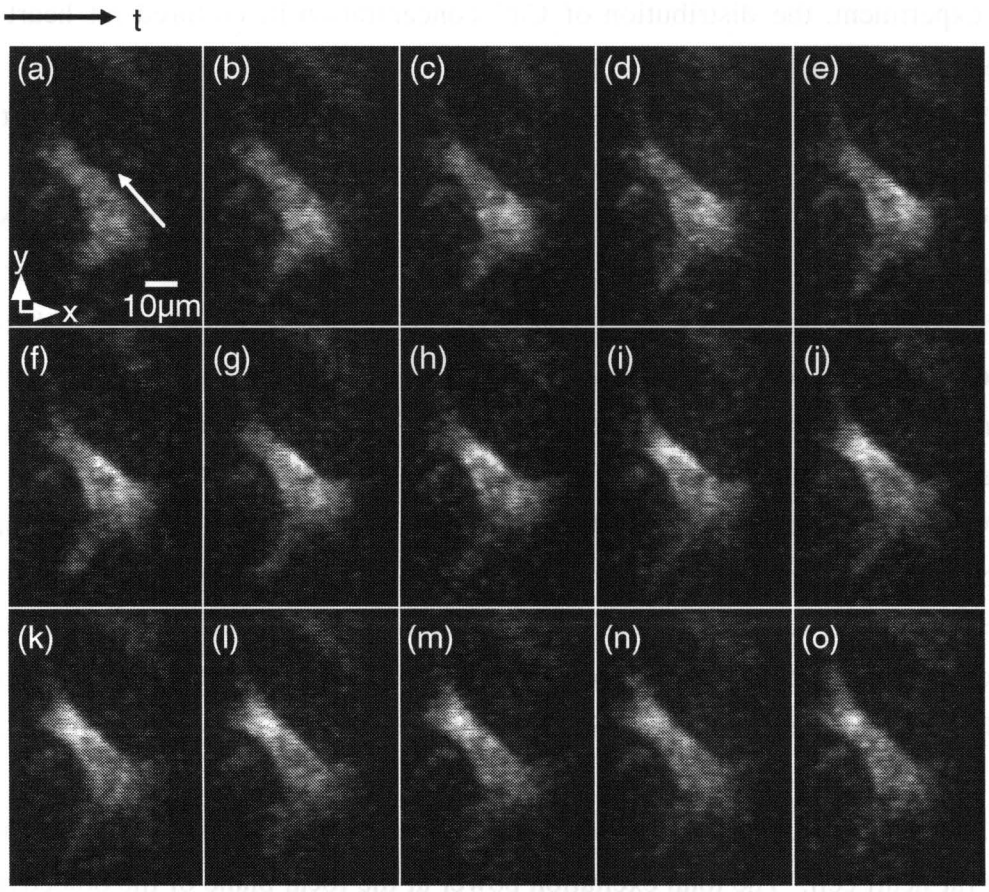

Fig. 3-8 Two-photon fluorescence image of the distribution of Ca^{2+} concentration in the cultured rat-heart cell. Time resolution for each image was about 33ms. Ca^{2+} wave was imaged in this experiment.

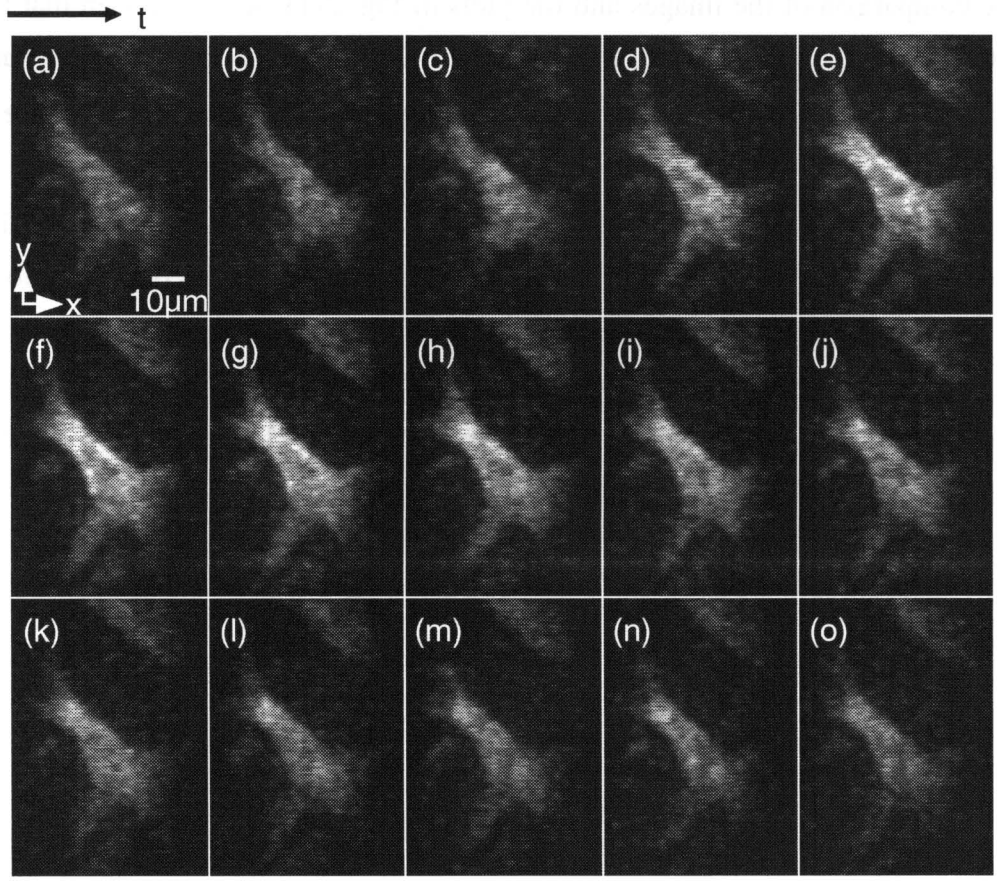

Fig. 3-9 Two-photon fluorescence image of the distribution of Ca^{2+} concentration in the cultured rat-heart cell. Time resolution for each image was about 33ms. Ca^{2+} transient was imaged in this experiment.

compared to another one shown in Fig. 3-10 (Cell-B). The images in Fig. 3-10 show a Ca^{2+} transient in Cell-B. Fig. 3-11 shows the comparison between both cells. Fig. 3-11(a) and 3-11(b) show an x-y and an x-t image of Cell-A, respectively, and Fig. 3-11(d) and 3-11(e) show those in Cell-B. X axis in Fig. 3-11(b) and 3-11(e) shows the lines indicated as A-C in Fig. 3-11(a) and D-F in Fig. 3-11(d), respectively. The variations in fluorescence at the point B in Fig. 3-11(a) and E in Fig. 3-11(d) are shown in Fig . 3-11(c) and 3-11(f), respectively. From the comparison of the images and the plots in Fig. 3-11, it can be seen that the decay time of Ca^{2+} concentration is shorter in Cell-A. In Cell-A, the decay time is measured to be about 400ms, while that in Cell-B is about 800ms. The slower decay time of Ca^{2+} concentration shows lower functionality of Ca^{2+} pump in SR or the cell membrane. Another difference can also be seen at the nuclei of the cells. In Cell-A, the Ca^{2+} concentration at the nucleus (at the center of the cell) does not increase at all in Fig. 3-8 and Fig. 3-9. However, in Cell-B, the Ca^{2+} concentration in the nucleus can be seen in the nucleus, and it is even stronger there than in the other parts of the cell. The increase of Ca^{2+} concentration in nuclei is often observed when cells are under apoptosis [Brown, 1997]. From above comparison, it is concluded that Cell-B was in a physiologically worse condition than Cell-A.

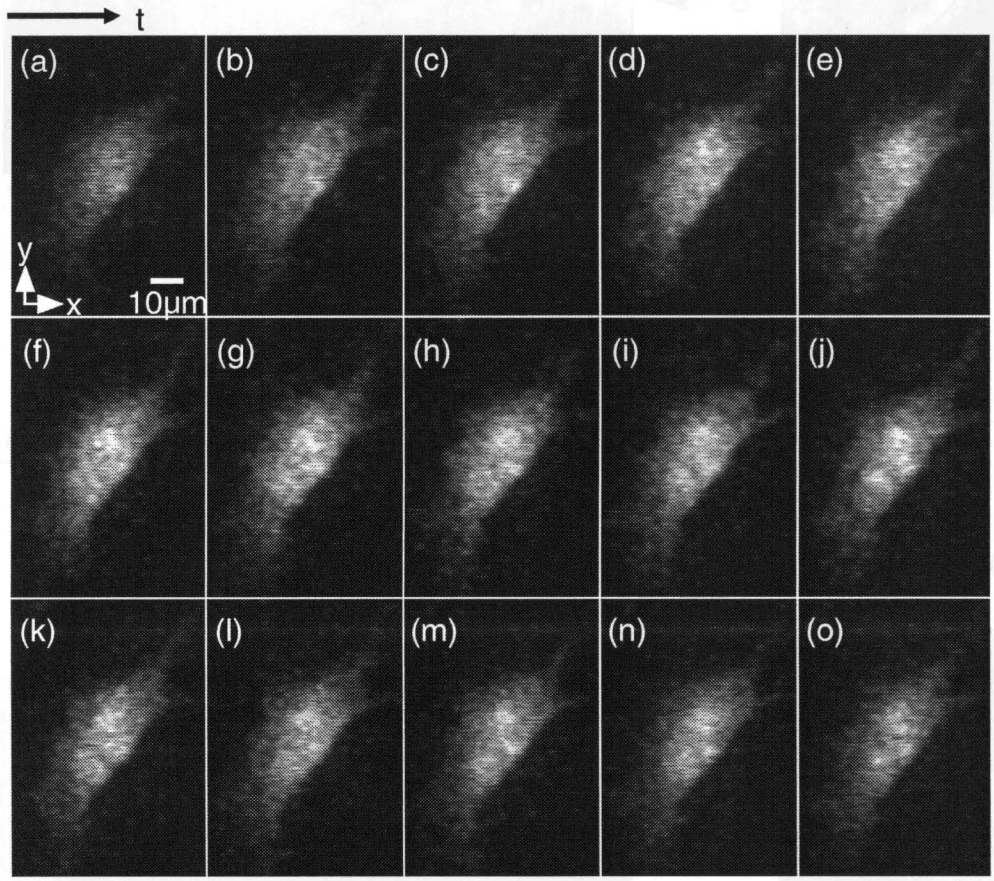

Fig. 3-10 Two-photon fluorescence image of the distribution of Ca^{2+} concentration in the cultured rat-heart cell. Time resolution for each image was about 33ms. Ca^{2+} transient was imaged in this experiment.

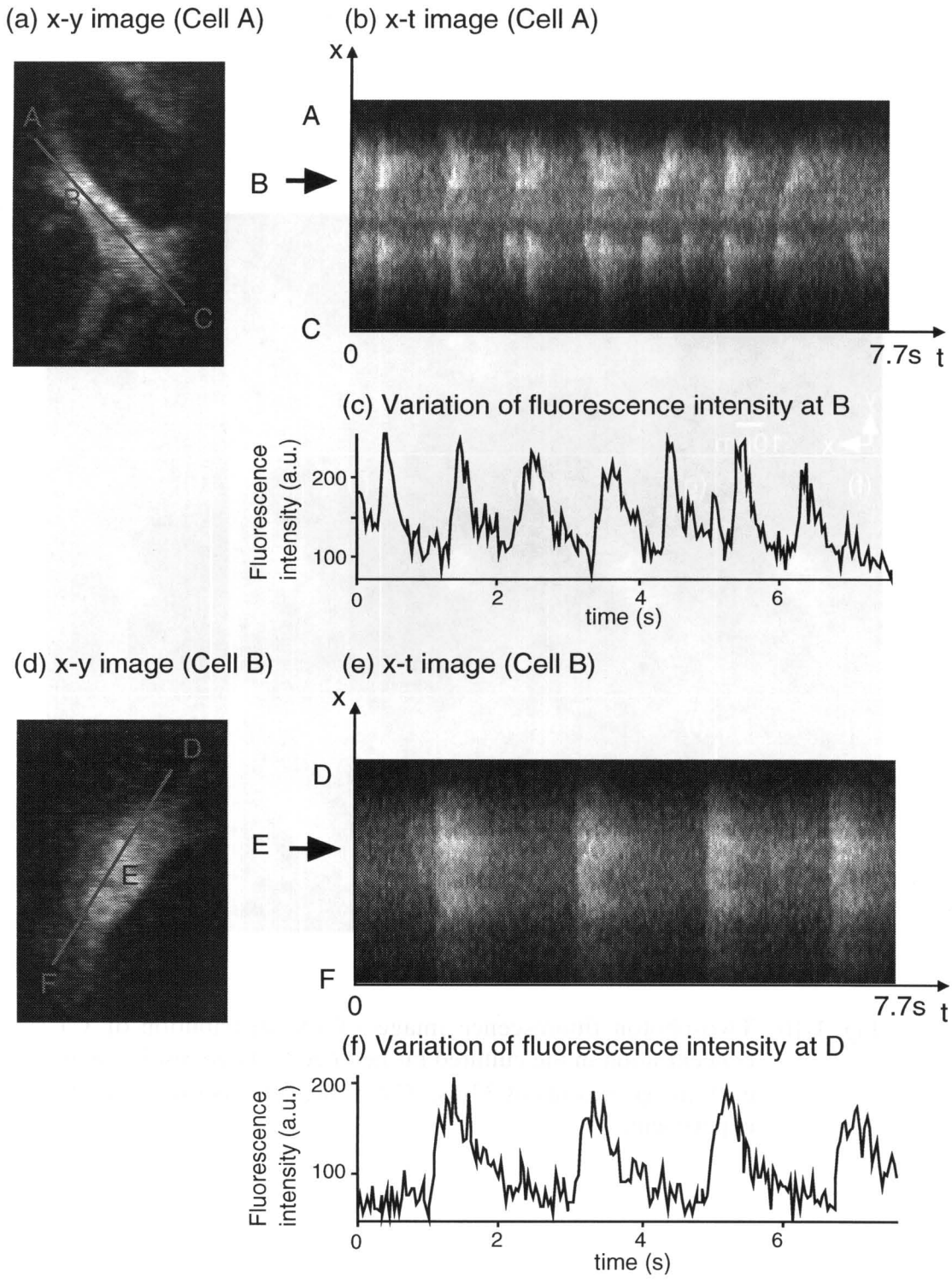

Fig. 3-11 The comparisons of the decay time of Ca^{2+} concentration in the cells which show the different Ca^{2+} dynamics.

2) Two-photon Ca^{2+} imaging in a whole heart of a rat

Two-photon Ca^{2+} imaging was also performed in situ with rat-heart muscle cells. A mode-locked Ti:Sapphire laser (Tsunami, SpectraPhysics, wavelength = 800nm, repetition rate = 82MHz, average output = 900mW) was used as an excitation light source. A water-immersion objective lens (Olympus, NA = 0.8) was used for excitation and observation of a specimen. Fluo-4AM (Molecular Probes) was used as the fluorescent Ca^{2+} indicator.

Fig. 3-12 shows the procedure of the experiments [Hama, 1998]. A whole heart of a rat was enucleated 5min after heparin injection (Step 1). Fig. 3-13 shows the heart 5min after the enucleation. The blood remaining in the heart was washed out by perfusing it with a Ca^{2+}-free Tyrode solution through the coronary vessels (Step 2, Langendorf perfusion) for 15min. As shown in Fig. 3-14, the Tyrode solution was infused into the heart from the aorta. Because of a valve existing at the joint of the aorta and the ventricle, the infused solution cannot flow into the atrium, but into the coronary vessels. For this time, the Tyrode solution worked as artificial blood to make the heart survive during the experiment. In this and the next step, the Ca^{2+}-free Tyrode solution was used to avoid the delibitation of the heart caused by its repetitious heartbeat. After removing the blood, Fluo-4AM (0.018mM) was loaded into the heart for 45min with the Ca^{2+}-free Tyrode solution (Step 3), and then the heart was perfused with the Tyrode solution including Ca^{2+} and observed (Step 4). During the observation, the movement of actin and myosin filament was restricted by BDM because it was impossible to fix the observation plane with the muscle constriction. Fig. 3-15 shows a picture of the heart during observation.

Figs. 3-16 and 3-17 show distributions of Ca^{2+} concentration in the right ventricle of the heart. The total excitation power at the focal plane of the objective lens was 150mW. In Fig. 3-16, a Ca^{2+} wave propagating from the lower right to the upper left was observed. In Fig. 3-17, a Ca^{2+} transient was observed. To know the depth-penetration functionality of the microscope, the specimen was scanned along the z direction. Fig. 3-18 shows the obtained x-z image of the Ca^{2+} concentration remaining in dead cells. In this result, the depth-penetration limit of the developed microscope for the heart muscle cells is around 20μm.

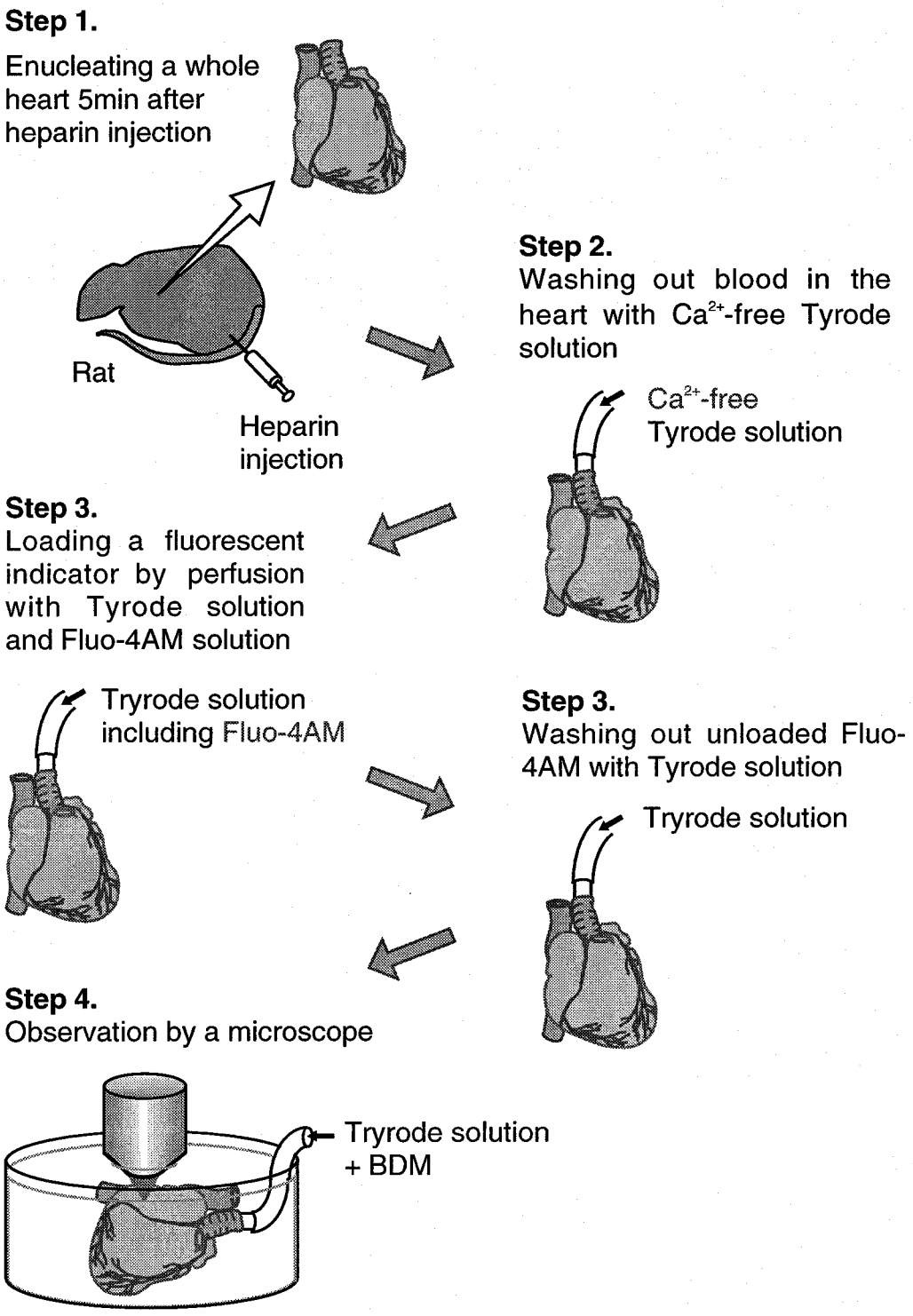

Fig. 3-10 A procedure of Ca^{2+} fluorescence imaging in a rat whole-heart.

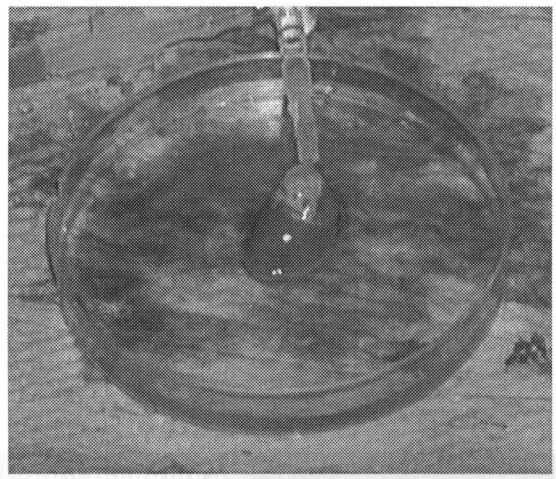

Fig. 3-13 A rat whole-heart 5 minutes after the enucleation.

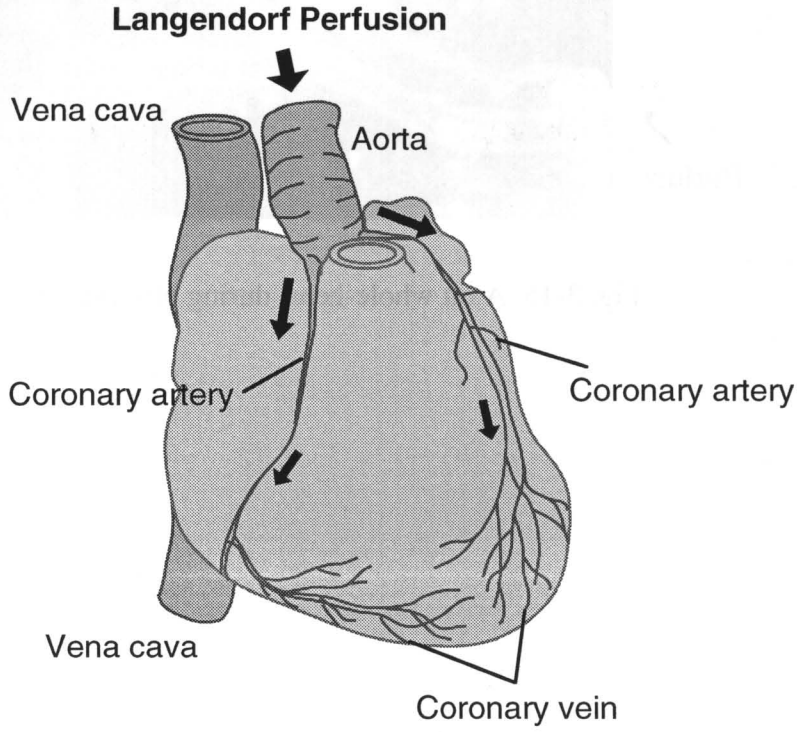

Fig. 3-14 Langendorf perfusion through coronay vessels

Fig. 3-15 A rat whole-heart during observation

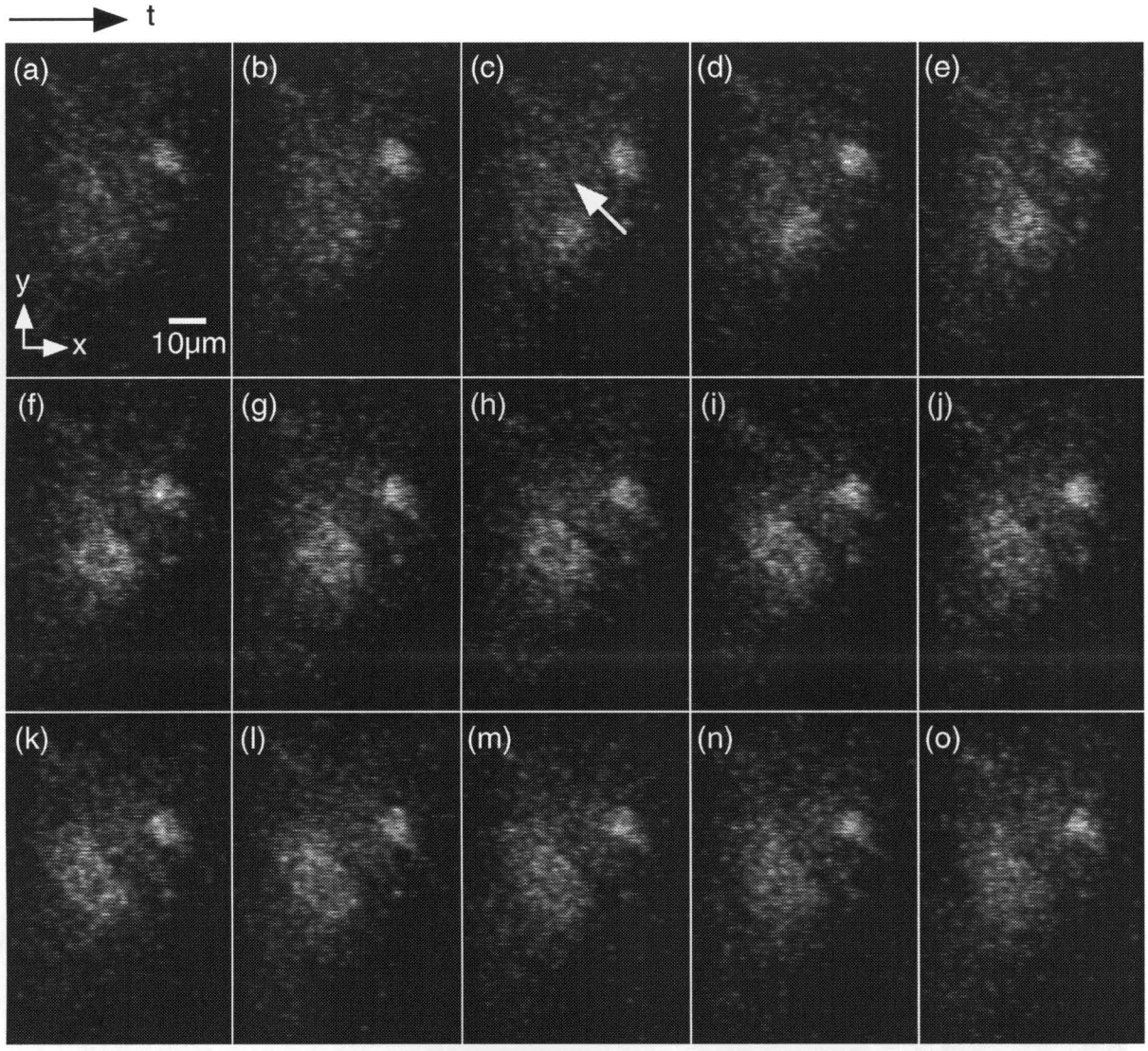

Fig. 3-16 Two-photon fluorescence images of Ca^{2+} wave propagating in a rat whole-heart. The time resolution of each image was about 33ms.

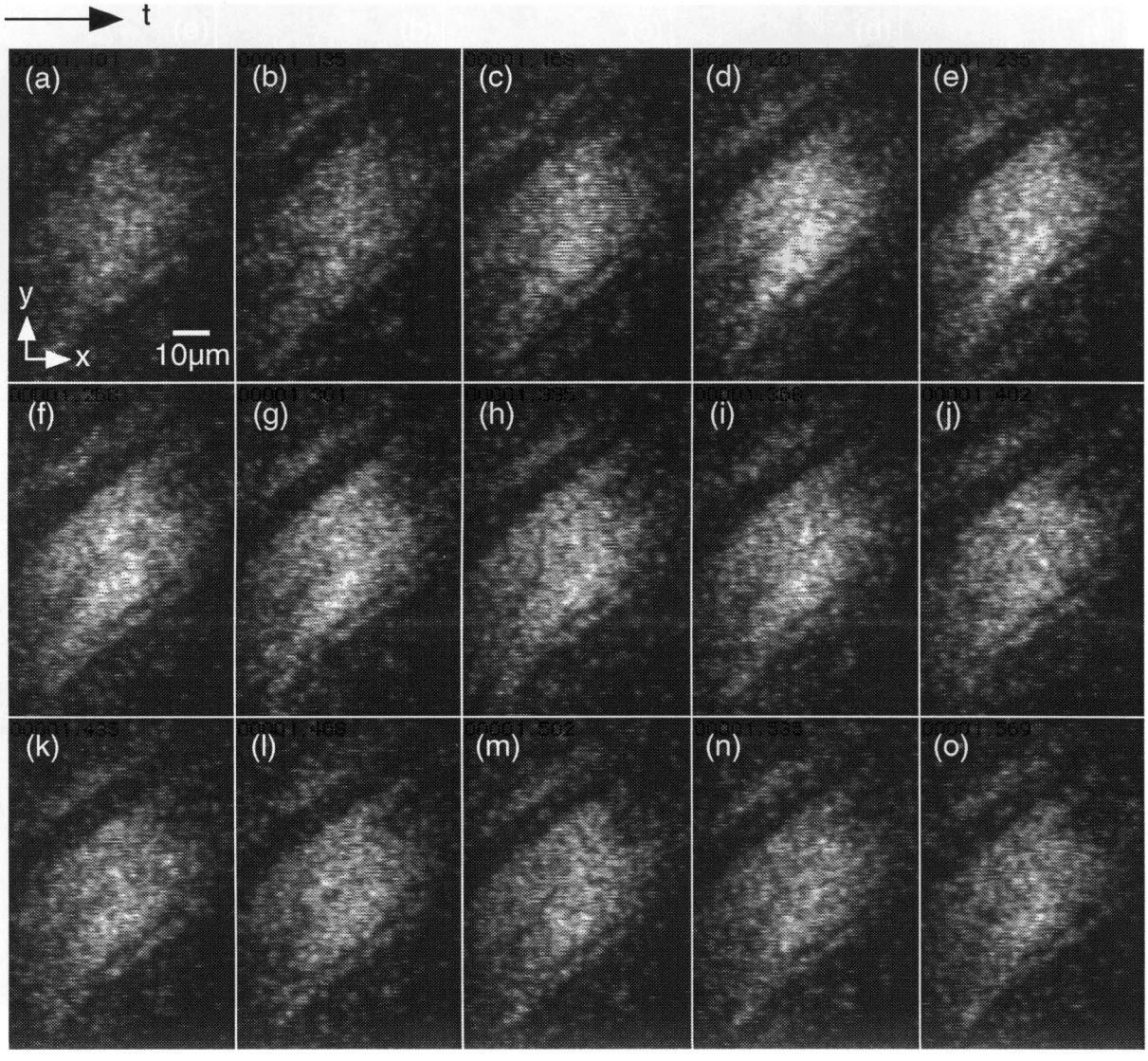

Fig. 3-17 Two-photon fluorescence images of Ca^{2+} transient propagating in a rat whole-heart. The time resolution of each image was about 33ms.

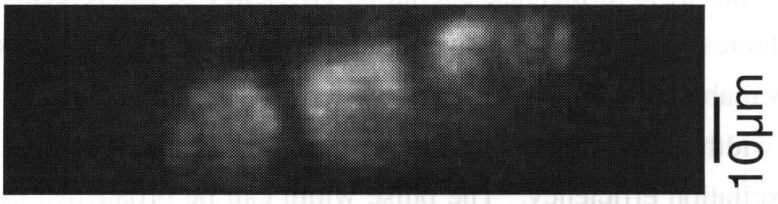

Fig. 3-18 An x-y cross-section image of a rat whole-heart obtained by the developed confocal two-photon excitation microscope.

3-4 Summary

In this chapter, techniques and experimental results of Ca^{2+} imaging with the developed two-photon multifocus fluorescence microscope were presented. In the experiments, Ca^{2+} wave and Ca^{2+} transient were successfully observed both in situ and in vitro.

In the obtained results, the penetration depth of the microscope was around 20μm in the heart muscle cells. This depth is almost the same as that of a single-photon fluorescence microscope. The reasons for this result can be considered as follows. First of all, the intensity of the excitation laser was not enough to induce sufficient two-photon excitation in the specimen. Let us consider the excitation rate of Fluo-3 in each focus for example (note that the two-photon absorption cross-section of Fluo-4 is not yet measured). From its two-photon absorption cross-section, NA of the used objective lens and the excitation power, the excitation rate can be estimated to be about 6%. This means that a higher excitation power can be introduced to obtain brighter fluorescence emission from the specimen.

It is possible to obtain more fluorescence by using fluorescent indicators which possess

larger two-photon absorption cross-sections. So far, only a few researchers have reported the two-photon absorption cross-section of commercially available indicators [Xu, 1996A, 1996B]. In their reports, two-photon absorption cross-sections were measured at only 700nm-900nm wavelengths. This experiment should be performed at a wider range of wavelengths in the future. Designing a new fluorescent indicator for two-photon excitation is also the one of the ways to increase excitation efficiency of fluorescence. Cheng et al. have developed a fluorescent dye which has a larger two-photon absorption cross-section than that of currently available dyes [Cheng, 1998].

The pulse width of the laser in a specimen is also an important factor which determines two-photon excitation efficiency. The pulse width can be broadened because of the group-velocity dispersion of light during the propagation through optics, especially in an objective lens, and decreases the peak intensity of the excitation light [Guild, 1997]. It is difficult to know the pulse width in such a thick specimen. However, it is worth to try to control the group-velocity dispersion by using pre-chirping optics while measuring the fluorescence intensity from the specimen [Fork, 1984].

Chapter 4.

High resolution microscopy with 4pi confocal optical system and phase conjugation

In this chapter, the use of a 4pi confocal optical system which increases the spatial resolution of a microscope is mentioned. The use of phase conjugation with a photorefractive crystal is proposed for further improvement of the optics. The verification of the proposed system is also shown with experimental results by a practical system.

4-1 Principle and imaging properties

A 4pi confocal optical system was introduced by Hell and his co-workers to increase the spatial resolution of a fluorescence microscope. They used two objective lenses to coherently illuminate a specimen from both sides and increase the spatial resolution in the axial direction to about 6 times as compared with that of a typical confocal microscope [Hell, 1992; Hell, 1994]. They applied this system to observe biological specimens with a two-photon excitation technique and also with a microlens array scanner [Shrader, 1999], and achieved about 100nm axial resolution. Fig. 4-1 shows the optical setup of a 4pi confocal microscope. In Fig. 4-1, Light from a laser is divided to two by a beam splitter, and each beam is incident on two different objective lenses. The illumination light from the two objective lenses interferes at the common focal point of the lenses and excites fluorescence in the specimen which is sandwiched between two cover slips. Fluorescence from the specimen is collected by the objective lens and detected through a pinhole after being reflected by a dichroic mirror. This optical system was named "4pi" since the solid angle of the illumination is close to 4π.

The interference of two counter-propagating beams at the common focal point of the two objective lenses gives a smaller point-spread function than that with a single objective lens. As shown in Section 1-3 of Chapter 1., the point-spread function of focusing light can be expressed with Eq. 1-5. The PSF in the 4pi optical system can be given by the interference term as

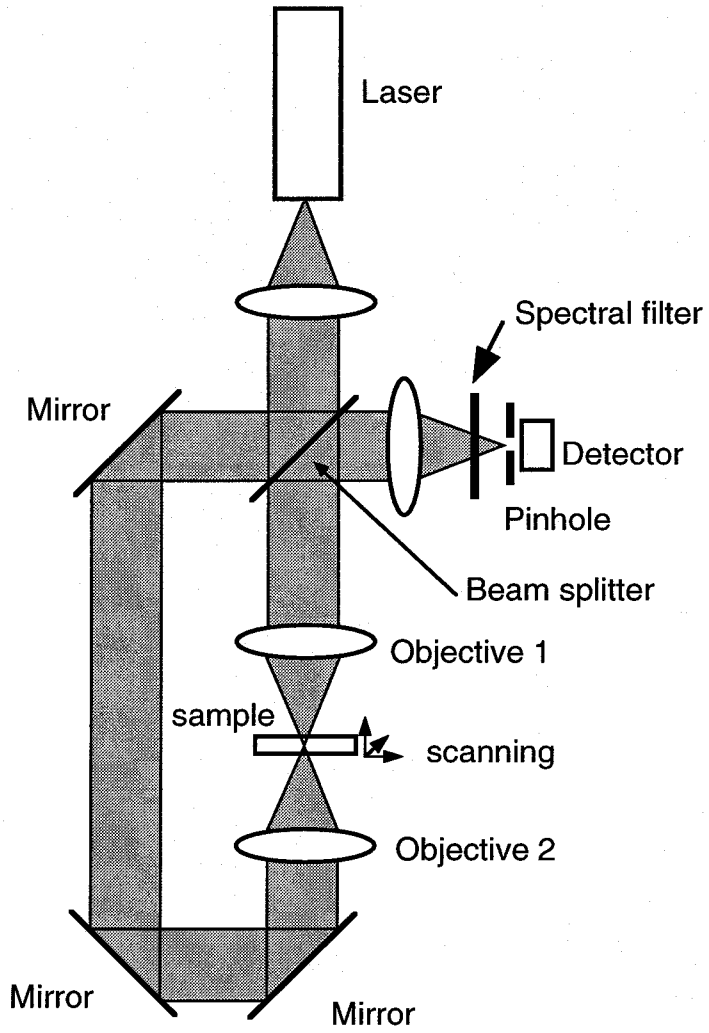

Fig. 4-1 Optical configuration of a 4Pi confocal microscope.

$$I_{4pi}(u,v) \propto \left| \int_0^1 J_0(v\rho) \exp(-\frac{1}{2} i u \rho^2) \rho \, d\rho + \int_0^1 J_0(v\rho) \exp(\frac{1}{2} i u \rho^2) \rho \, d\rho \right|^2 \quad (4\text{-}1)$$

Fig. 4-2(a) and 4-2(b) show the point-spread function (PSF) produced with two objectives and that with a single objective lens. An objective lens with an NA of 1.4 was used for the calculations. In Fig. 4-2(a), the interference effect can be seen as a standing wave of light on the PSF with a single lens. Fig. 4-3(a) and 4-3(b) show the plots of the intensity along the v axis and the u axis of Fig. 4-2(a), respectively. Fig. 4-3(c), (d) show the plots of the intensity along the v axis and the u axis of Fig. 4-2(b), respectively. The narrower peak in Fig. 4-3(b) compared with that in Fig. 4-3(d) corresponds to the 6-fold improvement of the spatial resolution in the axial direction. On the other hand, the lateral resolution of the 4pi system can be seen as same as that with a single objective lenses from the comparison of Fig. 4-3(a) and 4-3(c). In Fig. 4-3(b), strong sub-peaks can be seen, but not in Fig. 4-3(d). The number of the sub-peaks increases when objective lenses with lower NA are used with the increase of the size of the focus. For this reason, it is important to use objective lenses whose NA is as high as possible. These sub-peaks often bring artifacts in obtained fluorescence images, which should be removed by image processing with a deconvolution technique [Schrader, 1998].

The unique illumination system in 4pi confocal optical system also presents some difficulties in its commercialization. The alignment of the objective lenses is one of them. With a high NA objective lens, the size of focal spot is smaller than 1μm. It is not easy to keep the alignment condition so that the two objective lenses produce the common focal point in the specimen at this size. This alignment of the lenses has to be done everytime a specimen is replaced. Aberrations generated independently with each objective lens are another disadvantage. As shown in Fig. 4-4, when the light propagates through the specimen, the wave front of the light can be distorted by the distribution of refractive index in the specimen. This disadvantage is not only in a 4pi optical system but also in a typical microscope. However, it cannot be avoided even when the surface of the specimen is observed with a 4pi optical system.

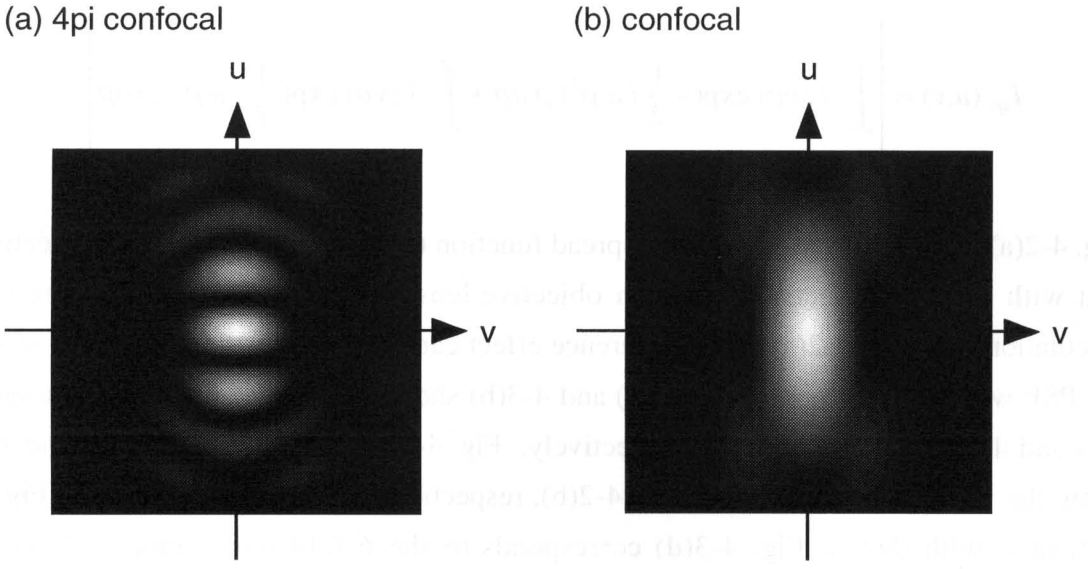

Fig. 4-2 The point-spread functions obtained with (a) two objective lenses and (b) one objective lens.

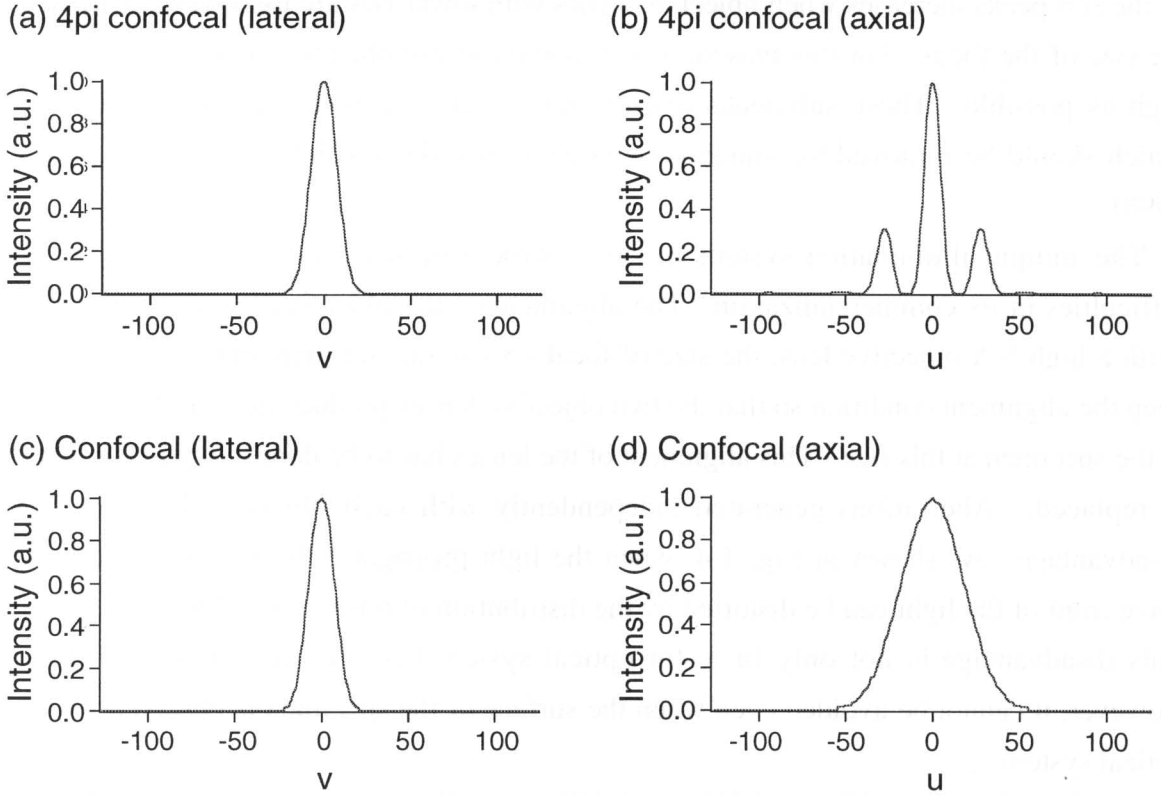

Fig. 4-3 The distribution of the intensity along the lateral and the axial direction.

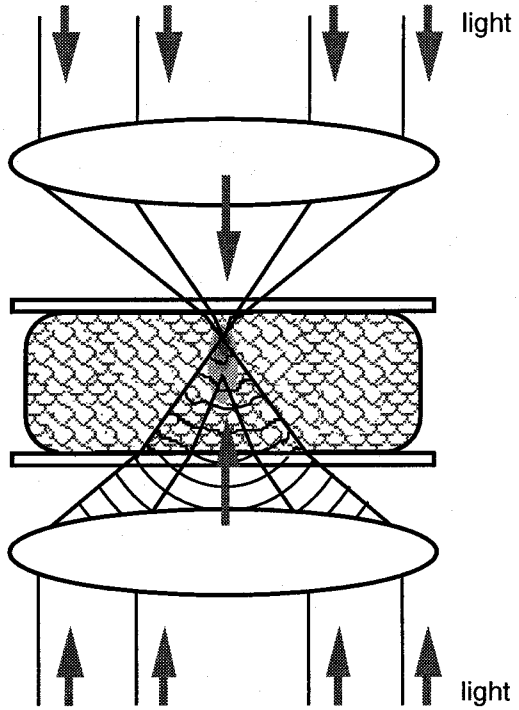

Fig. 4-4 Aberrations generated in thick samples.

4-2 The use of phase conjugation in a 4pi confocal optical system

The use of phase conjugation in a 4pi confocal optical system has the potential to reduce the previously mentioned disadvantages [Kawata, 1996]. Fig. 4-5 shows a 4pi confocal optical system with a phase conjugate mirror. In this optical system, a laser beam is incident to the first objective lens (Objective 1 in the figure), and illuminates a specimen from the front side. Transmitted light through the specimen is collected by the second objective lens (Objective 2 in the figure) and slightly focused into a phase-conjugate mirror which generates a phase-conjugate wave of the incident light. The generated phase-conjugate wave propagates back to the second objective lens and illuminates the specimen from the backside. The illumination from the front and the backside of the specimen interfere with each other at the common focal point of two objective lenses in the same way as that in a typical 4pi optical system.

Since the illumination from the back side of the specimen is a phase-conjugate wave, the focal spot of the backward beam can be formed at the same position as that of the first objective lens without precise alignment of the second objective lens [Fisher, 1983]. The phase-conjugate wave also compensates for aberrations generated in the specimen, slide glass, and the second objective lens, by propagating on the path of the forward beam. As shown in Fig. 4-6, it is theoretically possible to compensate most aberrations generated in the path between the focal spot and the phase-conjugate mirror. Therefore, it is possible to replace the second objective lens with a high NA condenser lens. The use of a high-NA objective lens enables one to prepare a specimen between a glass slide and cover slips, just like the usual way of sample preparation.

The extent of the spherical aberrations at the focal spots was compared theoretically between the proposed 4pi optical system and a conventional one. The geometric model used for the calculation is shown in Fig. 4-7. The thickness of the sample was set at 78λ. λ is the wavelength of the incident light. The refractive indices of the immersion oil, the cover slips, and the sample were set at 1.51, 1.51, and 1.33, respectively. The NA of the objective lenses was set at 1.3. It was assumed that the aberration of the objective lenses was corrected when the plane just under the upper cover slip was observed. Fig. 4-8(a) shows the distribution of the intensity along the optical axis in the proposed system. In this result, spherical aberration does not appear when the light is focused on the plane just under the upper cover slip ($a = 0$). With the increase of the focusing depth 10λ, 20λ, and 30λ, the intensity distribution of the spot is degraded by the spherical aberration generated in the forward light, but the focal spots

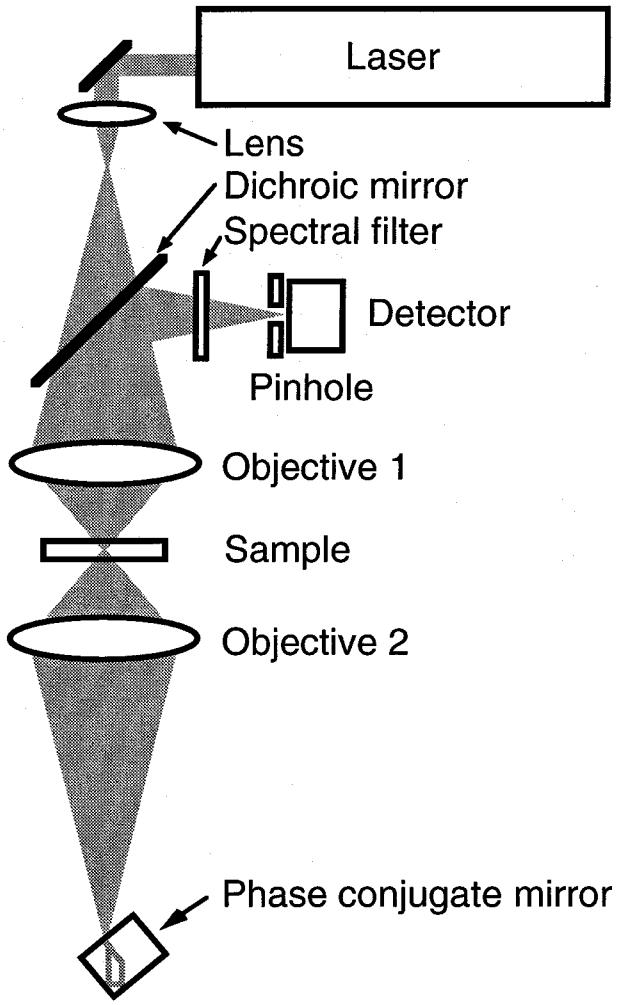

Fig. 4-5 Optics of a 4pi confocal fluorescence microscope with phase conjugation

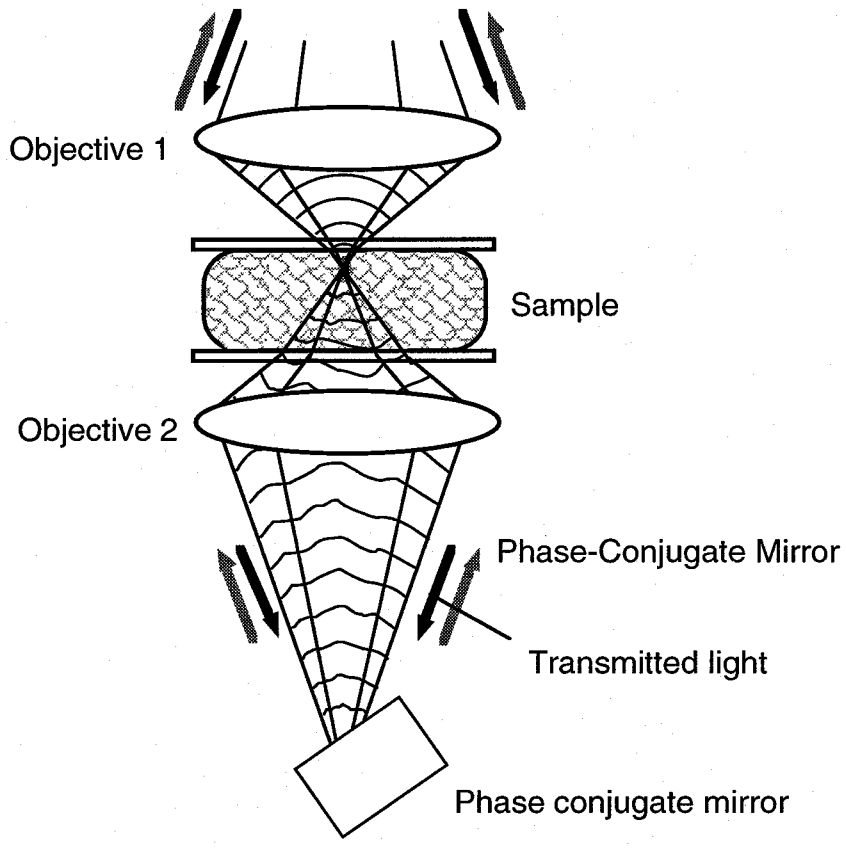

Fig. 4-6 Correction of aberration by using a phase conjugate mirror.

still keep the shape of the focus formed in the 4pi optical system. Fig. 4-8(b) shows the distribution of the intensity along the optical axis in a typical 4pi optical system. In this result, even when the focus is at the surface of the sample, the focal spot suffers from spherical aberration associated with the backward beam. At deeper parts of the sample, the shape of the focal spots is distorted further by spherical aberrations in the forward and the backward light, and the intensity of the peak is strongly reduced.

In the calculated result shown in Fig. 4-8(a) and 4-8(b), it can also be seen that the spherical aberration of the first objective lens appears in both systems. This is caused by a refractive index mismatch between the sample and the cover slip. In this condition, only a shallow part of a sample can be observed, even when the phase-conjugate mirror is used. However, the proposed microscope can compensate for spherical aberrations in the backward beam. This is an important property when thick samples are observed. On the other hand, in a typical 4pi optical system, both the backward and the forward beams have spherical aberration. Therefore, samples must be thin enough or sliced before the observation with a typical 4pi system.

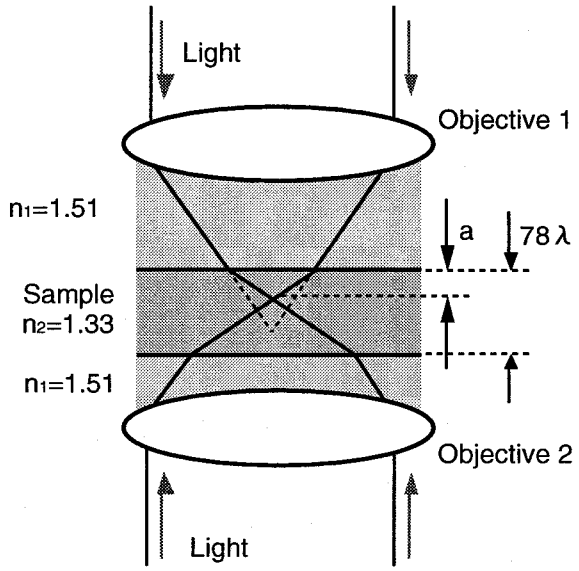

Fig. 4-7 The geometric model used for the calculation of aberration in thick samples.

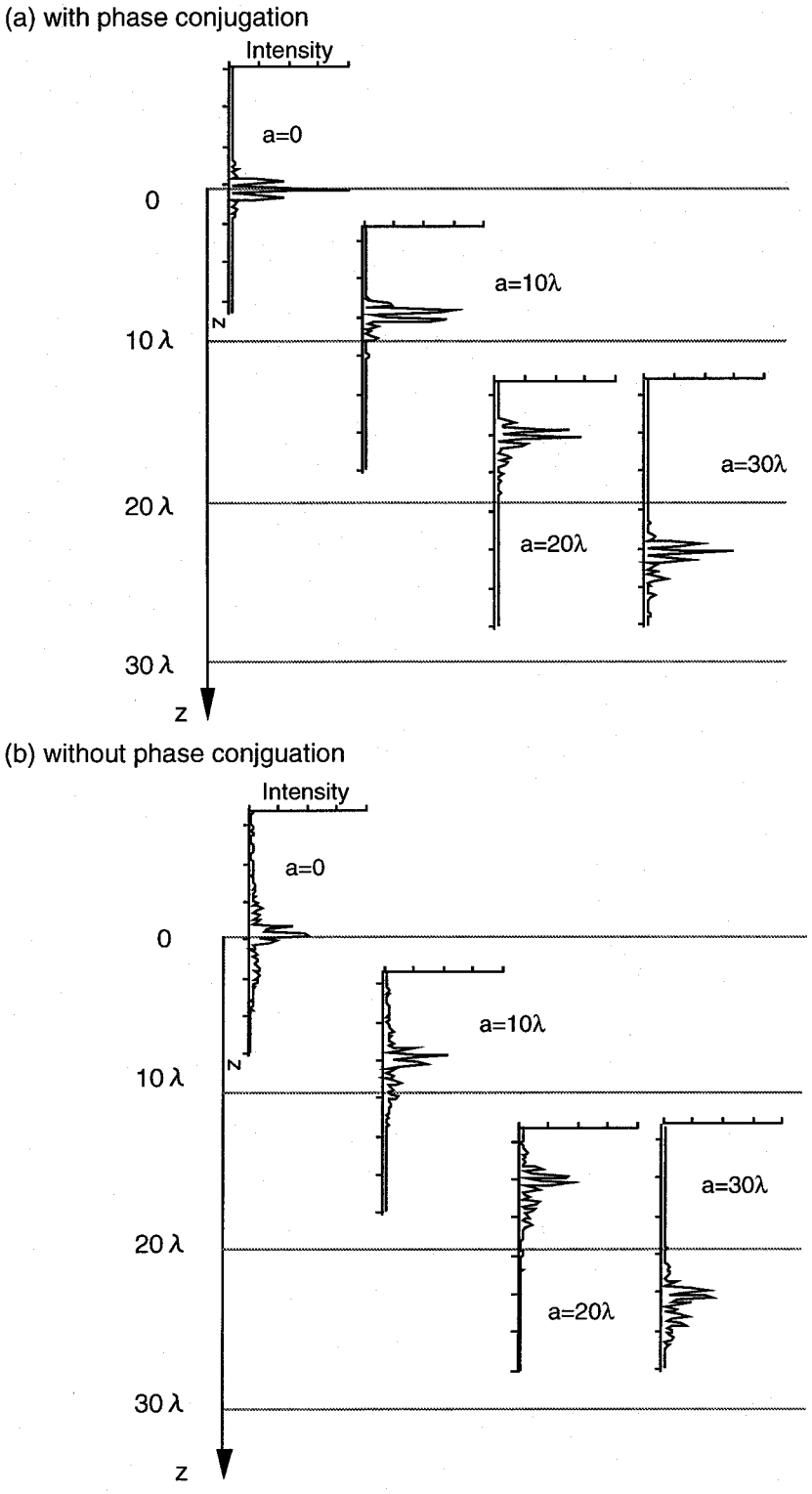

Fig. 4-8 Calculation results showing the axial response of (a) the proposed 4pi confocal configuration with phase conjugation and (b) a standard 4pi confocal system.

4-3 Experiments with a 4pi confocal microscope using a phase conjugate mirror

1) Fluorescence imaging

A 4pi confocal microscope with a phase conjugate mirror shown in Fig. 4-9 was constructed to investigate the usefulness of the proposed optical system. A water-cooled argon-ion laser (NEC, wavelength = 514.5nm, output power = 350mW) was used as a light source. A longitudinal-mode selector was installed in the laser to give enough long coherence length so that two counter-propagating beams in a sample interfere with each other. Two oil immersion objective lenses (Olympus, NA1.3oil) were used for illuminating and observing a specimen. A barium titanate crystal doped with cerium (Ce:BaTiO3) was used as a phase-conjugate mirror. A phase-conjugate wave was generated in the crystal by self-pumping [Fisher, 1983]. A fluorescent bead (Molecular Probes: ø = 40nm) fixed between two cover slips was used as a sample. The sample was scanned along the lateral and the axial direction by a piezo-electric scanning stage (MellesGriot, Nanoblock). The fluorescence from the sample was measured by a photomultiplier tube (Hamamatsu, H5874) through a pinhole (ø = 20μm) and a spectral filter which cut out the laser beam wavelength for excitation.

The fluorescent bead was scanned in the axial direction while measuring the intensity of the fluorescence. Since the size of the particle is much smaller than the size of the focal spot, the measured signal gives the response to a point object along the optical axis. This is called "axial response" and used to show the axial resolution of a confocal microscope. Fig. 4-10(a) shows the obtained axial response of the system. For comparison, the axial response of a typical confocal microscope, which was measured in the same setup without the phase-conjugate mirror, is shown in Fig. 4-10(b). In Fig. 4-10(a), it can be clearly seen that the sinusoidal modulation is present in the PSF produced by the interference of the two beams, while this modulation is absent in Fig. 4-10(b). From this result, it is concluded that the proposed system can function as a 4pi confocal optical system. The FWHM of the main peak in Fig. 4-10(a) is measured to be 116nm, which shows that our system holds about a 6-fold increased axial resolution as compared with that of a typical confocal system. The response in Fig. 4-10(a) does not include an additional aberration onto the confocal axial response. This result shows that additional aberrations do not appear with the use of phase conjugation for light illumination even at the focal region of a high NA objective lens. From the visibility of the interference on the response in Fig. 4-10(a), the reflectivity of the phase conjugate mirror

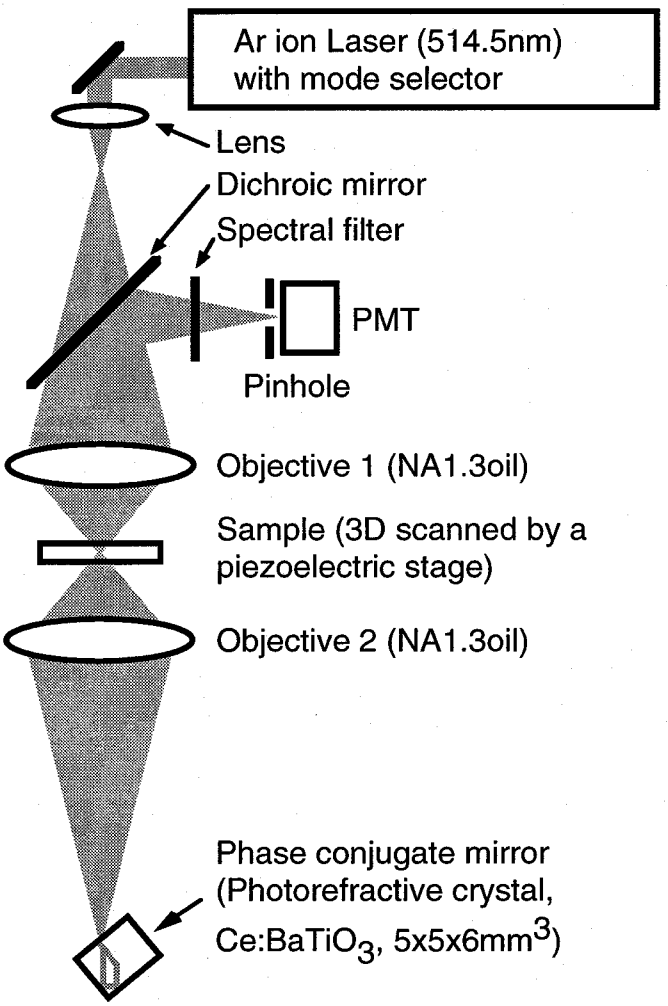

Fig. 4-9 Experimental setup of a 4pi confocal fluorescence microscope with phase conjugation.

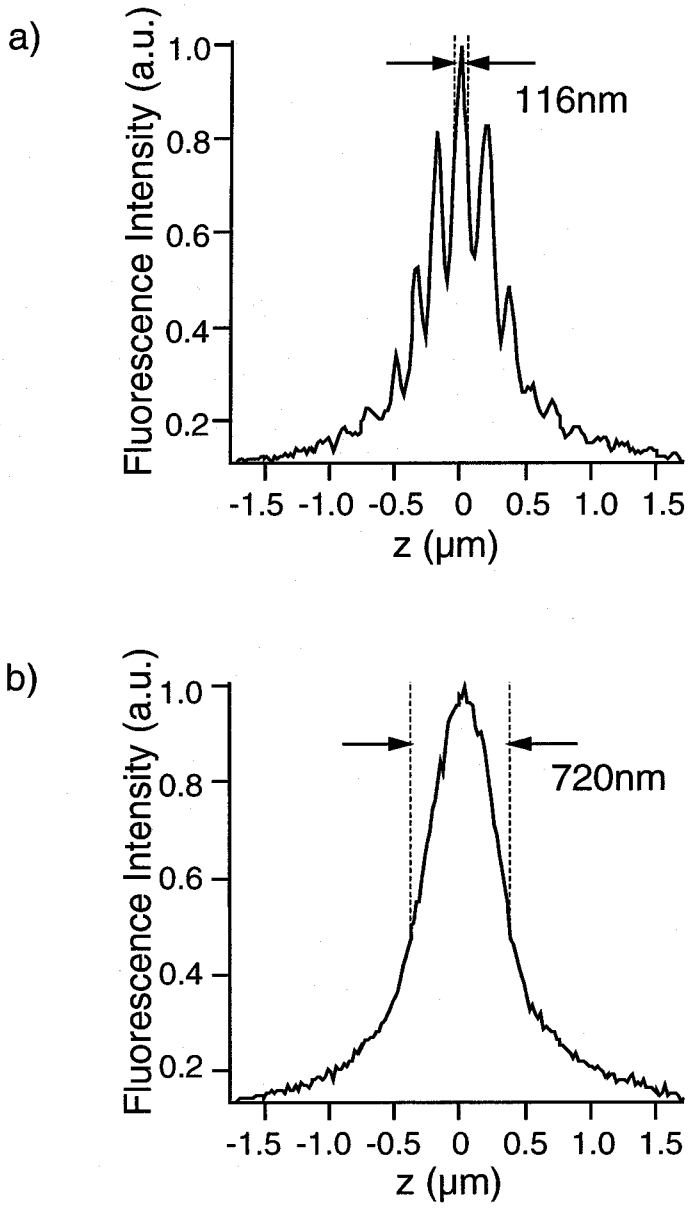

Fig. 4-10 Axial responses obtained with a 40nm-diameter fluorescent bead (a) with a phase conjugate mirror and (b) without a phase conjugate mirror.

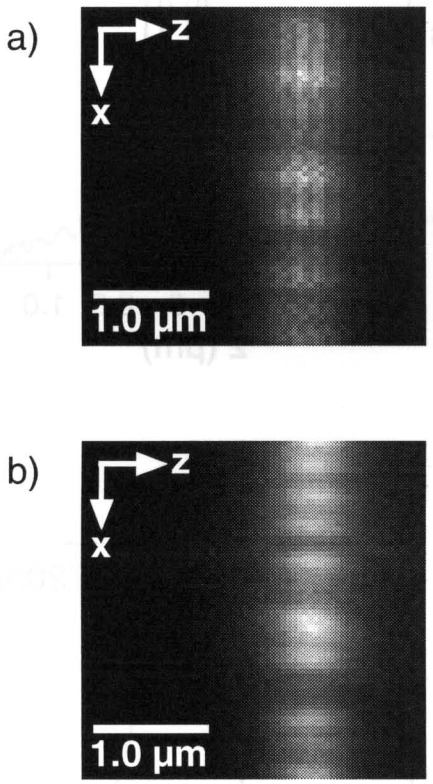

Fig. 4-11 X-Z cross-section images obtained with 40nm-diameter fluorescent beads (a) with a phase conjugate mirro and (b) without phase conjugate mirror.

is estimated to be around 4%.

Fig. 4-11(a) and 4-11(b) show an x-z fluorescence image of the same sample with and without the phase conjugate mirror, respectively. The fluorescence detection time at each pixel is around 100ms and it requires around 5 minutes for taking a 64pixel x 64pixel image. In Fig. 4-11(a), the interference fringe can be seen along the axial direction, but not in Fig. 4-11(b). These results also prove that the developed system can work as a 4Pi confocal fluorescence microscope. In Fig. 4-11(a), a slight movement of the main peak of the response can be seen along the lateral axis because of the phase shift of the phase conjugate light in the crystal [Gunter, 1989]

2) The compensation of the wave-front distortion in a sample

It was confirmed experimentally that the wave-front distortion of the beam is compensated with the backward illumination by the phase-conjugate wave. In this experiment, a diatom which has both phase and absorption structures was observed by a double-pass confocal absorption microscope (DPCAM) with a phase-conjugate mirror, and the image was compared with an image obtained by a conventional transmission laser-scanning microscope (Type-1 laser scanning microscope), where the phase structure cannot be imaged [Wilson, 1983].

Fig. 4-12(a) shows the optical setups of a DPCAM with a phase conjugate mirror for the experiments [Nakamura, 1996]. In both setups, an Ar-ion laser (wavelength = 488nm, average power = 50mW) was used as the light source. The beam from the source was focused into the sample by an objective lens (Olympus, NA0.4) and absorbed by the material in the sample. The transmitted light through the sample is collected by a collector lens which has the same numerical aperture as the first objective lens, and introduced into a phase-conjugate mirror. A photorefractive crystal (Ce:BaTiO3) was used as the phase-conjugate mirror and generated the phase-conjugate wave by self-pumping. The phase-conjugate wave propagated back to the second objective lens and was focused again in the sample. After transmitting through the sample twice, the beam was collected by the first objective lens and detected through a pinhole (ø = 20μm). The same as the setup for the 4pi optical setup shown in the previous section, the phase-conjugate wave compensates for aberrations generated by the second objective lens and the phase structure of the sample. Therefore, the phase structure could not be imaged by this microscope. Fig. 4-12(b) shows a DPCAM where a

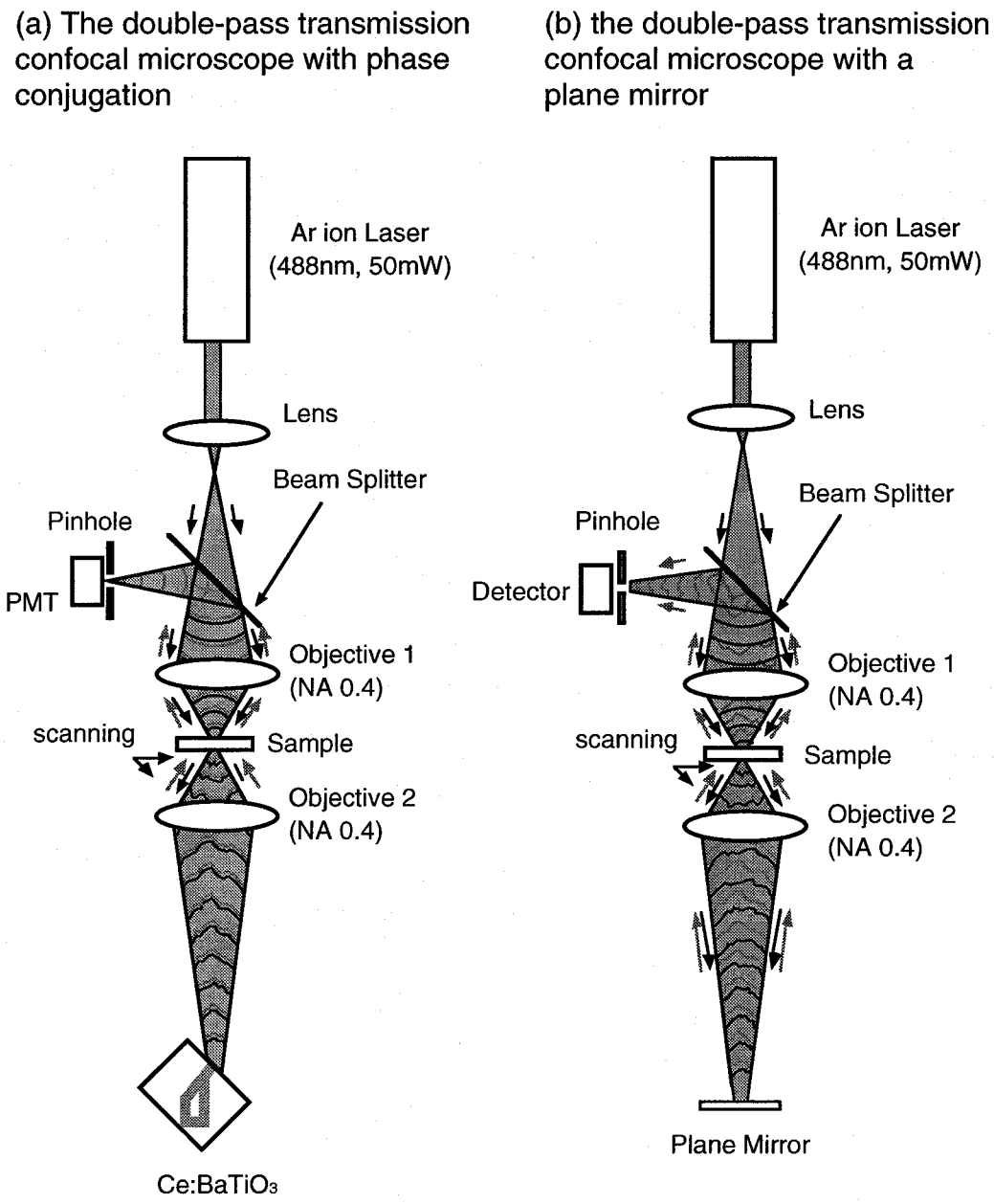

Fig. 4-12 Experimental setup for the double-pass transmission confocal microscope with a phase conjugate mirror and with a plane mirror

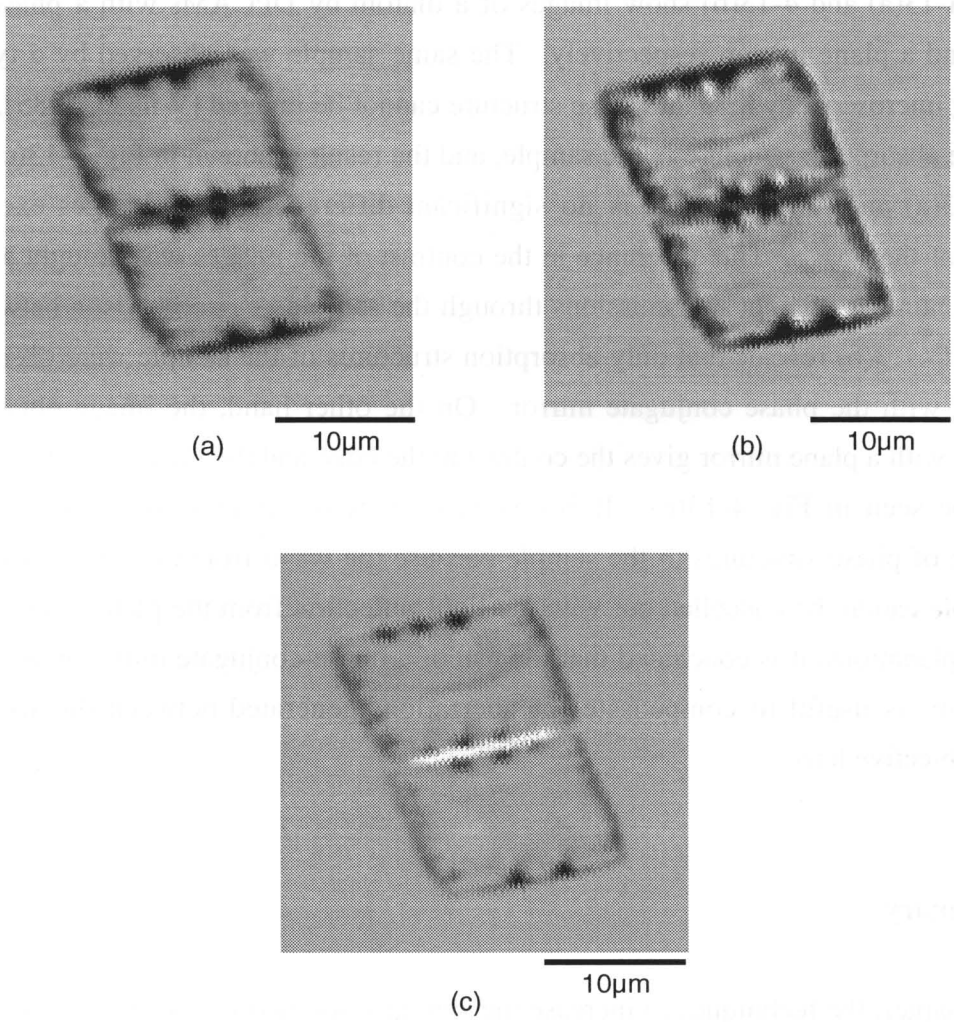

Fig. 4-13 Images of a kind of diatom obtained by the double-pass absorption confocal microscope with a phase conjugate mirror, the double-pass absorption confocal microscope with a plane mirror, and a laser scanning microscope (type1) are shown in (a),(b),and (c), respectively.

pine mirror was used instead of a phase-conjugate mirror. In this microscope, the wave-front distortion generated in the sample cannot be cancelled out. Therefore, the phase structure in the sample can be imaged.

Fig. 4-13(a) and 4-13(b) show images of a diatom by DPCAMs with a phase conjugate mirror and a plane mirror, respectively. The same sample was observed by a type-1 laser-scanning microscope, where the phase structure cannot be imaged [Wilson, 1985], in order to know the absorption structure in the sample, and the result is shown in Fig. 4-13(c). Between Fig. 4-13(a) and 4-13(c), there is no significant difference in the images except for the contrast of the image. The difference in the contrast of the images was brought about by the different number of light transmissions through the sample. A comparison between Fig. 4-13(a) and 4-13(b) reveals that only absorption structures of the sample were observed in the DPCAM with the phase conjugate mirror. On the other hand, the image obtained by the DPCAM with a plane mirror gives the contrast at the edge and the inside of the diatom, which cannot be seen in Fig. 4-13(c). It is considerable that this contrast of image shows the existence of phase structures in the sample because the wave-front distortion of the beam in the sample cannot be cancelled out with the light reflection from the plane mirror. From the given explanations, it is concluded that the use of a phase-conjugate mirror in a 4pi confocal microscope is useful to compensate for aberrations generated between the focus and the second objective lens.

4-4 Summary

In this chapter, the techniques to increase the spatial resolution of a fluorescence microscope using a 4pi optical system and phase conjugation were proposed. The usefulness of a phase conjugate mirror in a 4pi microscope was verified experimentally with a practical setup of the proposed optical system and a double-pass confocal absorption microscope. The experimental result of fluorescence imaging revealed that around 116nm axial resolution can be obtained with the proposed system, which corresponds to about 6-hold increased resolution as compared to that of a normal confocal microscope. The aberration-compensation property with the use of the phase-conjugate mirror was also verified by observing a diatom with the developed double-pass confocal absorption microscope.

The generation of spherical aberration in the sample in the proposed 4pi system and a

conventional one was also obtained theoretically. From the result, it was concluded that the observable part of the sample is limited at the shallow position of the sample, even when the phase-conjugate mirror is used. However, it was also shown that the proposed microscope does not give a limit to the thickness of samples, but so does the conventional 4pi system.

In the experiments, some problems which originate from the phase conjugate mirror used were also observed. The low reflectivity of the phase conjugate mirror degrades the contrast of an image, especially at the positions in the sample containing high spatial frequency. This problem also brings about a problem in the image restoration technique used for the reduction of the side lobe of 4Pi PSF [Schrader, 1998]. The low reflectivity of the phase conjugate mirror originates from the slow response of the crystal. It is possible obtain higher reflectivity than that obtained our system with higher incident power into the crystal and longer irradiation time. However, this leads to the problem of photobleaching in a fluorescence microscope. Another problem is the phase shift of the phase conjugate light generated by the movement of phase conjugation gratings in a crystal [Gunter, 1989], which causes destructive interference at the focal point and brings about artifacts of the sample. This problem can be overcome by the use of four-wave mixing (4WM) in nonlinear materials for the generation of a phase-conjugate wave. In 4WM, the phase condition of the phase-conjugate wave can be controlled by the pumping beam, therefore, it is possible to keep a constant phase at the focal point. All problems mentioned come from the property of the phase conjugate mirror, not from the use of the phase conjugation. I hope that these problems will be overcome by the improvement of phase conjugate mirrors in the future.

The proposed system can be combined with two-photon excitation of fluorescence. It has also been reported that a phase-conjugate wave of near-infrared pulse laser light can be generated by a photorefractive crystal [Yan, 1998]. The reported reflectivity of a phase conjugate mirror for near-infrared pulsed laser light is around 30%. In a two-photon excitation process, the low reflectivity of a phase conjugate mirror is not a significant problem because a point image at a detector can be represented as the fourth power of the PSF of the excitation (square of PSF, in single-photon excitation), which brings about higher visibility of the axial response than that with single-photon excitation at the same reflectivity. Apprehensive pulse broadening, which degrades the efficiency of two-photon excitation, by light propagation in the crystal can be automatically compensated in the crystal itself [Cheng, 1999].

It is also possible to combine a multifocus scanning technique with a 4pi optical system

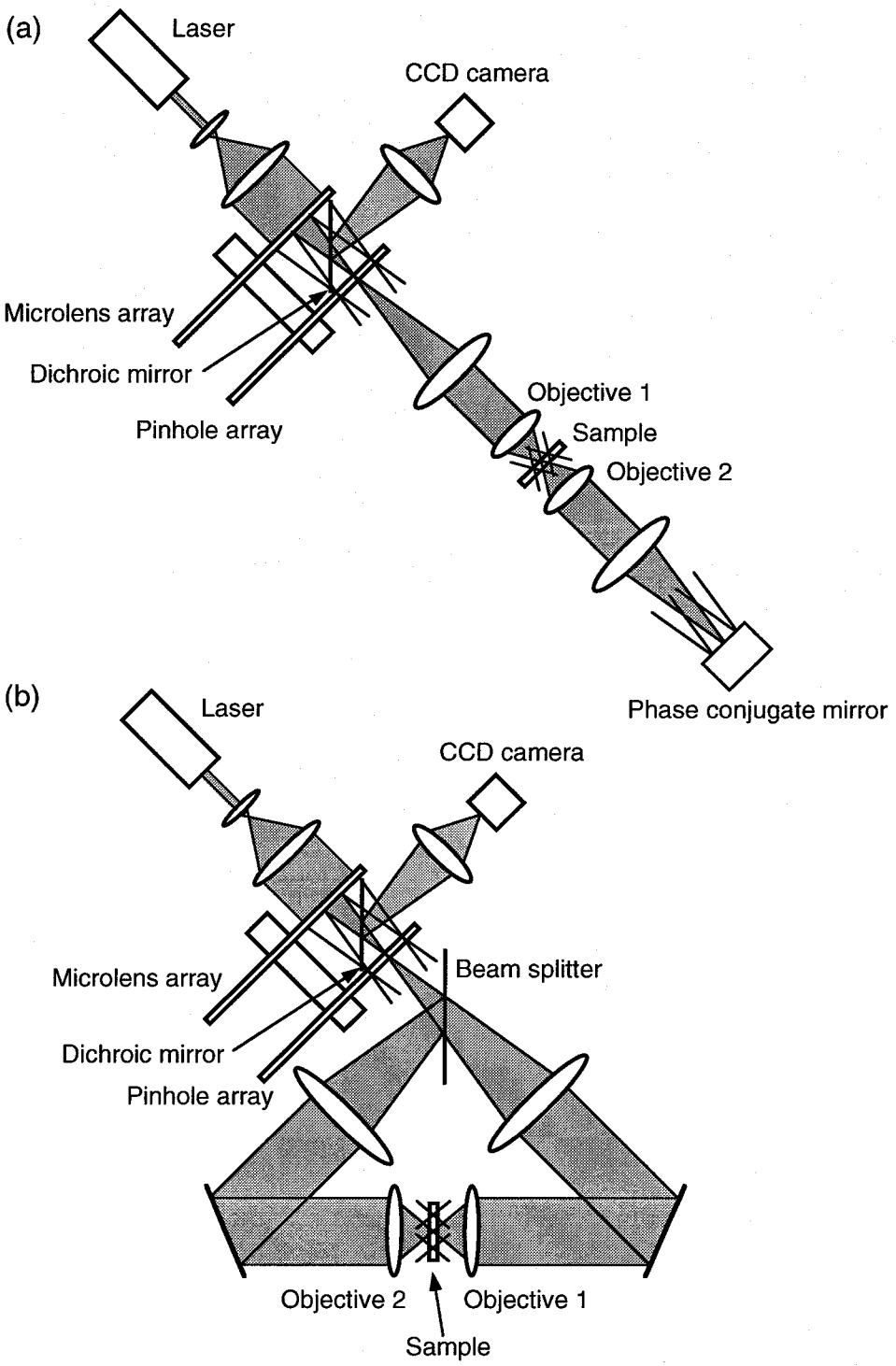

Fig. 4-14 Configuration of multifocus 4pi confocal fluorescence microscope (a) with and (b) without a phase conjugate mirror

[Schrader, 1999], and theoretically also with the proposed 4pi system as shown in Fig. 4-14. It is difficult to expect an increase in the scanning speed of the system with the phase-conjugate mirror because of its slow response time. However, as well as the case of the single-focus scanning mentioned in this chapter, the use of a phase-conjugate mirror is useful to reduce aberrations in the system.

Conclusions

In this research, a two-photon multifocus fluorescence microscope was developed for observations of living and moving biological specimens with the advantages of high image-acquisition rate and high spatial resolution. In Chapter 1, the principle and the optical properties of the developed microscope were discussed. A design of a microlens- and pinhole-array scanner and an estimation of fluorescence excitation efficiency for the developed microscope were also discussed in this chapter. Experimental results with the developed microscope presented in Chapter 2 showed the optical properties of the microscope, which are the enhancements in spatial resolution and contrast of images. In Chapter 3, the usefulness of the developed microscope was verified experimentally in the real-time observation of Ca^{2+} dynamics in living rat heart cells. Ca^{2+} waves and Ca^{2+} transients were observed in cultured rat heart cells and cells of a rat whole-heart. In Chapter 4, a use of 4pi optics and phase conjugation, which enhances the spatial resolution further, was introduced. A practical system with the techniques showed axial resolution of 116nm and the capability of phase conjugation for compensating for aberrations generated in the optics.

In the developed microscope shown in Chapter 2, a microlens-array disk was used to excite fluorescence specimens with multiple focus and to increase the image-acquisition rate of a two-photon microscope. In the developed setup, the scanning rate with the used microlens-array disk was about 360 frames/s. However, the actual image-acquisition rate was limited at 30 frames/s because of the use of a video-rate CCD camera. The use of a camera with higher speed can realize further improvement in the image-acquisition rate. The developed optical system is also useful in applications which use focused light, such as optical memories, optical fabrications, and optical surgery [Toriumi 1998; Maruo, 1997; König, 1999].

The introduction of a pinhole-array disk into a multifocus fluorescence microscope successfully increased the three-dimensional spatial resolution of a two-photon multifocus microscope and the contrast of the obtained image. These improvements were confirmed by comparison of the fluorescence images obtained with and without the pinhole-array disk. In the experiments, besides the improvement of the resolution by confocal detection, the rejection of scattered fluorescence at the pinhole array worked effectively to increase the

contrast of the images and also helped increase the resolution of the microscope. This effect also enhanced the observable depth. This shows contrasting results from that in a typical two-photon fluorescence microscope using single-focus scanning. From these experimental results, it was concluded that the use of a pinhole-array disk was indispensable in a two-photon multifocus fluorescence microscope.

The theoretical estimation of the fluorescence excitation efficiency in the multifocus excitation revealed that the maximum number of two-photon excitation spots was limited to a few tens of foci when a typical mode-locked Ti:Sapphire laser (average output ~ 1W) is used. This number should be increased because various applications in biology and medicine require a wider field of view with more excitation spots. An increase of the number of excitation spots directly corresponds to the enhancement of fluorescence acquisition rate also. In the current situation, the maximum output power of the commercially available Ti:Sapphire laser is about 2W. However, it can be easily estimated from the equations in Section 1-4 of Chapter 1 that this output is still not enough for many applications such as Ca^{2+} imaging as shown in Chapter 3. Note that the use of a regenerative amplifier in this application is not a good idea because of its low repetition rate and easily induced saturation effect of the fluorescence excitation.

The usefulness of the developed multifocus fluorescence microscope in biology was also verified with the observation of intracellular Ca^{2+} dynamics with cultured rat heart cells and a rat whole-heart. In these experiments, it was shown that the developed microscope could be used for such applications that require quantitative analysis of Ca^{2+} dynamics. The penetration depth obtained with the rat whole heart could not exceed that with a single-photon confocal microscope because of the low laser excitation power. An improvement of laser systems in the future is desired for pioneering a new application of this microscope.

The preliminary experiments with a 4pi optical system and phase conjugation for the further improvement of spatial resolution were performed. Even though the experiments were carried out using a single-photon excitation process, the results show enough potential for the enhancement of the spatial resolution in a two-photon multifocus microscope. In the experiments, the axial resolution of about 120μm was obtained. However, the low response of the phase-conjugate mirror used, brings about difficulties in implementing the use of this system into the multifocus system. Further investigations on the development of phase-conjugate mirrors are required for the application of the proposed system.

Acknowledgements

I wish to express my deepest appreciation to Professor Satoshi Kawata of Osaka University, Department of Applied Physics, for supervising my six year's studies in his laboratory. I have learnt a lot from his attitude toward research and it is a pleasure working under his direction. I also appreciate that he gave me chances for meeting many researchers not only in Japan, but also in foreign countries. This experience is a great treasure for me and will also be in the future.

Suggestions and comments for this dissertation from Professor Hiroshi Masuhara and Professor Hiroshi Iwasaki (Both from Osaka University, Department of Applied Physics) are deeply acknowledged.

I also would like to express my sincere gratitude to Associate Professor Osamu Nakamura of Osaka University, Department of Applied Physics, for his many technical support and advice. His grateful comments for my studies always showed me a right direction for my researches.

I would like to thank Professor Hideaki Kasai and Associate Professor Yoshihide Kimura (Both from Osaka University, Department of Applied Physics) for their critical reading of this dissertation.

Professor Tetsuro Takamatsu and Associate Professor Masahito Oyamada (Both from Kyoto Prefectural University of Medicine) gave me a lot of technical supports and comments for the studies of Ca^{2+} imaging shown in Chapter 3. I really appreciate that.

I would like to show my thankfulness to Dr. Tomoyuki Kaneko of Osaka University, Research Associate, for his technical support and useful discussion for this research.

I would like to thank Associate Professor Yoshimasa Kawata of Shizuoka University, Associate Professor Zouheir Sekkat of Osaka University, Department of Applied Physics, Assistant Professor Yasushi Inouye, and Assistant Professor Tadao Sugiura (Both from Osaka University, Department of Applied Physics) for their precious comments for my research and creating adequate situation for it.

I would also like to extend my thank to Professor Caesar Saloma and Assistant Professor Vincent Daria (Both from the University of the Philippines, Philippines) for accepting my studies in their laboratory and their kindness for my ten-month's staying in the Philippines. I also wish to express my appreciation to Dr. Stefan Hell in Max-plank Institute of Biophysical Chemistry in Göttingen, Germany, for his useful comments to my researches and his

acceptance of my stay in his laboratory.

I would like to express my appreciation to Dr. Akira Ichihara and Takeo Tanaami in Yokogawa Electric Corporation for the contribution of designing and developing microlens- and pinhole-array scanners used in this research.

Special thanks to Dr. Hiroshi Kano, Dr. Takuo Tanaka, Dr. Shoji Maruo, and Dr. Hiromitsu Furukawa for their technical support and advice.

Many thanks to members of Prof. Kawata's laboratory for helping my studies in various situation. I thank Jose Amistoso for editing my manuscript. I sincerely thank Masaki Hisaka and Kenji Okamoto throughout my studies in Osaka University and wish their brilliant future.

References

Alberts, B., Bray, D., Lewis, J., Raff, M., Roberts, K., and Watson, D., The Cell, (Garland publishing, 1990).

Bewersdorf, J., Pick, r., and Hell, S., Opt. Lett. Vol. 23, p.65 (1998).

Born, M., and Wolf, E., Principles of Optics, (Pergamon Press, 1959).

Brown, H. and Kozlowski, R., Physiology and pharmacology of the heart, (Backwell Science, 1997)

Buist, A., Müller, Mu., Squier, J., and Brakenhoff, J., J. Microsc. Vol. 192, Pt 2, p. 217 (1998).

Chalfie, M., Tu, Y., Euskirchen, G., Ward, W., Science, Vol. 264, p.802 (1994)

Cheng, P., Pan, S., Shin, A., Kim, K., Liou, W., and Park, M., J. Microsc., Vol. 189, Pt. 3, p. 199 (1998)

Cheng, Y., Minoshima, K., Seta, K., Matsumoto, H., Appl. Phys. Lett. (USA), Vol.74, No.14, p. 2062 (1999).

Denk, W., Strickler, J.,and Webb, W., Science, Vol.248, p.73 (1990).

Denk, W., Piston, D., and Webb, W. in "Handbook of biological confocal microscopy, J. B. Pawley ed.," p. 445 (Plenum Press, New York, 1995).

Denk, W., Proceedings of Focus on Microscopy, Abstract-48, Heidelberg (1999)

Diels, J., and Rudolph, W., Ultrashort Laser Pulse Phenomena, (Academic Press, SanDiego, 1996).

Fan, G., Fujisaki, H., Miyawaki, A., Tsay, R., Tsien, R., and Ellisman, M., Biophys. J., Vol.76, p. 2412 (1999).

Fisher, R. ed., Optical Phase Conjugation, (Academic, London, 1983).

Fork, R., Martinez, O., and Gordon, J., Opt. Lett., Vol. 9. No. 5, p. 150 (1985).

Fujita, K., Kaneko, T., Nakamura, O. Oyamada, M., Takamatsu, T., Kawata, S., Opt. Commn. (in press).

Gu, M., "Principles of three-dimensional imaging in confocal microscopes," (World Scientific, 1996).

Guild, J., Xu, C., and Webb, W., Appl. Opt., Vol. 36, No. 1, p. 397 (1997).

Gunter, P. and Hugnard, J. ed., Photorefractive Materials and Their Applications II, (Springer-Verlag, 1989).

Hama, T., Takahashi, A., Ichihara, A. & Takamatsu, T., Cell. Signal. Vol. **9.** p. 331 (1998).

Hell , S., and Stelzer, E., J. Opt. Soc. Am. A, Vol.9, No. 3, p. 2159 (1992).

Hell, S., Lindek, S., Cremer, C., and Stelzer, E., Appl. Phys. Lett. Vol. 64, p.1335 (1994)

Haugald, R., Handbook of fluorescent probes and research chemicals, (Molecular Probes, 1996).

Ichimura, A., Tanaami, T., Isozaki, K., Sugiyama, Y., Kosugi, Y. Mikuriya, K., Abe & Uemura, I., Bioimages, Vol. 4, p. 57-62 (1996).

Kawata, Y., Fujita, K., Nakamura, O., and Kawata, S., Opt. Lett., Vol. 21, p.1415 (1996).

Konig, K., Riemann, I., Fischer, P., and Halbhuber, K., Cell. Mol. Biol. Vol. 45, No. 2, p. 195 (1999).

Maruo, S., Nakamura, O., and Kawata, S., Opt. Lett., Vol 22, No. 2, p. 132 (1997).

Miyawaki, A., Llopis, J., Heim, R., McCaffery, J., Adams, J., Ikura, M., and Tsien, R., Nature, Vol. 388, p.882 (1997).

Minta A., Kao, J., Tsien, R., J Biol Chem., Vol. 264, No. 14, p.8171 (1989).

Nakamura, O., Optik, Vol. 93, p. 39 (1993).

Nakamura, O., Fujita, K., Kawata, Y., and Kawata, S., Jpn. J. Appl. Phys. Vol. 35, No.7A, p. L852 (1996).

Piston, D., Kirby, M., Cheng, H., Lederer, W., and Webb, W., Appl. Opt., Vol. 33, No.4, p.662 (1994).

Schrader, M., Bahlmann, K., and Hell, S, J. Biophys., Vol. 75, p. 1659 (1998).

Schrader, M., and Hell, S., Proceedings of Focus on Mcirscopy, ABSTRACT-55, Heidelberg, (1999)

Schrader, M., and Hell, S., Proceedings of Focus on Mcirscopy, ABSTRACT-55, Heidelberg, (1999)

Sheppard, C., and Gu, M., Optik, Vol. 86, p. 104 (1990).

Squirrell, J., Wokosin, D., White, J., and Bavister, B., Nature Biotechnology, Vol. 17, p. 763 (1999).

Straub, M., and Hell, S., Appl. Phys. Lett., Vol. 73, p.1769 (1998).

Svoboda, K., Denk, W., Kleinfeld, D., and Tank, D., Nature, Vol. 395, p.161 (1997)

Toriumi, A, Gu, M., and Kawata, S., Opt. Lett. Vol.23, No.24, p. 1924 (1998).

Wilson, T., and Sheppard, C., Theory and practice of scanning optical microscopy, (Academic Press, 1985).

Xiao, G., and Kino, G., Proc. SPIE - Int. Soc. Opt. Eng., Vol. 809, p. 107 (1987).

Xie, S., Holtom G., Sanchez, E., Novotony, L., and Arnett, D., Proceedings of Focus on Microscopy 1998, Abstracts-73, Sydney (1998).

Xu, C., Williams, R., Zipfel, M., and Webb, W., Bioimaging, Vol. 4, p. 198 (1996) .

Xu, C. and Webb, W.W. J. Opt. Soc. Am. B, Opt. Phys. Vol.13. p.481(1996).

Yan, H., Pan, E., Wang, P., Chang, C., Cheung, N., Chin, J., J. Phys., Vol.36, No.6, p. 791 (1998).

飯野正光, 蛋白質・核酸・酵素（増刊）, Vol. 43, No.2, p.1534（共立出版、1998）.

石川春律, 高松哲郎 編著, "新しい光学顕微鏡、第２巻：共焦点レーザ顕微鏡の医学・生物学への応用, "（学際企画, 1995）.

遠藤 寛, 蛋白質・核酸・酵素（増刊）, Vol. 43, No.2, p.1525（共立出版、1998）.

河田 聡 編著, 新しい光学顕微鏡、第１巻：レーザ顕微鏡の理論と実際, （学際企画, 1995）.

高松哲郎, 細胞, Vol. 30., No. 1, p.2 (1998).

竹迫和浩, 佐々木一美, 細胞, Vol. 30., No. 1, p.23 (1998).

List of publications

Original Papers

[1] K. Fujita, O. Nakamura, T. Kaneko, M. Oyamada, T. Takamatsu, and S. Kawata, "Confocal multipoint multiphoton excitation microscope with microlens and pinhole arrays," Opt. Commun. (in press).

[2] K. Fujita, O. Nakamura, T. Kaneko, M. Oyamada, T. Takamatsu, and S. Kawata, "Real-time imaging of two-photon induced fluorescence with a microlens-array scanner and a regenerative amplifier," J. Microsc., Vol. 194, Part 2/3, pp.528-531 (1999).

[3] M. D. Rosendo, A. Tarun, K. Fujita, and C. Saloma, "Temporal coherence behavior of a semiconductor laser under strong optical feedback," Opt. Commun., Vol.161, Issue1-3, pp. 123-127 (1999).

[4] K. Fujita and S. Kawata, "Laser feedback microscopy controlling the laser oscillation of semiconductor laser by reentered light," The Review of Laser Engineering (1996) (in Japanese).

[5] Y. Kawata, K. Fujita, O. Nakamura, and S. Kawata, "4Pi confocal optical system with phase conjugation," Opt. Lett., Vol. 21, No. 18, pp. 1415-1417 (1996).

[6] O. Nakamura, K. Fujita, Y. Kawata, and S. Kawata, "Double-pass absorption confocal microscopy with phase conjugation," Jpn. J. Appl. Phys., Vol. 35, No.7A, pp. L852-L853 (1996).

International conferences / proceedings

[1] K. Fujita,T. Kaneko, O. Nakamura, M. Oyamada, T. Takamatsu, and S. Kawata, "Real-time confocal two-photon fluorescence microscope using a rotating microlens array", Proceeding of SPIE,1999 International Conference on Optical Engineering and Nanotechnology, pp. 390-393(1999).

Nanotechnology, pp. 390-393(1999).

[2] K. Fujita, O. Nakamura, T. Kaneko, M. Oyamada, T. Takamatsu, and S. Kawata, "Confocal two-photon excitation fluorescence microscopy for real-time imaging", Focus on Microscopy (12th International Conference on 3D Image Processing in Microscopy, 11th International Conference on Confocal Microscopy), p. 17 (Heidelberg, 1999).

[3] K. Fujita, O. Nakamura, T. Kaneko, M. Oyamada, T. Takamatsu and S. Kawata, "Real-time imaging of two-photon induced fluorescence with a microlens-array scanner and a regenerative amplifier," Proc. of the 5th International Conference on Near Field Optics and Related Techniques (NFO-5), pp. 394-395 (Shirahama, 1998).

[4] K. Fujita, O. Nakamura, Y. Kawata, and S. Kawata, "Phase-conjugation confocal microscopy," Proc. 1997 Topical Meeting on Photorefractive Materials, Effects and Devices (PR'97), pp.499-502 (Chiba, 1997).

[5] K. Fujita, O. Nakamura, Y. Kawata, and S. Kawata, "4Pi Confocal Microscopy with a Phase Conjugate Mirror," Journal of Analytical Morphology (Proc. Focus on Multidimentional Microscopy, 10th International Conference on 3D Image Processing in Microscopy and 9th International Conference on Confocal Microscopy), Vol. 4, pp. 165-166 (1997).

[6] O. Nakamura, V. Daria, K. Fujita, Y. Kawata, S. Kawata, C. Palmes-Saloma, and H. Kondoh,"Two-photon Fluorescence Scanning Microscopy of a Turbid Medium," Journal of Analytical Morphology (Proc. 10th International Conference on 3D Image Processing in Microscopy and 9th International Conference on Confocal Microscopy), Vol. 4, pp.163-164 (1997).

[7] K. Fujita, O. Nakamura, Y. Kawata and S. Kawata, "The Use of Phase Conjugation in Scanning Laser Microscopy," ICO-17, Proceedings of SPIE, Vol. 2778, pp. (Taejon, 1996).

Domestic Meetings (in Japanese)

[1] T. Kaneko, H. Tanaka, K. Fujita, M. Oyamada, O. Nakamura, S. Kawata, and T. Takamatsu, "The observation of Ca^{2+} waves in perfused rat whole heart by real-time confocal laser scanning microscopy and two-photon excitation microscopy," Proc. of 24th mtg. of Jpn. Soc. Laser Microscopy (Kyoto, 1999).

[2] T. Kaneko, H. Tanaka, K. Fujita, M. Oyamada, O. Nakamura, S. Kawata, T. Takamatsu, "Observation and characterization of the Ca^{2+} waves in the perfused whole heart," 37th annual meeting of the biophysical society of Japan, Abstract p.s209-3PD049 (Wako, 1999).

[3] O. Nakamura, K. Fujita, and S. Kawata, "Real-time confocal two-photon fluorescence microscope using a rotating microlens array", Proc. of 23rd mtg. of Jpn. Soc. Laser Microscopy (SLM23), pp.50-53 (Tokyo, 1999).

[4] K. Fujita, O. Nakamura, and S. Kawata, "Development of a confocal scanner unit for a real-time two-photon excitation microscope," Extended Abstracts (The 46th Spring Meeting,1999);The Japan Society of Applied Physics, p. 1053 (Tokyo, 1999) .

[5] O. Nakamura and K. Fujita, "Fast scanning two-photon excitation laser microscopy," Proc. of 22nd mtg. of Jpn. Soc. Laser Microscopy (SLM22), pp. 8-13 (Hamamatsu, 1998).

[6] K. Fujita, T. Kaneko, O. Nakamura, M. Oyamada, T. Takamatsu and S. Kawata, "Dynamic observation of biological samples with a real-time two-photon fluorescence microscope," Proceedings of Optics Japan '98, pp. 257-258 (Okayama, 1998).

[7] K. Fujita, A. Egner, O. Nakamura, and S. Kawata, "Real-time two-photon fluorescence microscope with a microlens array and a Nipkow disk," Extended Abstracts (The 59th Autumn Meeting, 1998);The Japan Society of Applied Physics, p. 877 (Hiroshima, 1998).

[8] O. Nakamura, K. Fujita, M. Shirai, A. Egner, T. Kaneko, and S. Kawata, "Two-photon fluorescence microscope with a microlens-array scanner," Proc. of 21st mtg. of Jpn. Soc. Laser Microscopy (SLM21), p. A1 (Osaka, 1998).

[9] K. Fujita, O. Nakamura, and S. Kawata, "Fluorescent imaging by a 4Pi confocal microscope with phase conjugation," Extended Abstracts (The 58th Autumn Meeting, 1997);The Japan Society of Applied Physics, p. 952. (Akita, 1997).

[10] V. Daria, O. Nakamura, C. Palmes-Saloma, K. Fujita, C. Saloma, H. Kondoh, and S. Kawata,"Long depth imaging of turbid biological samples by two-photon fluorescence microscopy," Proc. 19th mtg. of Japan Society for Laser Microscopy (SLM-19), pp. 26-32 (Nagoya, 1997).

[11] O. Nakamura, K. Fujita, and S. Kawata, "4Pi confocal optical system with phase conjugation," The 7th Meeting on Phase Conjugation and Wave Mixing (Osaka, 1996).

[12] O. Nakamura, K. Fujita, Y. Kawata and S. Kawata, "Laser scanning microscopy with phase conjugation," Proc. of 16th mtg. of Jpn. Soc. Laser Microscopy (SLM16), pp.49-56 (1995).

[13] K. Fujita and S. Kawata, "Threshold-controlled imaging with a semiconductor laser-feedback microscope," Extended Abstracts (The 56th Autumn Meeting, 1995);The Japan Society of Applied Physics, p. 824 (Kanazawa, 1995).

[14] Y. Kawata, K. Fujita, O. Nakamura, and S. Kawata, "4Pi confocal optical system using phase conjugation," Extended Abstracts (The 56th Autumn Meeting, 1995);The Japan Society of Applied Physics, p. 814 (Kanazawa, 1995).

[15] K. Fujita and S. Kawata, "Laser feedback microscopy controlling the lasing state of a semiconductor laser," Proc. SLM-15 (Japan Society for Laser Microscopy), pp.11-17 (1995).

Award

The 5th JSAP Awards for Research Paper Presentation, "Real-time two-photon fluorescence microscope with a microlens array and a Nipkow disk," (November, 1998).